MITIGATING DISUSE BONE LOSS: ROLE OF RESISTANCE EXERCISE AND BETA-ADRENERGIC SIGNALING

A Dissertation

by

JOSHUA MICHAEL SWIFT

Submitted to the Office of Graduate Studies of
Texas A&M University
in partial fulfillment of the requirements for the degree of

DOCTOR OF PHILOSOPHY

May 2010

Major Subject: Kinesiology

MITIGATING DISUSE BONE LOSS: ROLE OF RESISTANCE EXERCISE AND BETA-ADRENERGIC SIGNALING

A Dissertation

by

JOSHUA MICHAEL SWIFT

Submitted to the Office of Graduate Studies of
Texas A&M University
in partial fulfillment of the requirements for the degree of

DOCTOR OF PHILOSOPHY

Approved by:

Co-Chairs of Committee,	Susan A. Bloomfield
	Harry A. Hogan
Committee Members,	Christopher R. Woodman
	James D. Fluckey
Head of Department,	Richard Kreider

May 2010

Major Subject: Kinesiology

ABSTRACT

Mitigating Disuse Bone Loss: Role of Resistance Exercise and Beta-Adrenergic Signaling. (May 2010)

Joshua Michael Swift, B.S., The Pennsylvania State University

Chair of Advisory Committee: Dr. Susan A. Bloomfield

Mechanical loading is an integral component to maintaining bone mass during periods of disuse (i.e. bedrest or casting) or reduced weightbearing activity. Recent data has shown a direct relation between the sympathetic nervous system (SNS) and bone metabolism, however the underlying mechanisms responsible for this relationship are unknown. Furthermore, the role that beta adrenergic stimulation during disuse has on cancellous bone mass and microarchitecture have yet to be defined. The *central hypothesis* of this research is that resistance exercise and beta-1 adrenergic (Adrb1) receptor agonist administration attenuate disuse-associated reductions in metaphyseal bone during 28 days of rodent hindlimb unloading (HU).

Study one determined whether an eccentric- (ECC) or combined isometric+eccentric- (ISO+ECC) based contraction paradigm, engaged during hindlimb unloading (HU), mitigates losses in musculoskeletal mass and strength. Both simulated resistance training (SRT) protocols inhibited reductions in disuse-sensitive cancellous bone mass and maintained plantarflexor muscle strength.

Study two determined whether combining the anabolic effects of SRT with the anti-resorptive effects of alendronate (ALEN) during HU positively impacts cancellous bone in an additive or synergistic fashion. ALEN significantly inhibited the anabolic response of cancellous bone to SRT during HU.

Study three determined whether an Adrb1 receptor agonist (dobutamine; DOB) mitigates disuse-associated losses in bone mass and formation rate (BFR) during HU. DOB administration significantly blunted reductions in bone mineral density (vBMD) by maintaining cancellous BFR.

Study four determined if Adrb1 receptor agonist administration during HU results in an attenuation of osteocyte apoptosis within cancellous bone and whether this relates to a decrease in Bax/Bcl-2 mRNA content ratio (pro- and anti-apoptotic proteins). HU significantly increased cancellous bone osteocyte apoptosis and Bax/Bcl-2 mRNA content ratio, which was reduced by the administration of DOB.

Collectively, these are the first studies to assess the role of beta-1 adrenergic signaling and resistance exercise in mitigating disuse-induced loss of cancellous bone mass in rodents. The long term goals of this research are to understand the exact molecular mechanisms by which both Adrb1 signaling and high intensity resistance exercise provide beneficial bone effects during prolonged periods of disuse and to apply these findings to current osteoporosis research.

DEDICATION

To my wife and son, who give meaning to everything I do.

ACKNOWLEDGEMENTS

I want to extend my deepest gratitude to Sue, my mentor who believed in my abilities from the beginning of my graduate career. She stood by and supported my research when others may not have been willing to do so. Her training has provided me with many valuable resources that I will undoubtedly call upon throughout my career. She treated me more as a colleague than a student, and always looked out for my best interest. She helped to open doors for me that I never dreamed possible, and provided me the opportunity to spend my life doing what I love, research. For all this and more, I will eternally be thankful.

I also want to thank Harry, the hardest working man I've ever met. His tireless work for his students' benefit is unmatched by any other mentor. He has inspired me in many ways beyond science. His humor always kept me in good spirits and I will forever appreciate his help and support.

My sincerest thanks to Matt Allen, who has selflessly offered his advice and guidance over the past 3 years. I would be thankful if I became even half the scientist that Matt is. He is a model researcher that I will always admire and strive to be like.

Additionally, I want to thank my committee members Jim Fluckey and Chris Woodman for their support and insight.

To Joanne Lupton and Nancy Turner, thank you for giving me the opportunity to be an NSBRI fellow and renewing my childhood dreams. I will forever be grateful for

the opportunities that this fellowship afforded me and I will never forget the experiences that I've had as a direct result of this program.

Thank you to my closest friend and colleague, Lt. Heath G. Gasier, for always listening and providing advice. I look forward to the many years to come of collaboration that we will have. To Michael Wiggs and Mats Nilsson, thank you for your friendship and stimulating scientific conversations over the past several years. Additionally, I want to thank all the members of the Muscle Biology Lab, including Justin Dobson, Kevin Shimkus, and Nic Greene. Thank you also to friends at Texas A&M who have since graduated, but who provided me an outlet from research. Thank you to these friends and fellow "Busters": Adam and Lindsay Barry, Yosuke Tsuji, Don and Beth Chaney, Tina Garcia, Kirk Zihlman, Rod Peterson, Stewart Walsdorf, Trevor Bopp, and Windy Dees.

I want to sincerely thank all the past and present members of the Bone Biology Lab, including Florence Lima, Brandon Macias, Liz Greene, Kyunghwa Baek, and Jan Stallone. Thank you all for your friendship, your assistance, and your commitment to excellence in research.

I want to thank my parents, Scott and Mary Swift, my sister, Danielle Swift, and my grandparents, Harold and Betty Swift. You may have thought that I was crazy 6+ years ago when I traveled across the country to pursue graduate school in Texas, but your love and support never wavered. Thank you for always listening, always loving, and always believing in me. I also want to thank Jim and Camille Miller for their love and support the past 5 years. I love you all so much.

Most importantly, I thank the love of my life, Sibyl. Before I met you, I never knew I could love someone so completely. You are my life-partner, my wife, my colleague, and my best friend. Without your many sacrifices and endless support none of this would have been possible. Thank you for always supporting my dreams and continuing to inspire me. Everything I do is for you and our son, Liam. I can't wait to see where this journey takes us! I love you!

Finally, I want to thank God for giving me the many opportunities to achieve greatness. I lost my way some time ago, but have found my path with Him in life again. He's given me the strength and courage to continue to fight through all of life's adversities. He's brought me more joy than I knew existed. I offer this work to Him.

"Science without religion is lame. Religion without science is blind." Albert Einstein

TABLE OF CONTENTS

CHAPTER Page

LIST OF TABLES

LIST OF FIGURES

Page

Page

Page

CHAPTER I

INTRODUCTION

During normal weightbearing, bone formation (osteoblasts) and bone resorption (osteoclasts) remain equal, and the skeleton is in a state of balance. During periods of decreased skeletal loading, bone formation and resorption become uncoupled, with increased resorption and decreased formation leading to a net loss of bone mass. This reduction in skeletal mass, if continued over a prolonged period of time, leads to osteopenia or osteoporosis and significantly increases the risk of skeletal fracture.

Outside of the realm of microgravity, periods of disuse or reduced mechanical loading are encountered by a large number of persons and are, therefore, of great importance for continued investigations. Individuals exposed to prolonged bed rest, limb immobilization, or spinal cord injury give clinical relevance to the accelerated bone loss associated with spaceflight. However, understanding the mechanisms underlying the processes of skeletal tissue loss during disuse and aging have yet to be determined, and many similarities between bone loss in these two models do exist. Therefore, research aimed at determining the mechanisms involved in disuse-associated reductions in skeletal loss will provide essential insight into age-related decrements in bone mass and osteoporosis.

This dissertation follows the style of Journal of Bone and Mineral Research.

Bisphosphonates are well established as the leading drugs for the treatment of osteoporosis and other skeletal diseases characterized by increased bone resorption. Alendronate (ALEN), a nitrogen-containing bisphosphonate, has been approved by NASA for in-flight experiments. Alendronate inhibits bone resorption and ultimately contributes to osteoclast apoptosis, thereby maintaining skeletal mass and strength. Additionally, ALEN is a proven agent in minimizing bone loss due to estrogen deficiency and disuse in rats.

Resistance exercise is an anabolic agent proven to stimulate bone growth, even during periods of bed rest and disuse. The high strains imparted on bone, typically encountered during high intensity resistance exercise, activate mechanical and chemical signaling within bone and ultimately lead to "modeling activity." As of yet, no animal studies have successfully inhibited reductions in cancellous bone mass and formation using resistance exercise protocols. Furthermore, no studies have addressed the effects that combining bisphosphonate treatment with a resistance exercise protocol, completed during disuse, has on disuse-sensitive cancellous bone.

The sympathetic nervous system (SNS) has been shown to mediate bone metabolism. However, the exact role that beta-1 adrenergic (Adrb1) receptors have in this process has not been elucidated. Although stimulation of the SNS has been documented to increase bone resorption, resulting in reduced cancellous bone mass and microarchitecture, this has been primarily attributed to stimulation of Adrb2 receptors. The role that Adrb1 receptor stimulation during reduced mechanical loading has on

disuse-sensitive cancellous bone is important to further understanding the underlying mechanisms responsible for bone loss.

In the first study included in this dissertation (Chapter III), we investigated the effects of two separate simulated resistance training (SRT) protocols, engaged during rodent hindlimb unloading, on bone and muscle mass and strength. Results from this investigation demonstrated that high-intensity muscle contractions, independent of weightbearing forces, can effectively mitigate losses in muscle strength and provide a potent stimulus to bone during prolonged disuse. Based on results from the first study, we hypothesized that by adding an anti-resorptive agent, alendronate (ALEN; bisphosphonate), to an anabolic stimulus, SRT, disuse-associated reductions in cancellous bone formation and microarchitecture would be completely inhibited. In the second study (Chapter IV), we investigated the individual and combined effects of a reduced volume and intensity of SRT and ALEN treatment during HU on cancellous bone parameters. Results from this investigation further demonstrate the anabolic effect of a low volume of high intensity muscle contractions during disuse and suggest that both bone resorption and formation are suppressed when SRT is combined with bisphosphonate treatment. Furthermore, this study describes the potential inhibitory effects of ALEN treatment on cancellous bone's response to SRT during rodent hindlimb unloading.

In the third study (Chapter V), we evaluated the effects of a beta-1 adrenergic (Adrb1) agonist, dobutamine (DOB), on unweighted tibiae and femoral bone content, density, area, and strength during 28 days unloading. DOB administration during HU

effectively attenuated significant declines in total volumetric bone mineral density (vBMD) at the proximal tibia by mitigating associated decrements in bone formation. The significant positive effects of DOB on unweighted bone are not observed in animals experiencing normal gravitational loading and provide evidence for the importance of Adrb1 signaling in maintaining bone mass. Based on results from the third investigation, we wanted to determine if the positive effects of DOB on unweighted cancellous bone resulted in enhanced metaphyseal microarchitecture and were directly related to reductions in osteocyte apoptosis. In the fourth study (Chapter VI) we tested the effects of an Adrb1 agent on osteocyte apoptosis and expression of a pro- and anti-apoptotic protein (Bax, Bcl-2) in unloaded bone. Results from this investigation illustrated the effectiveness of DOB treatment during HU to mitigate reductions in cancellous bone microarchitecture and increases in osteocyte apoptosis, perhaps by inhibiting increased Bax/Bcl-2 mRNA content.

Results of these investigations highlight the potential ability of high-intensity muscle contractions to completely abolish disuse-associated reductions in cancellous bone mass, formation, and deleterious changes in microarchitecture, and further emphasize the role that both resistance exercise and bisphosphonate treatment have to inhibit osteocyte apoptosis. In addition, these studies demonstrate the dynamic role that beta-1 adrenergic agonist signaling has on maintaining cancellous bone during periods of reduced weightbearing or unloading. Hence, these findings have important implications for humans experiencing extended periods of reduced weightbearing activity.

CHAPTER II

REVIEW OF LITERATURE

Bone Remodeling and Modeling in the Adult Skeleton

Skeletal remodeling, occurring throughout the lifetime of a mammal, is defined as the collaborative and sequential efforts of a BMU (bone multicellular unit). BMU's operate on periosteal, endosteal, and trabecular surfaces, as well as within cortical bone by replacing old with new bone. Osteonal BMU's originate on the periosteal or endosteal surfaces of bone, or along the walls of Haversian canals, and are activated by chemical, mechanical, or electrical signals. The process of bone remodeling is based upon the coupled action of bone-resorbing cells (osteoclasts) and bone-forming cells (osteoblasts). Osteoblasts, as well as chondrocytes, adipocytes, fibroblasts, and myoblasts, differentiate from mesenchymal stem cells (1). Osteoclasts, however, are derived from the hematopoietic mononuclear lineage (2). The primary functions of the remodeling cycle include: (1) the preventative maintenance of mechanical strength through replacement of fatigued bone by new, mechanically sound bone, and (2) maintenance of mineral homeostasis by providing access to stores of calcium and phosphorous.

There are 4 basic phases of the remodeling cycle, which include (1) activation, (2) resorption, (3) reversal, and (4) formation. Activation involves the recruitment of multinucleated osteoclast precursors from cells in the monocyte-macrophage lineage. Most remodeling is likely random, but can be targeted towards specific sites that need to

be repaired. Pre-osteoclasts, from hematopoietic stem cells, affix themselves to the bone matrix through binding between integrin receptors and organic matrix, creating a sealing zone. Osteoclasts are then able to create a bone-resorbing compartment between itself and the bone matrix. Activation of osteoclasts is regulated by local cytokines like RANKL, IL-1 and IL-6 (3,4).

Resorption, the second phase of remodeling, involves the catabolic actions of osteoclasts. Osteoclasts are multinucleated, macrophage-like cells that attach to the bone surface, form a peripheral seal, and break down bone within a sealed area by means of enzymes or chemicals (1). The osteoclast's membrane transfers protons to the resorbing compartment (attached to bone) lowering its pH to 4. This compartment becomes acidified by the secretion of lysosomal enzymes like TRAPC and cathespin K, which dissolves and digests the mineral and organic phases of the matrix. This resorption of bone creates a saucer-shaped cavity, called Howship's lacunae.

The process of bone resorption ends with osteoclast apoptosis and the reversal phase begins. During reversal, signals are sent out to "summon" osteoblasts into the newly formed resorption cavities to replace removed bone. Without efficient coupling mechanisms, remodeling would result in net bone loss. There are two theories of coupling signals: (1) osteoclasts release growth factors from bone matrix during resorption, which attract osteoblast precursors and stimulate osteoblast proliferation and differentiation; or (2) strain-regulated theory: strain levels are lower ahead of osteoclasts and higher behind them (in BMU as it moves through bone). Osteoblasts are activated in response to high strain, and osteoclasts are activated in response to reduced strain.

Following reversal, formation of new bone occurs. Formation is a two step process, whereby osteoblasts synthesize organic matrix and then regulate its mineralization. Osteoblasts mineralize organic matrix by deposition of Ca^{2+} and phosphate ions. After completion of their bone formation function, osteoblasts have three cell fates: (1) die by apoptosis, (2) become entombed in the mineralizing matrix as osteocytes, or (3) remain on the surface as bone lining cells. Osteocytes maintain contact with each other and cells on bone surface via gap junctions between cytoplasmic processes that extend through canaliculae. Osteocytes become part of network which can sense changes in mechanical properties surrounding bone and transmit this information to cells on bone surface (i.e. osteoblasts) to initiate or regulate bone remodeling when necessary.

Modeling differs from remodeling, as this process is not defined by the coordinated actions of osteoblasts and osteoclasts. Instead, modeling involves the shaping or reshaping of bones by independent actions of these cells. During modeling, bone formation is not coupled to resorption, and vice versa. Modeling occurs during growth or, in an adult skeleton, in response to increased mechanical loading. Additionally, modeling occurs less frequently than remodeling in adults, particularly in cancellous bone.

Disuse Bone Loss

Spaceflight Effects on Bone (Human)

Mechanical loading is an integral component to maintaining bone mass during periods of disuse (i.e. bedrest or casting) or reduced weightbearing activity. In-flight measures of bone mass and geometry are not possible to obtain, therefore serum and urine biomarkers of bone formation and resorption have become useful pieces of evidence to our understanding how bone responds to microgravity. Early studies from Skylab missions (1973-1974) sought to determine transient changes in bone metabolic biomarkers during 28, 59, and 84 days of space flight. Data from these missions demonstrated nearly 2-fold increases in-flight in urinary excretion of bone resorption markers type 1 cross-linked N-telopeptide of (NTX), deoxypyridinoline (DPD), and pyridinoline (PYD), and hydroxyproline vs. pre flight values (5,6). Later investigations on MIR cosmonauts extended results from these Skylab missions. Extensive microgravity exposure (up to 180 days) significantly reduced bone alkaline phosphatase (BAP; bone formation biomarker) and increased DPD and type 1 cross-linked C-telopeptide (CTX; bone resorption biomarkers) up to 80% (7-10). A study by Smith and colleagues (10) demonstrated no change in BAP or osteocalcin during 180 days of space flight. However, these authors noted a significant loss of Ca^{++} absorption (~250mg/d) during microgravity. Assessment of changes in biomarkers of bone metabolism pre vs. post-flight, demonstrated that, although bone formation markers were unchanged during microgravity exposure, osteocalcin and BAP were significantly increased post-flight (11).

Although bone biomarkers provide readily accessible data in-flight data (from urine or serum), their amounts vary considerably from day to day and from subject to subject (12). For this reason, more reliable ground-based measures of bone mass and geometry were necessary to document skeletal changes attributable to space flight. Long duration exposure to microgravity leads to an accelerated loss of bone mass (~1-2%/month) and results in osteopenia (13,14). Vico and colleagues (14) completed peripheral quantitative computed tomography (pQCT) scans on tibiae and radii of cosmonauts before and after long-duration MIR missions and demonstrated that prolonged microgravity exposure (6+ months) results in greater reductions in cancellous than cortical bone mineral density (BMD), and that these reductions in tibia cancellous BMD are not fully restored by 6 months of recovery. Furthermore, microgravity exposure affects bone mass in weightbearing (i.e. lower body) bones only. Recent data gathered from crew members on the International Space Station (ISS) illustrates the significant losses of bone mineral density (BMD) and geometry of the femoral neck (15). Dual-energy x-ray absorptiometry (DXA) and QCT scans were taken on 14 ISS astronauts before and after 4-6 month missions. Data from this investigation demonstrated that the greatest reductions in areal BMD (aBMD) and trabecular volumetric BMD (vBMD) occurred at the hip at a rate of 1.4-1.5% and 2.2-2.7%/month, respectively (15). A subsequent study by Lang and colleagues (16) illustrated a significant increase in estimated fracture risk during 4.5-6 month ISS missions that remains even 1 year after returning to Earth. Pre- and post-flight peripheral pQCT scans were administered to astronauts serving a single 4-6.5 month mission aboard ISS, and

finite element models (FEM) of these scans were completed to assess estimated proximal femoral strength during stance or a fall onto the posterolateral aspect of the greater trochanter. For those crew members experiencing the greatest bone loss, reductions in modeled proximal femur strength after a microgravity exposure approached the estimated lifetime loss in stance strength for Caucasian women (17). Furthermore, lack of recovery of BMD in ISS and MIR crew members has been documented 6 months post-flight (14), with indications that it may not be fully restored for 3 years (18).

Taken together, these data suggest that microgravity results in reduced bone mass, which is attributable to increased bone resorption and decreased (or unchanged) bone formation and negative calcium balance (in-flight). Furthermore, these reductions in bone mass put astronauts at increasingly greater risk of fracturing their hip upon return to Earth's 1-gravity atmosphere. Most importantly, losses in bone typical of exposure to microgravity are not fully restored by an equal amount of recovery time (i.e. 6 months).

Simulating Bone Loss with Spaceflight in Rodents: Hindlimb Unloading/Tail Suspension

The rodent hindlimb unloading (HU) model was developed by Emily Morey-Holton in the 1970's to most effectively mimic the effects of spaceflight on multiple systems of the body (19). This model was the first to successfully model microgravity-induced alterations in cardiovascular, muscular, and skeletal tissues, all the while not overly stressing the animal. The HU model has become the gold-standard Earth-based

model to simulate microgravity effects, as it allows the animal ambulation using only the forelimbs, unloads the hindlimbs without paralysis, and produces cephalic fluid shifts (20). Furthermore, ground-based studies using the HU model provide a more efficient avenue to continue to study the effects of microgravity on the body, in comparison to actual shuttle experiments, which are costly and extremely competitive.

Similar to the effects of microgravity in humans, rodent hindlimb unloading significantly reduces cancellous bone within the metaphyses of the unweighted femur and tibia (14,21). The effects of HU in adult male rats are compartment-specific, as 28 days of unloading primarily impacts cancellous and not cortical bone sites (21). HU results in significant reductions in disuse-sensitive cancellous bone mass, architecture and material properties, due to early increases in bone resorption followed by prolonged depressions in bone formation rate (BFR) (21-24). These reductions in cancellous bone mass are accounted for by decreased trabecular thickness (25-27) and number (27) and increased trabecular spacing (24).

Resistance Exercise Effects on Skeletal Tissue

It has been well established that bone responds to increased and reduced mechanical loading in opposing manners. Resistance exercise (RE) training incurs an integrated physiological response typical of intense exercise (e.g., increased sympathetic nervous system outflow, blood flow, and IGF-1 production), but which has not been demonstrated with other models of mechanical loading (28-31). Squats, a lower-body

form of RE, produces significant lower leg muscle hypertrophy and increased skeletal muscle protein synthesis (32-34).

Resistance exercise that includes eccentric contractions provides an anabolic stimulus for both skeletal muscle and bone in human and rodent models (35-38), and has generally proven more effective in promoting increased bone and muscle mass than endurance exercise protocols such as running. Furthermore, eccentric contractions (during muscle lengthening) generate larger muscle forces than do concentric contractions (muscle shortening), providing greater increases in BMD (36).

Resistance Exercise Effects on Bone (Humans)

In humans, bone responds to increased mechanical stress, evidenced during high-impact and resistance exercise (RE), and has demonstrated the ability to increase lumbar spine and femoral neck (FN) bone mass and strength (39-41). Resistance exercise provides the necessary load to increase bone mass in healthy individuals and prevents skeletal losses in estrogen deficient women, thereby decreasing the risk of fracture during a fall (30,42-45). Furthermore, high-intensity RE (39,46) elicits a greater anabolic response on bone than lower-impact activities like running or walking (47), making it an attractive countermeasure to inhibit bone loss encountered in persons experiencing reduced activity.

Modeling Resistance Exercise Effects on Bone in Small Animal Models

Animal studies demonstrate similar results, as high-intensity RE and jump training provide greater anabolic stimulus to bone than repetitive, low-load, high-frequency exercise (i.e. running) (48,49). Drop training, whereby an animal is dropped from a set height and lands with high amount of force on its hindlimbs, results in greater proximal tibia total and cancellous volumetric bone mineral density (vBMD), (as a consequence of greater trabecular thickness (TbTh) compared to ambulatory controls) (50,51). Jump exercise, experienced when an animal jumps vertically in response to a visual stimulus, in rats and mice leads to greater bone volume (BV/TV) and osteoblast activity (MAR) at cancellous-rich bone sites (48,49) as well as increased cortical bone mass and strength (50,52). Furthermore, jumping with weighted backpacks (i.e. jump RE) has demonstrated the ability to increase trabecular thickness (TbTh), trabecular number (TbN), and bone volume in the proximal tibia (38).

Resistance Exercise Effects on Bone During Extended Bed Rest (Human)

Only a few long-term bed rest investigations have successfully mitigated bone loss with exercise paradigms. Combined supine flywheel resistive and treadmill exercise during 90-day bed rest in young men attenuates reductions in trochanter and hip BMD (53). Vigorous resistance training during 17-week bed rest increased lumbar spine and diminished reductions in total hip BMD, as well as attenuated losses of leg muscle masses and strength compared with bed rest controls (54). These initial studies provide promising data suggesting that losses in skeletal BMD, at sites where greatest bone loss

occurs during disuse, can be attenuated if a high-intensity resistance exercise training program is begun immediately upon initiation of unloading.

Applying Resistance Exercise During Rodent Hindlimb Unloading

Previous investigations have sought to define the osteogenic effect of mechanical loading during periods of disuse. Rubin et al (55) ,employing low-magnitude, high-frequency loads, found that 10min/d of loading was effective at maintaining metaphyseal bone volume (BV/TV) and did attenuate losses in bone formation at the proximal tibia. More recent studies have utilized electrical stimulation as a countermeasure to disuse-induced bone loss. Transcutaneous stimulation of the thigh, producing peak strains of ~200με, did not effectively prevent disuse osteopenia in hindlimb unloaded rodents, but did reduce tibial bone loss (56). A novel rodent resistance exercise device using flywheel technology was used by Fluckey et al (57) to demonstrate the effects of maximal voluntary squats, performed during suspension, on changes in metaphyseal bone mass. The flywheel exercise protocol maintained distal femur BMD and inhibited unloading-induced losses in bone mass at this site. Lam and Qin (58) recently demonstrated the beneficial effects of high frequency electrical stimulation of the leg musculature on bone during disuse. Although this treatment did effectively mitigate losses of cancellous bone volume in the unloaded distal femur, there was no demonstrable effect on bone formation. These studies provide initial evidence outlining the role of resistance exercise in mitigating reductions in metaphyseal bone mass and microarchitecture during periods of disuse or unloading.

Bisphosphonate Effects on Bone and Disue-Induced Bone Loss

Pharmacology of Bisphosphonates

Bisphosphonates are a class of anti-resorptive drugs which are strongly attracted to bone and inhibit osteoclast-mediated bone resorption. This characteristic makes bisphosphonates especially suitable for the treatment of many skeletal diseases all characteristic of severe bone loss. There are two main classifications of bisphosphonates: non-nitrogenous and nitrogenous. All bisphosphonates have a common phosphate-carbon-phosphate (P-C-P) moiety as part of their basic structure (59). Attached to the central P-C-P backbone are two side chains (R_1 and R_2), as shown in Figure 1. Each bisphosphonate differs in its side chains, which are primarily responsible for the binding affinity to mineral (R_1) and biochemical activity on osteoclast enzymatic activity (R_2).

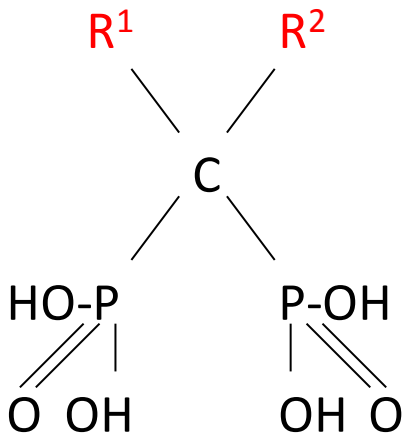

Fig. 1. Basic structure of a bisphosphonic acid.

Bisphosphonate Mechanisms of Action

The major effect of bisphonates on the skeleton is the inhibition of the osteoclast-mediated bone resorption. The phosphate ends of the bisphosphonate bind to calcium hydroxyapetite on the bone surface and are incorporated into bone during remodeling. Uptake of bisphosphonates by osteoclasts during remodeling leads to osteoclast apoptosis and the inhibition of key enzymes in the mevalonate pathway (also known as the HMG-CoA reductase pathway), preventing the generation of lipids necessary for the prenylation of small GTPase proteins (60). This restricts osteoclastic ability to bind to and resorb bone, as the ruffled border of the osteoclast is unable to be maintained, resulting in significantly reduced bone loss. Bisphosphoantes work to slow overall bone turnover. Bone remodeling units exit for longer time periods, which results in a greater degree of mineralization of skeletal tissue.

In addition to inhibiting osteoclast-mediated bone resorption, recent studies suggest that osteocytes may be important target cells for bisphosphonates in bone. Many bisphosphonates appear to protect osteocytes (and osteoblasts) from apoptosis (61). The ability of bisphosphonates to inhibit apoptosis in osteocytes contrasts with their ability to induce apoptosis in osteoclasts. The inhibition of osteocyte apoptosis by bisphosphonates appears to be mediated by activation of extracellular signal-regulated kinases (ERKs) (62). This dual role of bisphosphonates and potential interaction with osteocytes in vivo needs further investigation before the exact mechanisms of bisphosphonates' actions can be fully understood.

Alendronate Effects on Skeletal Tissue During Prolonged Human Bed Rest

Few bed rest investigations on the effects of alendronate (ALEN) have attempted to elucidate the mechanics of this bisphosphonate's action on bone. Ruml and colleagues (63) administered 20 mg/day of ALEN to healthy males during 3 weeks of bed rest and observed a reduction in urinary calcium excretion as compared to controls. The only other bed rest study investigating the anti-resorptive capabilities of alendronate was by Le Blanc and colleagues (64). A dose of 10 mg/d of ALEN was administered daily to eight male subjects during17 weeks of bed rest. Daily ALEN treatment successfully prevented reductions in lumbar spine and femoral neck BMD and attenuated increases in urinary markers of bone resorption [cross-linked N-teleopeptide of type I collagen (NTX), pyridinium (Pyd), an deoxypyridinium (D-Pyd)]. However, ALEN during bed rest resulted in significant reductions in serum markers of bone formation (alkaline phosphatase, bone-specific alkaline phosphatase, and osteocalcin), which remained unchanged in bed rest subjects not administered ALEN.

Alendronate Effects on Skeletal Tissue During Rodent Hindlimb Unloading

The effectiveness of alendronate to inhibit disuse-induced bone loss has been demonstrated in numerous rodent hindlimb unloading investigations. Alendronate (100 μg/kg/d), administered prior to HU, prevented reductions in total and proximal tibia bone mass and proximal tibia calcium content. ALEN treatment decreased relative osteoclast surface and mitigated reductions in bone formation (26). Additionally, ALEN, administered during 14-day HU, abolished losses in tibia and femur BMD, but

was unable to rescue disuse-induced reductions in bone strength (65). Apseloff et al. (66) administered 30 μg/kg alendronate during 28 days of unloading and revealed significant reductions in osteoid perimeter, cancellous bone formation, and bone resorption with bisphosphonate treatment during HU (as compared to controls). The resulting increase in bone mass with alendronate treatment resulted from greater inhibition of resorption than from stimulation of formation.

Beta-Adrenergic Signaling in Skeletal Tissue

Sympathetic Nervous System and Beta-Adrenergic Receptors

Beta-adrenergic receptor agonists, activated by the sympathetic nervous system (SNS), may affect bone metabolism through separate avenues and have opposing effects on bone mass. Three subunits of β-adrenergic receptors (Adrb1, 2, 3) are present in tissues within the body and variant effects. Adrb2 receptors, present in the lungs, cause bronchile dilation, and on osteoblasts and osteoclasts, stimulate apoptosis and result in diminished bone mass (67,68). Adrb1 receptors are present on the heart, increasing cardiac contractility when activated, and are also present on osteoblasts and osteoclasts (69,70). Activation of β-3 adrenergic receptors, the primary adrenoreceptor on adipocytes, results in enhanced lipolysis (71,72). Adrb1 and Adrb2 receptors are both present on osteoblasts, but β-2 adrenergic receptors are the predominant subtype (67,68,73-75).

Beta-1 Adrenergic Agonist Effects on Bone

Dobutamine (DOB) is a non-specific, Adrb receptor agonist with dominant β-1 adrenergic receptor activity and a small amount of Adrb2 activity (76). The ability of DOB to primarily activate Adrb1 receptors make it an attractive synthetic catecholamine to study in coordination with rodent disuse. To our knowledge, only one study has attempted to assess the effects of chronic Adrb1 receptor stimulation on skeletal tissue. DOB administered during HU significantly blunted reductions in femoral midshaft cortical bone area and cross-sectional moment of inertia (CSMI), as well as mitigated the HU-associated decrease in femoral mid-diaphyseal cortical bone mineral apposition rate (77). This preliminary investigation, while lacking mechanisms, provides initial data outlining the potential positive effects of increased Adrb1 receptor stimulation during disuse.

Beta-2 Adrenergic Agonist Effects on Bone

Few studies have attempted to define the role that β-2 receptor activation has on skeletal tissue, beyond a few investigations completed in female rats. Adrb2 receptor agonist administration leads to increased bone resorption, resulting in reduced cancellous bone mass and microarchitecture. Bonnet and colleagues (78) treated skeletally immature, female rats daily (4mg/kg/d) with salbutamol or clenbuterol for 6 weeks. This study demonstrated the significantly deleterious effects of Adrb2 receptor agonists on metaphyseal bone, and clenbuterol-treated rats had lower distal femur trabecular number (-40%), connectivity (-3-fold), and bone volume (-43%) as compared to controls.

Furthermore, although bone formation was not measured, based on data from urinary markers the authors concluded the deleterious effects of Adrb2 agonists were related to increased resorption and not decreased formation. A subsequent study by Bonnet and colleagues (79) further emphasized the significant reductions in metaphyseal bone in a subsequent investigation. The authors demonstrated that chronic treatment of salbutamol or clenbuterol in growing female rats significantly decreased proximal tibia and lumbar spine bone volume, trabecular thickness, trabecular number, and biomechanical properties. Furthermore, Bonnet and colleagues (80) verified that salbutamol further increases the deleterious effects of estrogen deficiency (ovariectomized) on cancellous bone loss in adult rodent. Additionally, stimulation of Adrb2 receptors on osteoblasts increases osteoclast differentiation and activity, resulting in increased bone loss (81).

Adrenergic Receptor Knock-Out Mouse Models and Effects on Skeletal Tissue

A very limited number of in vivo investigations have attempted to systematically define the precise roles of β-1 and β-2 receptors and their relation to bone mass. Adrb2 receptor knock-out (KO) and Adrb1 receptor KO mice demonstrate a high and low bone mass phenotype, respectively, vs. wild type controls (67,82). Furthermore, reduced bone volume in β-less receptor mice (β-1,2,3 KO) is attributed to a marked reduction in cancellous BFR (83). Estrogen deficiency (OVX) further increased the significant reductions in metaphyseal bone volume and trabecular number in mice lacking β-adrenergic receptors as compared to controls. Finally, Adrb1 receptor deficient mice

demonstrated an inability to respond to mechanical loading, whereas Adrb2 receptor and wild-type littermates were found to respond normally (82).

Taken together, these data suggest that the higher bone mass phenotype in Adrb2 receptor KO mice may be caused by enhanced β-1 adrenergic receptor activity stimulating bone formation in the absence of the inhibitory effects of β-2 adrenergic receptors on osteoblasts. Therefore, defining the role that Adrb1 receptor stimulation during reduced mechanical loading has on disuse-sensitive cancellous bone is important to fully understanding underlying mechanisms responsible for bone loss with disuse.

CHAPTER III

SIMULATED RESISTANCE TRAINING DURING HINDLIMB UNLOADING ABOLISHES DISUSE BONE LOSS AND MAINTAINS MUSCLE STRENGTH*

Introduction

President George W. Bush announced his Exploration Vision for the National Aeronautics and Space Agency (NASA) in 2004, proposing lengthy stays at a Lunar outpost by 2020 and eventual expeditions to Mars thereafter (84). Mission success may ultimately depend on improvements in our ability to maintain astronaut health and functional capabilities during such lengthy trips. To date, current exercise countermeasures (cycle ergometer, treadmill, and resistance exercise device) (85) used by crew on the International Space Station (ISS) have not effectively mitigated losses of bone mineral density (BMD) or geometry (15), resulting in a significant increase in estimated fracture risk that remains even 1 year after returning to Earth (16). For those crew members experiencing the greatest bone loss, reductions in modeled proximal femur strength after a 6-month ISS mission approach the estimated lifetime loss in stance strength for Caucasian women (16,17). Furthermore, lack of recovery of BMD in ISS and MIR crew members has been documented 6 months post-flight (14), with indications that it may not be fully restored for 3 years (18). In addition to skeletal losses, reductions in ISS crew member skeletal muscle volume of the lower leg are

---

*Reprinted with permission from Swift JM, Nilsson MI, Hogan HA, Sumner LR, Bloomfield SA 2010 Simulated resistance training during hindlimb unloading abolishes disuse bone loss and maintains muscle strength. J Bone Miner Res **25**(3): 564-74.

coupled with significant decrements (nearly 30%) in plantarflexor muscle strength (85).

These changes in humans exposed to microgravity parallel alterations in bone and muscle mass observed during prolonged bedrest (53,54,86,87) and during the more severe losses incurred after spinal cord injury (SCI). Electrical stimulation has been utilized in patients with SCI to enable active contractions of the paralyzed lower limbs to perform aerobic (cycling) and resistive training. If this training is started months to years after the injury, acting on bone and muscle that is severely compromised by disuse, only marginal improvements in muscle strength and BMD in the paralyzed limbs are achieved (88-90). Far more successful is a strategy that starts early after the onset of paralysis; stimulated contractions of the plantarflexor muscles begun within 6 weeks of a SCI significantly mitigated the loss of muscle torque and contractile speed of the paralyzed lower leg, as well as the loss of cancellous bone in the distal tibia (91).

The rodent hindlimb unloading (HU) model is a well-established ground-based model for investigating disuse effects on bone and muscle (20). Hindlimb unloading results in significant reductions in disuse-sensitive cancellous bone mass, architecture and material properties, due to early increases in bone resorption followed by prolonged depressions in bone formation rate (BFR) (21-24). Additionally, skeletal muscle atrophy and reduced functional properties (i.e. strength) have been demonstrated as early as 4 days after HU begins and may remain depressed for some time upon reambulation (57,92,93). To date, no method has successfully prevented deficits in both muscle and bone during long duration unloading.

Resistance exercise that includes eccentric contractions provides an anabolic stimulus for both skeletal muscle and bone in both humans and rodent models (35-38), and has generally proven more effective in promoting increased bone and muscle mass than endurance exercise protocols such as running. Eccentric contractions (during muscle lengthening) generate larger muscle forces than do concentric contractions (muscle shortening), providing greater increases in BMD (36). Until the launching of improved training equipment late in 2008, ISS astronauts were unable to train at the high intensities (>70% maximum) demonstrated as osteogenic in land-based studies (94).

The purpose of the present investigation was to determine the effectiveness of high intensity simulated resistance training (SRT), achieved without weightbearing, in maintaining hindlimb muscle and bone (tibia) mass and strength during hindlimb unloading in skeletally mature rats. We sought to maximize the ability of high intensity exercise, begun early in the unloading period, to mitigate loss of both muscle and bone during unloading and so tested two separate contraction paradigms, an eccentric-based (HU+ECC) and a protocol combining both isometric and eccentric contractions (HU+ISO/ECC). We hypothesized that SRT would effectively attenuate disuse-induced bone and muscle loss and that doubling muscle contraction time with the addition of an isometric component would significantly enhance the effectiveness.

Materials and Methods

Animals and Experimental Design

Fifty male Sprague-Dawley rats were obtained from Harlan (Houston, TX) at 6 months of age and allowed to acclimate to their surroundings for 14 days prior to

initiation of the study. All animals were housed in a temperature-controlled (23 ± 2ºC) room with a 12-hour light-dark cycle in an American Association for Accreditation of Laboratory Animal Care-accredited animal care facility and were provided standard rodent chow (Harlan Teklad 8604) and water ad-libitum. Animal care and all experimental procedures described in this investigation were conducted in accordance with the Texas A&M University Laboratory Animal Care Committee rules.

Five experimental groups were studied: (1) cage control (CC, n=12), (2) hindlimb unloaded (HU, n=12), (3) HU animals exposed to similar duration of isoflurane anesthesia (Minrad Inc., Bethlehem, PA) as trained HU rats (ANHU, n=6), (4) HU subjected to eccentric muscle contraction training (HU+ECC, n=10), and (5) HU rats subjected to a combined isometric and eccentric hindlimb simulated resistive exercise (HU+ISO/ECC, n=10). Due to the labor-intensive nature of these experiments, it was necessary to perform experiments in two successive cohorts of animals. Rats in cohort I (CC, HU, and HU+ECC) and II (ANHU and HU+ISO/ECC) were randomly assigned to their respective groups by total vBMD at the proximal tibia metaphysis one day prior to study initiation. HU+ECC and HU+ISO/ECC animals underwent 14 sessions of simulated resistive exercise conducted every other day during the 28 day protocol, with each session consisting of 4 sets of 5 contractions. The HU and ANHU groups were similarly unloaded for 28 days, whereas the CC animals were allowed normal ambulatory cage activity; all animals were singly housed.

Hindlimb Unloading

Hindlimb unloading was achieved by tail suspension as previously described (77). Briefly, while the rat was under anesthesia, the tail was cleaned and dried thoroughly. A thin layer of adhesive (Amazing Goop, Eclectic Products, LA) was applied to the proximal half of the tail along the medial and lateral sides. A standard porous tape (Kendall, Mansfield, MA) harness was pressed firmly to the glue and allowed to dry (~30 min). A paper clip was used to attach the animal's tail harness to a swivel apparatus on the wire spanning the top of an 18" x 18" x 18" cage. The height of the animal's hindquarters was adjusted to prevent any contact of the hindlimbs with the cage floor, resulting in approximately a 30° head-down tilt. The forelimbs of the animal maintained contact with the cage bottom, allowing the rat full access to the entire cage.

Calcein injections (25 mg/kg body mass) were given subcutaneously 9 and 2 days prior to sacrifice to label mineralizing bone for histomorphometric analysis. HU animals were anesthetized before removal from tail suspension at the end of the study to prevent any weight bearing by the hindlimbs. At necropsy, left soleus, plantaris, and gastrocnemius muscles were excised and wet weights were recorded. Additionally, proximal left tibiae were removed, cleaned of soft tissue, and stored at -80°C in PBS soaked gauze for mechanical testing, whereas the distal portions of the left tibia were stored in 70% ethanol at 4°C for cortical histomorphometry of the TFJ (tibiofibular junction) region.

Muscle Contraction and Training Paradigms

Left plantarflexor muscles from animals in the HU+ECC and HU+ISO/ECC groups were trained every other day during 28-day HU using a custom-made rodent isokinetic dynamometer, as previously described (Fig 2A) (95). Animals were anesethetized with isoflurane gas (~2.5%) mixed with oxygen while remaining suspended, to prevent any weight bearing of the hindlimbs. Once unconscious, the lateral side of the rat's left leg was shaved and aseptically prepared. Each rat was then placed in right lateral recumbency on a platform, the left foot was secured onto the foot pedal, and the left knee was clamped so that the lower leg was perpendicular to the foot and the femur and tibia were at right angles to each other. This was referred to as the resting, 0° position. For isometric contractions, the foot pedal was held fixed in this position. For all contractions, the footplate was rotated in synchronization with muscle stimulation by a Cambridge Technology servomotor system (Model 6900) interfaced with a 80486 66-MHz PC using custom software written in TestPoint (v.4.0; Capital Equipment Corp., Billerica, MA). In either case, the torque generated around the footplate pivot (at the rat's ankle joint) was measured through the servomotor. Plantarflexor muscle stimulation was performed with fine wire electrodes consisting of insulated chromium nickel wire (Stablohm 800B, H-ML Size 003, California Fine Wire Co.), inserted intramuscularly straddling the sciatic nerve in the proximal thigh region. The stimulation wires were then attached to the output poles of a Grass Instruments stimulus isolation unit (Model SIU5; Astro-Med, Inc; W. Warwick, RI) interfaced with a

stimulator (S88; Astro-Med, Inc; W. Warwick, RI) which delivered current to the sciatic nerve and induced muscle contraction.

Eccentric-Based Simulated Resistive Exercise Training

An eccentric-based SRT protocol was utilized for training (HU+ECC). At the beginning of each session, the daily peak isometric torque (P_0) was determined. The foot was held fixed at 0° and successive stimulations were conducted at different voltages, with the frequency kept constant at 175 Hz (~4-6 contractions, 200ms duration, 45s rest between contractions). The voltage and magnitude of P_0 were recorded. This voltage was maintained for the eccentric contractions, and the stimulation frequency was varied until the torque matched P_0 (i.e., 100% peak isometric torque). This normally took 3-5 contractions, each at 200ms, with 45s of rest between contractions). A rest period of 2 minutes was given between the isometric and eccentric contraction optimization protocols. Upon completion of eccentric frequency optimization, the training program was initiated. Four sets of 5 repetitions (12 and 120 seconds of rest inserted between contractions and sets, respectively) were completed during each training session, which lasted approximately 25 minutes. Each eccentric contraction stimulus was 1000 ms long. During each plantarflexor muscle lengthening contraction, the footplate was rotated in dorsiflexion through a 40° arc (centered at the 0° position) (Fig 2B). After each contraction, the foot and pedal returned to the initial 0° resting position. Plantarflexor muscles fatigued by an average of 17.8% (maximum torque generated during the last set vs. the first set) during a typical training session.

Isometric Plus Eccentric Simulated Resistive Exercise Training

The ability of a longer duration contraction with isometric and eccentric components (both at 100% P_0) to maintain musculoskeletal health during unloading was also tested (HU+ISO/ECC). Voltage optimization of the peak isometric torque and frequency optimization of the eccentric torque were performed at the beginning of each session, as described in the previous paragraph. The total number sets, repetitions, and training sessions were identical to those of the HU+ECC group. In this case, however, the training protocol consisted of a 1000ms isometric contraction (175 Hz; 0°), immediately followed by a 1000ms eccentric contraction the same as those used for the eccentric contractions in experiment 1 (Fig 2C). By the end of a typical training session, plantarflexor muscles fatigued by an average of 34.2% and 39.8% for isometric and eccentric contractions, respectively. These reductions in torque are similar to previous investigations utilizing 2-second muscle stimulation contractions (95).

Muscle Function Testing

Functional assessments of the left leg plantarflexor muscles were completed on days 0 and 28 on animals in the ANHU, HU+ECC, and HU+ISO/ECC groups using the same isokinetic dynamometer (93) used for the SRT protocols. The anesthesia used, preparation of the animal, and electrodes' placements were identical to those used during training. Briefly, stimulation voltage was optimized using 0.1-ms pulses at 300 Hz to yield the peak isometric torque during a trial of 4-6 tetanic contractions. Peak torque produced about the ankle was recorded using custom software written in TestPoint.

A.

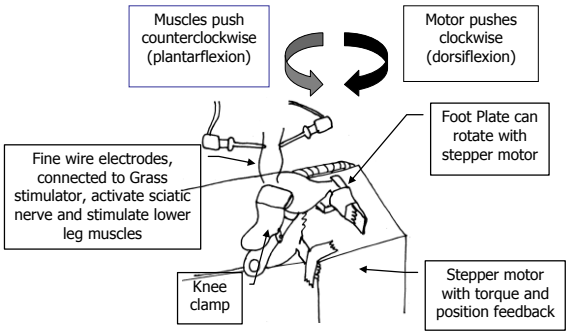

B.

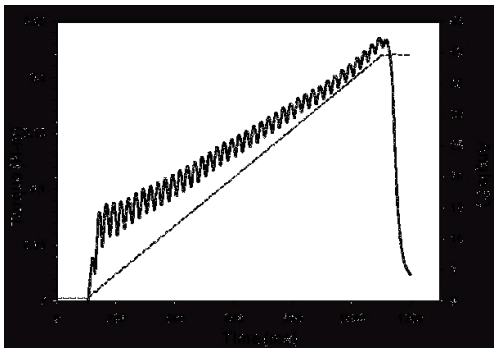

C.

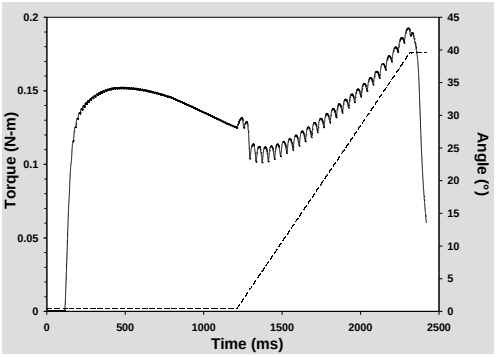

Fig. 2. Simulated resistive exercise apparatus used for muscle contractions (A) and sample torque/angle vs. time graphs during 28-day hindlimb unloading (B – HU+ECC; C – HU+ISO/ECC). Arrows illustrate movement of the footplatre for eccentric contractions; footplate held steady for isometric contractions (A). Electrodes run from Grass Instruments (S88) stimulator; Cambridge servomotor (Model 6900) quantitates torque around the ankle and determines eccentric/isometric nature of contractions. Dotted line on the graphs (B and C) represents change in foot-pedal and ankle angle during contraction; solid line represents muscle torque output.

Peripheral Quantitative Computed Tomography Scans

On days -1 and 28 of the study, tomographic scans were performed in vivo at the proximal and mid-diaphysis of the left tibia with a Stratec XCT Research-M device (Norland Corp., Fort Atkinson, WI), using a voxel size of 100 μm and a scanning beam thickness of 500 μm. Daily calibration of this machine was performed with a hydroxyapatitie standard cone phantom. Transverse images of the left tibia were taken at 5.0, 5.5, and 6.0 mm from the proximal tibia plateau, as well as one slice at the midshaft (50% of the total tibia length). A standardized analysis for either metaphyseal bone (contour mode 3, peel mode 2, outer threshold of 0.214 g/cm^3, inner threshold of 0.605 g/cm^3) or diaphyseal bone (separation 1, threshold of 0.605 g/cm^3) was applied to each section.

Values of total and cancellous volumetric bone mineral density (vBMD), total bone mineral content (BMC), total bone area, and marrow area were averaged across the 3 metaphyseal slices for each outcome variable. For each mid-diaphyseal slice, the outcome variables were cortical vBMD, BMC, cortical bone area, and the polar cross-sectional moment of inertia (CSMI). Machine precision (based on manufacturer's data) is ±3 mg/cm^3 for cancellous vBMD and ±9 mg/cm^3 for cortical vBMD. Coefficients of variation were ± 1.24, 2.13, and 1.95% for in vivo proximal tibia total vBMD, cancellous vBMD, and total area, respectively, as determined from repeat scans on adult male rats.

Histomorphometry Analysis

Undemineralized distal left tibia were subjected to serial dehydration and embedded in methylmethacrylate (Sigma-Aldrich M5, 590-9). Serial cross-sections (150-200 μm) of mid-shaft cortical bone were cut starting 2.5 mm proximal to the tibial-fibular junction with an Isomet diamond wafer low-speed saw (Buehler, Lake Bluff, IL). Sections were hand ground to reduce thickness (<80 μm) before mounting on glass slides. The histomorphometric analyses were performed using the OsteoMeasure Analysis System, Version 1.3 (OsteoMetrics, Atlanta, GA). Measures of labeled surfaces and interlabel widths were obtained at 100x magnification of up to 3 slides per animal. Periosteal and endocortical mineral apposition rates (MAR, μm/d) were calculated by dividing the average interlabel width by the time between labels (7 days), and mineralizing surface (MS) for both periosteal and endocortical bone surfaces was calculated using the formula %MS/BS = {[(single labeled surface/2) + double labeled surface]/surface perimeter} X 100. Bone formation rate (BFR) was calculated as (MAR x %MS/BS).

Biomechanical Testing

Proximal tibiae from animals in the CC, HU, and HU+ECC groups were tested for changes in cancellous bone material properties using reduced platen compression (RPC) test as previously described (96). Briefly, a 2-mm thick cross-section was cut from the proximal tibia just distal to the primary spongiosa of the metaphysis. Each specimen thus consists of a central core of cancellous bone encompassed by the

surrounding cortical shell. Contact radiographs were made of each specimen to determine the appropriate size for the loading platens such that the platens contact only the cancellous bone and not the cortical shell. Quasi-static loading was applied at 2.54 mm/min to compress the specimen until failure occurred using an Instron 1125 load frame (Norwood, MA). Load and displacement were recorded digitally in real time at 10Hz. Load-displacement data were analyzed to determine the stiffness (slope of linear loading portion) and the ultimate load (maximum force during test). Cancellous bone material properties (elastic modulus, EM; and ultimate stress, US) were estimated assuming uni-axial compression of the cancellous bone material only, that is, assuming an "effective" specimen with a height equal to the specimen thickness and a cross-sectional area equivalent to that of the platen surface area. The equations used are: EM = (stiffness x specimen thickness) / platen surface area, and US = ultimate load/platen surface area.

Whole left tibiae were tested in three-point bending to assess cortical bone structural and material properties at the mid-diaphyseal pQCT sampling site (50% of total bone length). Thawed tibia from animals in the ANHU and HU+ISO/ECC groups were placed lateral side down on custom-built metal pin supports having a span of 18mm. The loading pin was centered above the lower supports and contacted the medial surface at the midpoint of the specimen (mid-diaphysis). Quasi-static loading was applied at 2.54 mm/min through the loading pin until fracture occurred. Load and displacement were recorded at 10 Hz. Load-displacement curves were analyzed to determine the structural variables of ultimate force (UF) and stiffness (S), the latter of

which was defined to be the slope of the elastic linear portion of the loading curve. The yield point was defined to be the intersection of the load-displacement curve with a line having a slope 90% of the stiffness. The corresponding load value was the yield force (YF). Material properties were estimated by normalizing structural properties for the bone geometry using the bending cross-sectional moment of inertia (bCSMI; from pQCT), bone diameter (D; measured by calipers), and the support span distance (L=18mm). The cross-sectional moment of inertia for bending, bCSMI, was estimated as half of the polar CSMI. Standard beam theory was applied to estimate the material properties of elastic modulus (EM) and ultimate stress (US) as follows: $EM = (S \times L^3) / (48 \times bCSMI \times 1000)$; $US = [UF \times L \times (D/2)] / (4 \times bCSMI)$.

Statistical Analyses

All data were expressed as means ± SEM and evaluated using the statistical package SPSS (v.15; Chicago, Ill). In vivo pQCT and body mass delta scores and muscle mass at sacrifice were first analyzed using a two-factor ANOVA to compare group differences between HU, ANHU, HU+ECC, and HU+ISO/ECC. A Tukey's post-hoc test was used for pair-wise comparisons. Subsequently, a one-factor ANOVA was used to compare individual group change scores vs. that of the comparator cage control (CC) group (Tukey's post-hoc test for pairwise comparisons), and paired t-tests to determine (using absolute date values pre-post within group) whether that change score represented a significant change from Day 0. Comparisons of mechanical properties of cancellous bone, cortical bone histomorphometric variables, and delta scores for muscle

peak torque values were tested using a one-factor ANOVA, with a Tukey's post-hoc test for pairwise comparisons. Paired t-tests were used on absolute values of muscle peak torque pre- and post-values to determine if the change score represented a significant change from Day 0. Cortical bone mechanical properties in HU+ISO/ECC and ANHU animals were compared with unpaired t-tests. For all data, statistical significance was accepted at $p<0.05$.

Results

Two animals from the HU+ECC group and one from the HU+ISO/ECC group died from complications due to isoflurane aministration. No other animals suffered any deleterious effects of either HU or anesthesia during the study that led to their removal.

Simulated resistance training attenuates muscle mass and strength losses during disuse. HU alone resulted in no change in body mass, whereas all 3 HU groups receiving anesthesia did exhibit some loss in body mass (-5.5 to -7.8%) by 28 days (Table 1). Simulated resistance training paradigms did not attenuate HU-induced losses in body mass. Unloading resulted in significantly lower left plantarflexor muscle masses as compared to CC rats, and this reduction was partially attenuated by both exercise paradigms (Table 1). Additionally, when normalized to body mass, total plantarflexor muscle mass of the trained left leg in both SRT groups was significantly higher than both HU and ANHU groups ($p<0.05$).

Table 1. Effects of hindlimb unloading (HU) and high intensity muscle contractions on whole-body and left plantarflexor muscle masses.

	CC	HU	HU+ALEN	HU+SRT	HU+SRT/ALEN
Body Mass (g)					
Day 0	454.58 ± 6.56	447.73 ± 15.89	438.31 ± 6.39	442.42 ± 7.78	436.36 ± 6.09
Day 28	478.75 ± 8.50*	412.00 ± 13.35*	414.15 ± 9.58*	409.08 ± 8.28*	389.36 ± 8.04*
Body Mass Change (g)	24.17 ± 3.08*	35.73 ± 5.25^{ab}†	(-24.15 ± 5.81^{a}†)	(-33.33 ± 4.65^{a}†)	(-47.00 ± 5.24^{b}†)
%-Change	*(5.32%)*	*(-7.98%)*	*(-5.50%)*	*(-7.53%)*	*(-10.77%)*
Ankle Plantarflexor Masses (g)					
Gastrocnemius	2.312 ± 0.135	1.732 ± 0.035†	1.845 ± 0.057†	1.607 ± 0.058†	1.663 ± 0.044†
Plantaris	0.513 ± 0.009	0.392 ± 0.010†	0.401 ± 0.011†	0.374 ± 0.015†	0.359 ± 0.010†
Soleus	0.199 ± 0.006	0.088 ± 0.004^{a}†	0.107 ± 0.007^{b}†	0.096 ± 0.004^{ab}†	0.101 ± 0.004^{b}†
Total Mass	3.025 ± 0.128	2.212 ± 0.039†	2.353 ± 0.068†	2.072 ± 0.064†	2.100 ± 0.051†
Relative Total Mass/BW (mg/g)	*6.347 ± 0.297*	*5.41 ± 0.165*^{a}†	*5.682 ± 0.290*^{a}†	*4.662 ± 0.421*^{b}†	*4.922 ± 0.465*^{ab}†

Values are group mean ± standard error of the mean. Those HU groups not sharing the same letter for each variable are significantly different from each other ($p<0.05$); comparisons with CC (by t-test): †Significantly different vs. CC ($p<0.05$); $^{*}p<0.05$ vs. pre value.

Eccentric (HU+ECC) and combined eccentric+isometric-based (HU+ECC/ISO) hindlimb muscle contractions successfully prevented any loss in P_0 (Fig 3). Additionally, the 14 sessions of anesthesia exposure combined with 28 days of mechanical unloading (ANHU) resulted in a significant 10.2% reduction in peak isometric torque.

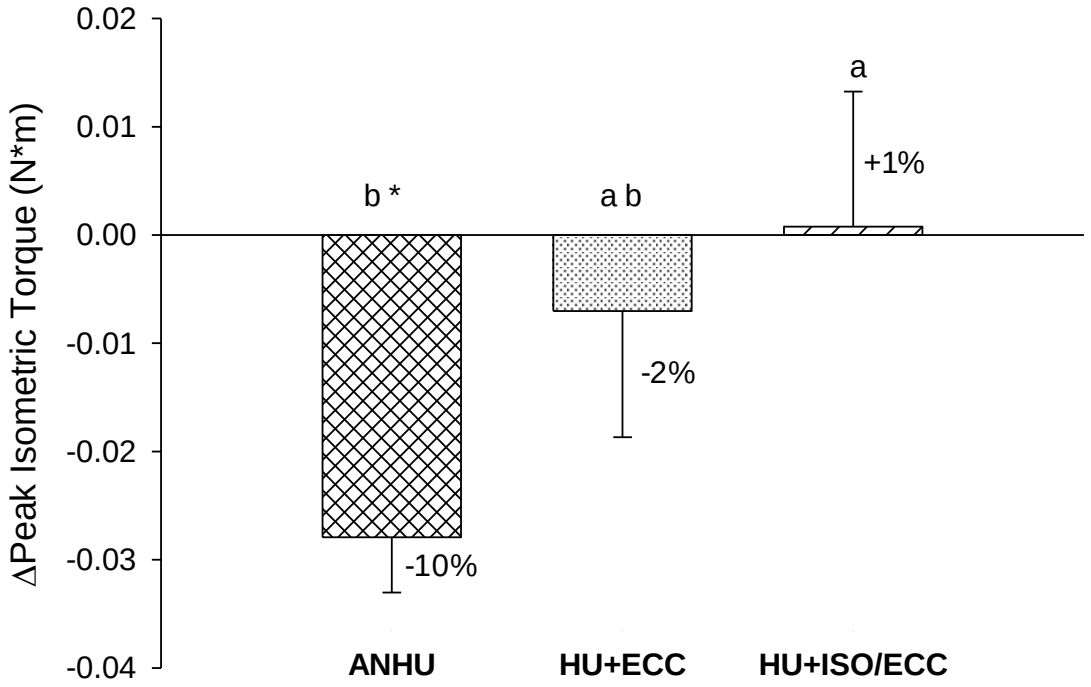

Fig. 3. Effects of hindlimb unloading and high intensity muscle contractions on in vivo measurement of peak isometric torque of the ankle plantarflexor muscles. Values are change in group mean ± standard error of the mean. Those groups not sharing the same letter for each variable are significantly different from each other ($p<0.05$). *Significantly different for Post vs. Pre value ($p<0.05$).

Simulated resistance training not only mitigates loss of bone mass but stimulates gain during disuse. Hindlimb unloading resulted in reduced total BMC (-11%) and total bone area (-8%) at the PTM (Fig 4B-C); most of this bone loss appears to occur in the cancellous compartment, as cancellous vBMD declined by 14% (Fig 4D). SRT during HU not only prevented the loss of total metaphyseal vBMD (Fig 4A) but resulted in significantly increased total vBMD (+12-13% post vs. pre values; both SRT groups) and total BMC (+17% post vs. pre; ISO/ECC group) at this disuse-sensitive site. In

addition, both SRT paradigms led to a complete maintenance of cancellous bone during unloading. HU+ECC rats experienced significantly greater reductions in marrow area as compared to HU rats (Fig 4E), possibly resulting from endocortical formation.

Similar to the effects at the PTM, both SRT protocols increased bone mass at the midshaft tibia after 28 days (Fig 5). Although no significant changes were noted in cortical vBMD with either hindlimb unloading or SRT (Fig 5A), cortical BMC increased by 15 and 11% in HU+ECC and HU+ISO/ECC rats, respectively, surpassing the 7% gain observed in CC rats (Fig 5B). For structural and geometric properties, unloading resulted in a suppression of growth-related increases (Fig 5C-D; HU and ANHU groups), but the beneficial effect of both SRT protocols was again strongly evident. Bone area increased by 14 and 10% in the HU+ECC and HU+ISO/ECC groups, respectively (Fig 5C), and the change in polar CSMI was significantly greater in the HU+ECC group as compared to non-exercised unloaded animals (Fig 5D).

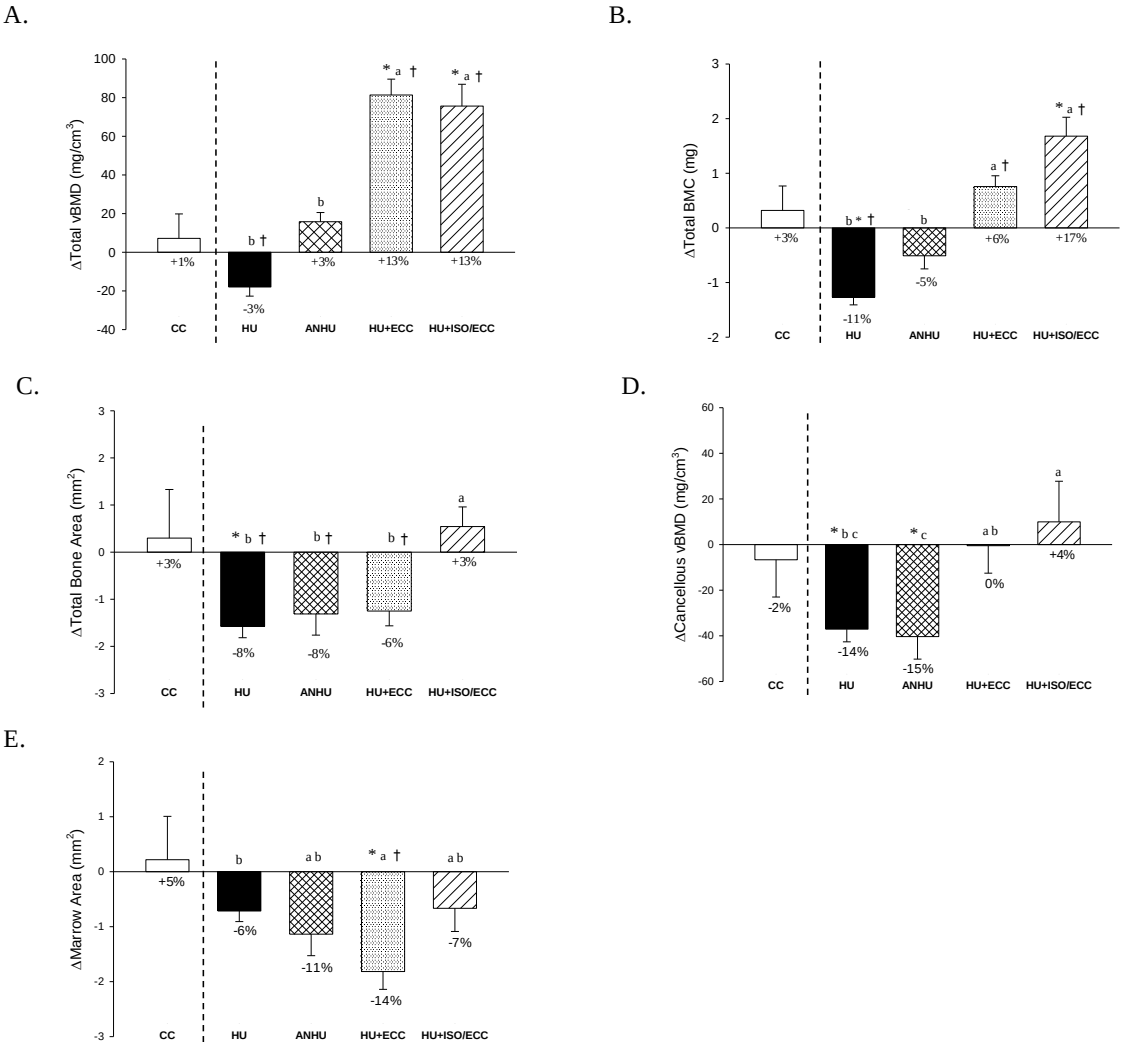

Fig. 4. Effects of hindlimb unloading and high intensity muscle contractions on changes in structural and geometric properties of the proximal tibia metaphysis as taken by in vivo peripheral quantitative computed tomography scans. *A*: Total volumetric bone mineral density (vBMD). *B*: Total bone mineral content (BMC). *C*: Total bone area. *D*: Cancellous volumetric bone mineral density (vBMD). *E*: Marrow area. Vertical dashed line indicates separation of CC from the experimental groups for preliminary ANOVA. Those HU groups not sharing the same letter for each variable are significantly different from each other ($p<0.05$); comparisons with CC (by t-test): †Significantly different vs. CC ($p<0.05$); $^{*}p<0.05$ vs. pre value.

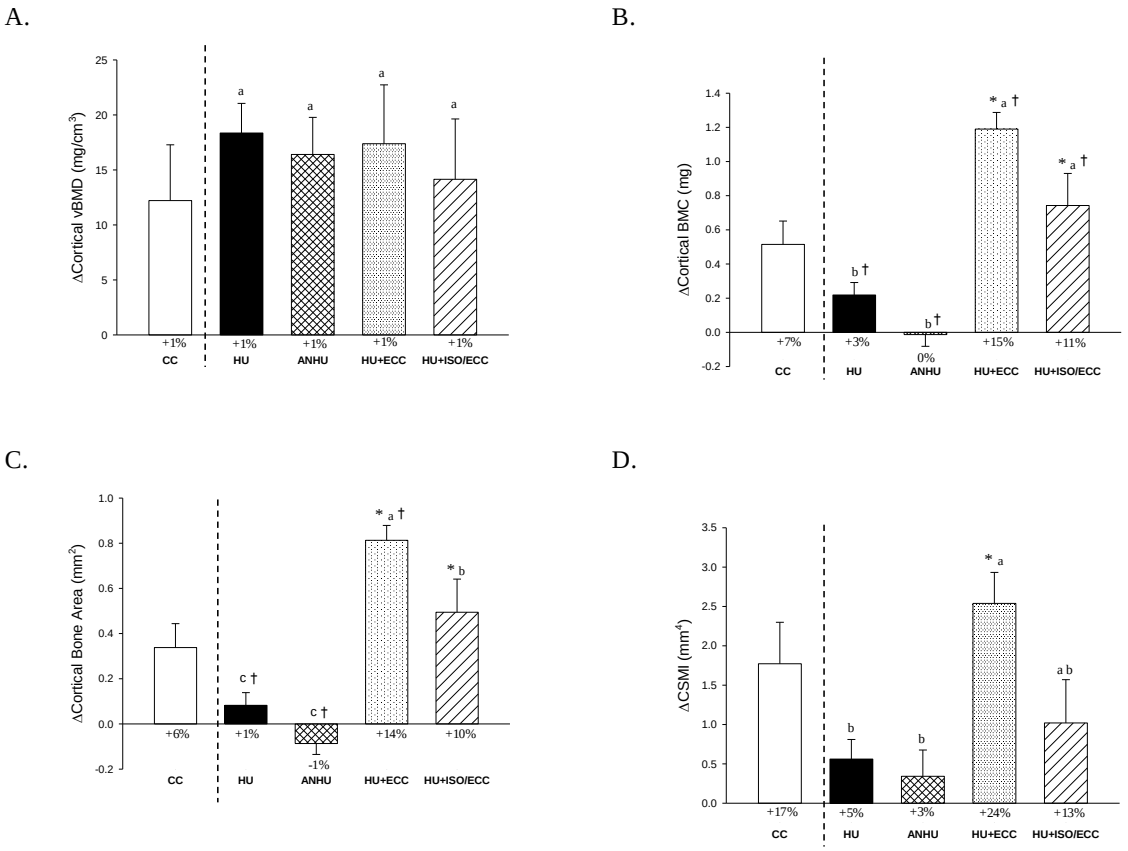

Fig. 5. Effects of hindlimb unloading and high intensity muscle contractions on changes in structural and geometric properties of the tibial mid-diaphysis as taken by in vivo peripheral quantitative computed tomography scans. *A*: Cortical volumetric bone mineral density (vBMD). *B*: Cortical bone mineral content (BMC). *C*: Cortical bone area. *D*: Polar cross-sectional moment of inertia (CSMI). Vertical dashed line indicates separation of CC from the experimental groups for preliminary ANOVA. Those HU groups not sharing the same letter for each variable are significantly different from each other ($p<0.05$); comparisons with CC (by t-test): †Significantly different vs. CC ($p<0.05$); $^{*}p<0.05$ vs. pre value.

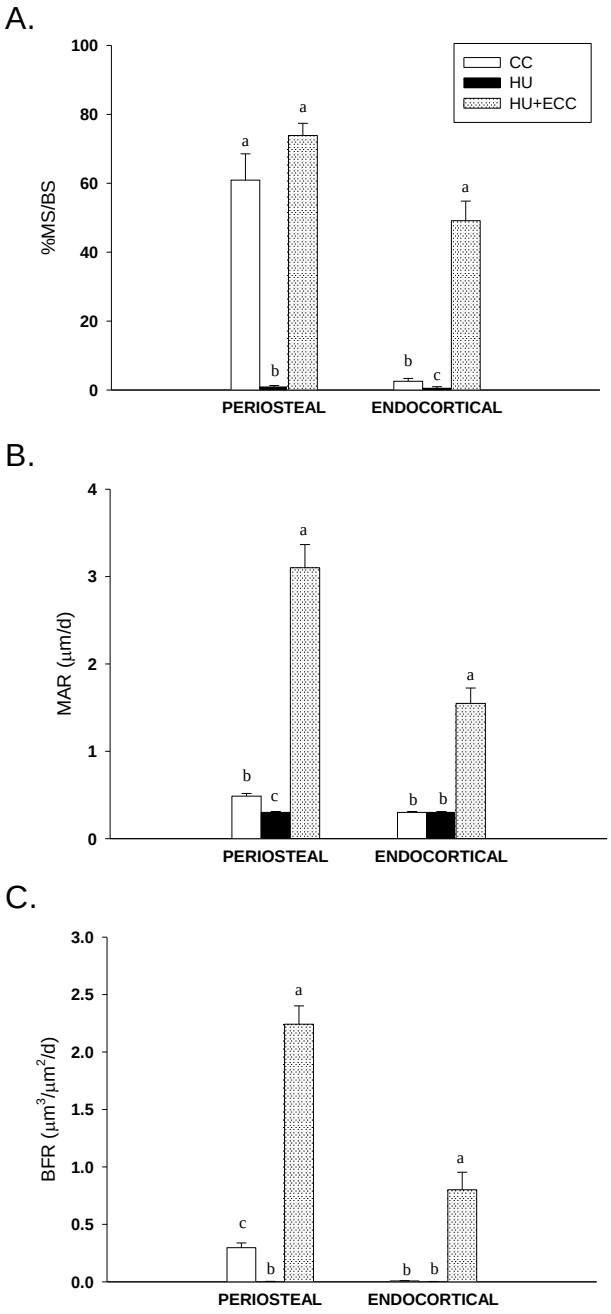

Fig. 6. Effects of hindlimb unloading and high intensity eccentric muscle contractions on periosteal and endocortical surface dynamic histomorphometry analyses measured at the tibia diaphysis. *A*: Mineralizing Surface (%MS/BS). *B*: Mineral Apposition Rate (MAR). *C*: Bone Formation Rate (BFR). Those groups not sharing the same letter for respective surface measures are significantly different from each other ($p<0.001$).

Simulated resistance exercise increases bone formation on cortical surfaces.

Hindlimb unloading virtually abolished periosteal %MS/BS, MAR, and BFR (Fig 6 A-C). These results are all endpoint values (day 28 only), and the differences between the HU and CC groups are -99%, -38%, and -99% for %MS/BS, MAR, and BFR, respectively. SRT effectively abolished the deficit in %MS/BS observed in hindlimb unloaded animals and stimulated a dramatic increase in periosteal MAR and BFR , with values 5- and 6-fold greater, respectively, than those observed in CC rats. There was little evidence of bone formation activity on endocortical surfaces in ambulatory CC and HU rats, whereas HU animals subjected to SRT exhibited much higher values for %MS/BS, MAR and BFR. Few fluorochrome labels were present on either surface in HU rats (Fig 7B).

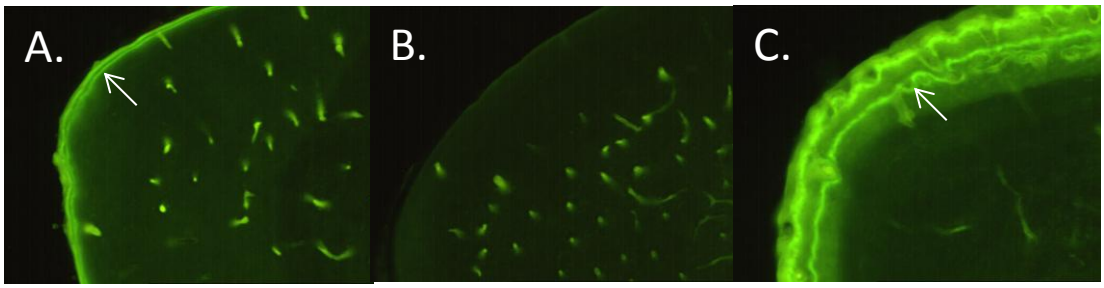

Fig. 7. Visual depiction (100x) of calcein labeling on the periosteal surface of cortical bone at the tibia diaphysis. *A*: CC *B*: HU *C*: HU+ECC. Note the extensive flurochrome labeling (arrows) in CC and HU+ECC and large interlabel width (HU+ECC).

Muscle contractions improve cancellous but not cortical bone material properties.

Reduced platen compression (RPC) testing was used determine the effects of HU and the

eccentric-based SRT protocol on material properties of cancellous bone. Eccentric-based exercise during HU resulted in significantly higher estimated values for both the elastic modulus and ultimate stress values (Table 2). The elastic modulus of the HU+ECC animals was 3.1 and 4.6-fold higher than values in CC and HU rats, respectively. The ultimate stress of the HU+ECC animals was 2.6 times higher than in CC rats and 4.6 times higher than in HU animals. Although HU rats exhibited lower elastic modulus and ultimate stress values (by 33% and 4%, respectively), as compared to ambulatory aging controls, these differences were not statistically significant.

The effects of eccentric-based muscle contractions on changes in mechanical properties of left tibia cortical bone with unloading yielded no significant effects of a combined isometric and eccentric muscle stimulation protocol during 28-day hindlimb unloading (data not shown). Extrinsic (maximal force, yield force, and stiffness) and intrinsic (elastic modulus, ultimate stress, and yield stress) mechanical properties of cortical bone were not significantly different in ANHU compared to HU+ISO/ECC groups.

Table 2. Effects of hindlimb unloading and high intensity muscle contractions on mechanical properties of cancellous bone at the proximal tibia metaphysis.

	CC	HU	HU+ECC
Elastic Modulus (MPa)	21.0 ± 7.7^{b}	14.1 ± 3.4^{b}	65.5 ± 19.2^{a}
Ultimate Stress (MPa)	0.9 ± 0.2^{b}	0.5 ± 0.1^{b}	2.3 ± 0.5^{a}

Values are group mean ± standard error of the mean. Those HU groups not sharing the same letter for each variable are significantly different from each other ($p<0.05$); group comparisons made with ANOVA.

Discussion

Our main objective was to determine if high intensity simulated resistance training during hindlimb unloading would effectively mitigate disuse associated losses in musculoskeletal mass and strength. We hypothesized that the in vivo exercise paradigms tested would lessen any HU-associated losses in both tibial bone and plantarflexor muscles and that doubling the contraction time would further increase this response.

Most significantly, our data demonstrate that, if an isometric component is added to eccentric muscle contractions, bone loss is not only attenuated but an absolute increase in total and cancellous vBMD at the disuse-sensitive proximal tibia metaphysis results. Additionally, we demonstrate large gains in mid-shaft cortical bone area and BMC with SRT, both of which were suppressed in HU animals (Fig 5B-C). The increased bone mass at the tibial mid-diaphysis resulted from strikingly higher cortical bone formation on the periosteal surface and activation of endocortical formation in eccentrically trained animals that was virtually absent in ambulatory controls and hindlimb unloaded rats. The HU+ECC and HU+ECC/ISO simulated resistive exercise paradigms successfully preserved in vivo muscle isometric strength (post vs. pre), whereas unloaded animals experienced a 10% reduction in strength. The SRT protocols also mitigated unloading-associated losses in muscle mass. Thus, our data suggest that a low volume of high intensity muscle contractions, with isometric and eccentric components, can effectively maintain musculoskeletal mass and strength during 28 days of hindlimb unloading.

Lower leg disuse in rodents leads to significant hindlimb muscle atrophy in as little as 4 days (97,98). Previous studies have shown that maximal voluntary isometric exercise during HU effectively maintains soleus mass and strength (99), but muscle stimulation is unable to diminish reductions in medial gastrocnemius mass or protein content (100). Additionally, more physiological contractions (combined isometric + concentric + eccentric) during unloading were able to maintain muscle mass and myofibril protein content (95). None of these previous studies tested changes in unloaded muscle beyond 14 days of unloading, and few examine outcomes for a functional muscle group (as opposed to the disuse-sensitive soleus muscle). Our investigation sought to prevent unloading-induced changes in plantarflexor muscle mass and strength over a much longer duration and provides the first report of longitudinal in vivo measures of muscle strength (in rodents). Both resistive exercise protocols used in the present study mitigated losses in gastrocnemius and soleus mass, as well as total and relative plantarflexor masses (Table 1). Importantly, isometric strength of these muscles was maintained at pre-HU levels, whereas hindlimb unloading without intervention significantly reduced muscle strength by more than 10% (Fig 3).

Previous investigations have sought to define the osteogenic effect of mechanical loading during periods of disuse. Rubin et al. (55),employing low-magnitude, high-frequency loads, found that 10min/d of loading was effective at maintaining metaphyseal bone volume (BV/TV) and did attenuate losses in bone formation at the proximal tibia. More recent studies have utilized electrical stimulation as a countermeasure to disuse-induced bone loss. Transcutaneous stimulation of the thigh, producing peak strains of

~200με, did not effectively prevent disuse osteopenia in hindlimb unloaded rodents, but did reduce tibial bone loss (56). Lam and Qin (58) recently demonstrated the beneficial effects of high frequency electrical stimulation of the leg musculature on bone during disuse. Although this treatment did effectively mitigate losses of cancellous bone volume in the unloaded distal femur, there was no demonstrable effect on bone formation. Their model stimulates muscle contraction in an unrestrained leg, generating relatively small muscle forces and presumably low strain levels on the associated bone. By contrast, our simulated resistive exercise protocols provide a more physiological loading of muscle with quantifiable torque production at the restrained ankle. The loading stimulus can be manipulated to any desired intensity, even exceeding 100% peak isometric torque during eccentric contractions, and can generate concentric, eccentric or isometric contractions.

Significant increases in periosteal bone formation rate in the HU+ECC group (Fig 6C) contributed to absolute gains in cortical bone mass as compared to controls, more than reversing the losses observed in HU animals (Fig 5). Periosteal bone formation at mid-shaft tibia was approximately 7-fold higher in HU+ECC rats than in CC animals, which was largely attributable to a 5-fold higher mineral apposition rate.

Both of our resistive exercise paradigms effectively mitigated bone loss in unloaded hindlimbs and actually led to gains in cortical bone mass (Fig 5), while maintaining disuse-sensitive cancellous bone at the proximal tibia (Fig 4D). Combined isometric and eccentric contractions resulted in a 5% increase in cancellous vBMD over 28 days, whereas untreated HU animals exhibited 14-15% reductions. Those animals

treated with only eccentric-based contractions effectively maintained cancellous vBMD during the period of disuse. Importantly, this cancellous bone compartment exhibited dramatic increases in material properties, with ultimate stress and elastic modulus values approximately 4-fold higher in HU+ECC vs. unloaded animals (Table 2). Discrepancies in effects on cancellous vBMD versus changes in mechanical properties are not uncommon because bone density, volume, and mass can sometimes be imperfect measures of bone condition, particularly for cancellous bone. Other prominent factors contributing to mechanical performance include the cancellous architecture and the quality of the solid bone tissue, with the latter encompassing mineral and organic matrix compositional and ultrastructural features. Changes in these bone quality-related variables sometimes gives rise to a disassociation between density or volume and bone strength. An example of this effect was reported by Allen et al. (101) describing changes in mechanical properties of cancellous bone with raloxifene treatment. The treated and control groups had essentially the same BV/TV, yet material properties were substantially higher in the treated group (ultimate stress 130% higher, elastic modulus 89% higher). Accordingly, our results suggest that the exercise protocol may very well have induced positive adaptations in the organic matrix of the cancellous bone and/or enhancements in cancellous bone microarchitecture. To our knowledge, these are the first exercise paradigms utilized during disuse that effectively produce absolute gains in cancellous bone mass and/or in cancellous bone material properties.

The simulated resistance training protocols tested were successful in achieving, at minimum, maintenance of cortical and cancellous bone mass and attenuation of

muscle mass and strength losses associated with hindlimb unloading. However, the degree to which each regimen achieved these was not equal. Both exercise regimens significantly increased cortical BMC and bone area, yet only in the HU+ECC animals did the gain in area result in a significant increase in polar cross-sectional moment of inertia. When an isometric component was added to the eccentric contraction, greater benefits to disuse-sensitive cancellous bone occurred. Although both SRT groups experienced equivalent increases in total vBMD at the proximal tibia, only the HU+ISO/ECC protocol significantly increased total BMC and mitigated reductions in bone area. In sum, these data suggest a bone compartment-specific response to the different contraction paradigms. Training using eccentric-only contractions had the greater effect on the mid-diaphysis cortical bone shell, whereas a combined eccentric+isometric training paradigm resulted in greater effects in cancellous bone, as measured by in vivo pQCT scans. Additionally, both exercise protocols were successful in preventing hindlimb unloading-associated losses in muscle strength and mitigating loss of muscle mass.

The effectiveness of our simulated resistance training protocols in maintaining plantarflexor muscle strength and increasing bone mass during disuse may offer some important insight regarding the efficacy of exercise interventions for human subjects exposed to prolonged bed rest. Only a few long-term bed rest investigations have successfully mitigated bone loss with exercise paradigms. Combined supine flywheel resistive and treadmill exercise during 90-day bed rest in young men attenuates reductions in trochanter and hip BMD (53). Treadmill exercise combined with lower-

body negative pressure effectively maintains total hip and femoral shaft BMD (87) and lumbar spine muscle strength (86). Vigorous resistance training during 17-week bed rest increased lumbar spine and diminished reductions in total hip BMD, as well as attenuated losses of leg muscle masses and strength compared with bed rest controls (54). These data mirror the findings of our rodent protocol, with the exception that our exercised animals experienced absolute gains in bone mass and not merely mitigation of losses. Our present study, using invasive measures feasible only in an animal model, illustrates the efficacy of a high intensity resistive exercise intervention in maintaining musculoskeletal mass and strength during long duration disuse. Our results suggest that, should newer exercise equipment now being installed in the ISS more effectively provide for higher intensity resistance training, the currently intractable problem of bone loss during prolonged missions may be partially solved.

There were several limitations to the current investigation. This study utilized two separate cohorts of animals, which were not equally and randomly assigned to all representative groups. To most fairly represent the data across these two cohorts, we normalized all longitudinal data (in vivo pQCT and muscle strength) by expressing them as change values. Additionally, lacking detailed histomorphometric measures at the proximal tibia metaphysis, we cannot verify tissue-level mechanisms (increased formation and/or decreased resorption) for the gains in cancellous vBMD and in material properties in this bone compartment observed with our exercise interventions.

In summary, our data demonstrate that high intensity simulated resistance training during unloading leads to absolute increases in disuse-sensitive cancellous bone

mass and material properties, while maintaining muscle strength. The exercise paradigms used in this investigation during disuse also stimulated increases in midshaft BMC and bone area, which gains were found to be attributed to dramatic increases in periosteal bone formation. These data provide the first direct evidence that high-intensity, eccentric-based resistive exercise, begun early during the period of unloading, can prevent the loss of bone mass and muscle strength routinely observed during a period of disuse or exposure to microgravity.

CHAPTER IV

CANCELLOUS BONE RESPONSE TO SIMULATED RESISTANCE TRAINING IS BLUNTED BY CONCOMITANT ALENDRONATE TREATMENT DURING DISUSE

Introduction

Significant bone loss remains a persistent problem for humans exposed to microgravity, with little evidence of consistent recovery upon return to Earth. Recently, Lang and colleagues (15) have demonstrated significant reductions in bone mineral density (BMD) and geometry in astronauts aboard the International Space Station (4-6 month missions), which losses result in increased estimated fracture risk up to 1 year after returning to Earth (16,17). Additionally, lack of recovery of BMD in ISS and MIR crew members has been documented 6 months post-flight (14), with indications that it may not be fully restored for 3 years (18). The ability of current resistance exercise countermeasures installed on ISS (iRED, interim resistance exercise device; and aRED advanced resistance exercise device) to mitigate reductions in lower leg bone mass and strength has yet to be validated (85). Furthermore, if these exercise devices are unable to provide sufficient mechanical loading and a crew member fracture did occur in microgravity, it would be debilitating and may compromise mission objectives, particularly if crews are to be working on the lunar or Martian surface as currently planned in the National Aeronautics and Space Administration's (NASA) "Vision for Space Exploration" (102).

The rodent hindlimb unloading (HU) model is a well-established ground-based model for investigating disuse effects on bone and muscle (20). Hindlimb unloading results in significant reductions in disuse-sensitive cancellous bone mass, architecture and material properties, due to early increases in bone resorption followed by prolonged depressions in bone formation rate (BFR) (21,103-105). These reductions in metaphyseal bone mass are associated with increased osteocyte and osteoblast apoptosis. Recent data demonstrate a striking 66% increase in apoptotic osteocytes at the proximal tibia with 14 days of HU and increased cancellous and cortical osteocyte apoptosis in unweighted tibiae by day 3 of HU (106,107). Reducing osteocyte apoptosis within the metaphyseal region of hindlimb bone during unloading may be crucial to preserving cancellous bone mass and reducing bone resorption.

Previously, our lab has demonstrated the significant positive effects of high intensity muscle contractions, produced during rodent simulated resistance training (SRT), on unweighted tibia bone. SRT, completed every other day, results in absolute increases in disuse-sensitive cancellous bone mass and material properties, while maintaining muscle strength (105). Furthermore, significant gains in mid-diaphyseal tibia cortical bone mineral density were associated with a 5-fold greater periosteal bone formation rate (BFR) as compared to control animals. However, we have not yet identified the cellular mechanisms by which our SRT protocol inhibits unloading-induced reductions in cancellous bone mineral density (BMD).

The inability of current exercise hardware to prevent microgravity-induced losses in skeletal tissue may be inconsequential if the use of pharmacological agents in-flight

proves to be a more effective and less time-intensive countermeasure. Alendronate (ALEN), an anti-resorptive agent, has been approved by NASA for in-flight experiments (108). Alendronate is a nitrogen-containing bisphosphonate that inhibits bone resorption by adsorbing to bone mineral; it interferes with osteoclast activity by inhibiting enzymes of the mevalonate pathway, and ultimately contributes to osteoclast apoptosis (109). Additionally, ALEN is currently in use for treatment of various disorders characterized by increased osteoclast-mediated bone resorption, and is a proven agent in minimizing bone loss due to estrogen deficiency and disuse in rats (65,66,110,111). Combining anti-resorptive therapy with the muscle-anabolic effects of resistance exercise might prove to be an effective approach for protecting both bone and skeletal muscle during bed rest and spaceflight.

The aim of this current investigation was to determine whether combining the anabolic effects of SRT with the anti-resorptive effects of ALEN during 28 days of HU positively impacts cancellous bone. Furthermore, we sought to define the effects of our SRT protocol and ALEN on the prevalence of cancellous osteocyte apoptosis. We hypothesized that administering ALEN in rats also subjected to SRT during HU will better prevent or ameliorate deleterious changes in cancellous bone than will ALEN or SRT administration alone and that this effect may be due to both treatments' ability to mitigate disuse associated increases in prevalence of apoptotic osteocytes.

Materials and Methods

Animals and Experimental Design

Sixty male Sprague-Dawley rats were obtained from Harlan (Houston, TX) at 6 months of age and allowed to acclimate to their surroundings for 14 days prior to initiation of the study. All animals were singly housed in a temperature-controlled (23 ± 2ºC) room with a 12-hour light-dark cycle in an American Association for Accreditation of Laboratory Animal Care-accredited animal care facility and were provided standard rodent chow (Harlan Teklad 8604) and water ad-libitum. Animal care and all experimental procedures described in this investigation were conducted in accordance with the Texas A&M University Laboratory Animal Care Committee rules.

Five experimental groups were studied: (1) cage control (CC, n=12), (2) hindlimb unloaded (HU, n=12), (3) HU animals administered 0.01 mg/kg alendronate via subcutaneous injection 3 times/week (HU+ALEN, n=12), (4) HU subjected to simulated resistance training one time/3 days (HU+SRT, n=12), and (5) HU rats subjected to both ALEN and SRT (HU+SRT/ALEN, n=12). HU+SRT and HU+ALEN/SRT animals underwent 9 sessions of simulated resistive exercise conducted once every three days during the 28 day protocol. The HU group was similarly unloaded for 28 days and exposed to the same duration (25 min) of isoflurane anesthesia (Minrad Inc., Bethlehem, PA) as trained HU rats, whereas the CC animals were allowed normal ambulatory cage activity.

Calcein injections (25 mg/kg body mass) were given subcutaneously 9 and 2 days prior to sacrifice to label mineralizing bone for histomorphometric analysis. HU animals

were anesthetized before removal from tail suspension at the end of the study to prevent any weight bearing by the hindlimbs. At necropsy, left soleus, plantaris, and gastrocnemius muscles were excised and wet weights were recorded. Additionally, proximal left tibiae were removed, cleaned of soft tissue, and stored in 70% ethanol at 4°C for cancellous histomorphometry of the proximal tibia metaphysis. Distal left femora were decalcified and stored at 4°C for paraffin embedding.

Hindlimb Unloading

Hindlimb unloading was achieved by tail suspension as previously described (105). Briefly, while the rat was under anesthesia, the tail was cleaned and dried thoroughly. A thin layer of adhesive (Amazing Goop, Eclectic Products, LA) was applied to the proximal half of the tail along the medial and lateral sides. A standard porous tape (Kendall, Mansfield, MA) harness was pressed firmly to the glue and allowed to dry (~30 min). A paper clip was used to attach the animal's tail harness to a swivel apparatus on the wire spanning the top of an 18" x 18" x 18" cage. The height of the animal's hindquarters was adjusted to prevent any contact of the hindlimbs with the cage floor, resulting in approximately a 30° head-down tilt. The forelimbs of the animal maintained contact with the cage bottom, allowing the rat full access to the entire cage.

Simulated Resistance Training (SRT) Paradigm

Simulated resistance training was completed as previously mentioned (105). Briefly, left plantarflexor muscles from animals in the HU+SRT group were trained once

every 3 days during 28-day HU using a custom-made rodent isokinetic dynamometer. Animals were anesthetized with isoflurane gas (~2.5%) mixed with oxygen while remaining suspended, to prevent any weight bearing of the hindlimbs. Once unconscious, the lateral side of the rat's left leg was shaved and aseptically prepared. Each rat was then placed in right lateral recumbency on a platform, the left foot was secured onto the foot pedal, and the left knee was clamped so that the lower leg was perpendicular to the foot and the femur and tibia were at right angles to each other. This was referred to as the resting, 0° position. For isometric contractions, the foot pedal was held fixed in this position. For all contractions, the footplate was rotated in synchronization with muscle stimulation by a Cambridge Technology servomotor system (Model 6900) interfaced with a 80486 66-MHz PC using custom software written in TestPoint (v.4.0; Capital Equipment Corp., Billerica, MA). In either case, the torque generated around the footplate pivot (at the rat's ankle joint) was measured through the servomotor. Plantarflexor muscle stimulation was performed with fine wire electrodes consisting of insulated chromium nickel wire (Stablohm 800B, H-ML Size 003, California Fine Wire Co.), inserted intramuscularly straddling the sciatic nerve in the proximal thigh region. The stimulation wires were then attached to the output poles of a Grass Instruments stimulus isolation unit (Model SIU5; Astro-Med, Inc; W. Warwick, RI) interfaced with a stimulator (S88; Astro-Med, Inc; W. Warwick, RI) which delivered current to the sciatic nerve and induced muscle contraction.

Voltage optimization of the peak isometric torque and frequency optimization of the eccentric torque were performed at the beginning of each session, as described

previously (105). The eccentric phase of the muscle contraction was titrated to equal ~75% of each animal's daily peak isometric torque. The HU+SRT and HU+SRT/ALEN animals completed a combined isometric+eccentric simulated resistance training (SRT) exercise paradigm, consisting of 4 sets of 5 repetitions, once every 3 days during HU (n=9 total exercise sessions). The training paradigm consisted of a 1000ms isometric contraction (175 Hz; 0°), immediately followed by a 1000ms eccentric contraction (75% of the peak isometric contraction).

Bisphosphonate Treatment

Animals in the HU+ALEN, and HU+SRT/ALEN groups were administered 10 μg/kg alendronate (Merck and Co.; Rathway, New Jersey) via subcutaneous injection 3x/week for the duration of the 28-day study. The ALEN dose of 10 μg/kg was the lowest dose found to effectively mitigate reductions in cancellous vBMD at the proximal tibia during 28-day HU in a small pilot study (unpublished data) and is similar to the 15 μg/kg ALEN (2x/week) shown to maintain femur and lumbar spine bone mass and strength in ovariectomized (OVX) rodents (112). Furthermore, this dose of ALEN is lower than the dose used in previously published clinical studies in OVX rats demonstrating pronounced increases in bone mass and strength (113). Rats in the CC, HU, and HU+SRT groups were administered an equal volume of vehicle (phosphate-buffered saline).

Peripheral Quantitative Computed Tomography Scans

On days -1 and 28 of the study, tomographic scans were performed in vivo at the proximal metaphysis of the left tibia with a Stratec XCT Research-M device (Norland Corp., Fort Atkinson, WI), using a voxel size of 100 μm and a scanning beam thickness of 500 μm. Daily calibration of this machine was performed with a hydroxyapatite standard cone phantom. Transverse images of the left tibia were taken at 5.0, 5.5, and 6.0 mm from the proximal tibia plateau. A standardized analysis for metaphyseal bone (contour mode 3, peel mode 2, outer threshold of 0.214 g/cm^3, inner threshold of 0.605 g/cm^3) was applied to each section.

Values of total volumetric bone mineral density (vBMD), total bone mineral content (BMC), total bone area, and cancellous vBMD were averaged across the 3 slices at the proximal tibia to yield a mean value. Machine precision (based on manufacturer's data) is ± 3 mg/cm^3 for cancellous vBMD. Coefficients of variation were ± 0.6, 1.6, 1.9, and 2.13% for in vivo proximal tibia total vBMD, total BMC, total area, and cancellous vBMD respectively, as determined from 3 repeat scans on each of 6 adult male rats.

Histomorphometry Analysis

Undemineralized proximal left tibia were subjected to serial dehydration and embedded in methylmethacrylate (Aldrich M5, 590-9). Serial frontal sections were cut 8 μm thick and left unstained for fluorochrome label measurements. Additionally, 4 μm thick sections treated with von Kossa staining were used for measurement of cancellous bone volume normalized to tissue volume (%BV/TV), and osteoid (Os/BS), osteoblast

(ObS/BS), and osteoclast (OcS/BS) surfaces as a percent of total cancellous surface. Adipocyte density was calculated as number of adipocytes (Ad.N) divided by the marrow area (Ma.Ar) of the region of measurement. The histomorphometric analyses were performed by using the OsteoMeasure Analysis System, Version 1.3 (OsteoMetrics, Atlanta, GA). A defined region of interest was established ~1 mm from the growth plate and within the endocortical edges encompassing 8-9 mm^2 at x40 magnification. Total bone surface (BS), single labeled surface (SLS), double-labeled surface (DLS), interlabel distances, bone volume, and osteoid/osteoclast/osteoblast surfaces were measured at x200 magnification. Mineral apposition rate (MAR, μm/day) was calculated by dividing the average interlabel width by the time between labels (7 days), and mineralizing surface (MS) for cancellous bone surfaces (BS) was calculated by using the formula %MS/BS = {[(SLS/2) + DLS]/surface perimeter} X 100. Bone formation rate (BFR) was calculated as (MAR x MS/BS). All nomenclature for cancellous histomorphometry follows standard usage (114).

Osteocyte Apoptosis

Distal left femora were fixed in 4% phosphate-buffered formalin for 48 hours at 4°C and then decalcified in 10% EDTA and 4% phosphate-buffered formalin for 14 days. Following decalcification, the distal left femora were embedded in paraffin and serial frontal sections were cut 10 μm thick and mounted on slides. Apoptosis of osteocytes was detected by in situ terminal deoxynucleotidyl transferase dUTP nick end labeling (TUNEL) using the DNA fragmentation TdT enzyme and fluorescein-dUTP label (Roche

Diagnostics Corp., Indianapolis, IN) in distal femoral sections counterstained with hematoxylin QS (Vector Laboratories; Burlingame, CA). A defined region of interest was established ~1 mm from the growth plate and within the endocortical edges encompassing 8-9 mm^2 at x40 magnification. Quantification of osteocytes residing in trabeculae within the region of interest was performed by using the OsteoMeasure Analysis System, Version 1.3 (OsteoMetrics, Atlanta, GA). The total number of osteocytes (N.Ot) within the region was first counted (under normal light), followed by identification of TUNEL+ osteocytes using ultraviolet light at 200x magnification. The percentage of apoptotic osteocytes was calculated as (N.Ot /TUNEL+ Ot) x 100.

Statistical Analyses

All data were expressed as means ± SEM and evaluated using the statistical package SPSS (v.15; Chicago, Ill). In vivo pQCT, body mass delta scores, muscle mass at sacrifice, histomorphometry, and apoptosis assays were first analyzed using a two-factor ANOVA (exercise and alendronate) to compare group differences between HU groups (HU, HU+ALEN, HU+SRT, and HU+SRT/ALEN). A Tukey's post-hoc test was used for pair-wise comparisons. Subsequently, a one-factor ANOVA was used to compare individual group change scores vs. that of the comparator cage control (CC) group (Tukey's post-hoc test for pairwise comparisons), and paired t-tests to determine (using absolute date values pre-post within group) whether that change score represented a significant change from Day 0 (pQCT and body mass data only). For all data, statistical significance was accepted at $p<0.05$.

Results

Simulated resistance training does not prevent disuse-associated reductions in total body or ankle plantarflexor muscle masses. Hindlimb unloading significantly reduced total body mass (-8%), which was not attenuated by ALEN (-5.5%), SRT (-7.5%), or the combination of both ALEN and SRT (-11%) during 28-day HU (Table 3). Unloading resulted in lower gastrocnemius, plantaris, and soleus muscle masses as compared to ambulatory controls (24-56%). Reduced left ankle plantarflexor muscle masses were not affected by SRT alone, although ALEN and SRT/ALEN mitigated the decrease in soleus mass. Additionally, when normalized to body mass, SRT did not prevent reduced total plantarflexor muscle mass of the trained left leg (Table 3).

High intensity muscle contractions, performed during unloading, inhibit reductions in cancellous bone mass. Hindlimb unloading significantly reduced PTM total vBMD (-5%), total BMC (-8%), and total bone area (-3%). ALEN prevented HU-associated losses in total vBMD, but not the reductions in total BMC and bone area (Fig 8A-C). SRT and SRT/ALEN prevented HU-associated reductions in these parameters, resulting in significant increases in PTM total vBMD (7%) and total BMC (8-10%). Cancellous vBMD, reduced 8% by HU-alone, was maintained with ALEN treatment (Fig 8D). Simulated resistance training not only inhibited disuse-associated reductions in cancellous vBMD, but resulted in absolute gains.

Table 3. Effects of hindlimb unloading (HU) with or without alendronate (ALEN) treatment and/or simulated resistance training (SRT) on body mass and left ankle plantarflexor muscle masses.

	CC	HU	HU+ALEN	HU+SRT	HU+SRT/ALEN
Body Mass (g)					
Day 0	454.58 ± 6.56	447.73 ± 15.89	438.31 ± 6.39	442.42 ± 7.78	436.36 ± 6.09
Day 28	478.75 ± 8.50*	412.00 ± 13.35*	414.15 ± 9.58*	409.08 ± 8.28*	389.36 ± 8.04*
Body Mass Change (g)	24.17 ± 3.08*	35.73 ± 5.25^{ab}†	(-24.15 ± 5.81^{a}†)	(-33.33 ± 4.65^{a}†)	(-47.00 ± 5.24^{b}†)
%-Change	*(5.32%)*	*(-7.98%)*	*(-5.50%)*	*(-7.53%)*	*(-10.77%)*
Ankle Plantarflexor Masses (g)					
Gastrocnemius	2.312 ± 0.135	1.732 ± 0.035†	1.845 ± 0.057†	1.607 ± 0.058†	1.663 ± 0.044†
Plantaris	0.513 ± 0.009	0.392 ± 0.010†	0.401 ± 0.011†	0.374 ± 0.015†	0.359 ± 0.010†
Soleus	0.199 ± 0.006	0.088 ± 0.004^{a}†	0.107 ± 0.007^{b}†	0.096 ± 0.004^{ab}†	0.101 ± 0.004^{b}†
Total Mass	3.025 ± 0.128	2.212 ± 0.039†	2.353 ± 0.068†	2.072 ± 0.064†	2.100 ± 0.051†
Relative Total Mass/BW (mg/g)	*6.347 ± 0.297*	*5.41 ± 0.165*^{a}†	*5.682 ± 0.290*^{a}†	*4.662 ± 0.421*^{b}†	*4.922 ± 0.465*^{ab}†

Values are group mean ± standard error of the mean. Those HU groups not sharing the same letter for each variable are significantly different from each other ($p<0.05$); comparisons with CC: †Significantly different vs. CC ($p<0.05$); $^{*}p<0.05$ vs. pre value. Group means with no labels are not significantly different.

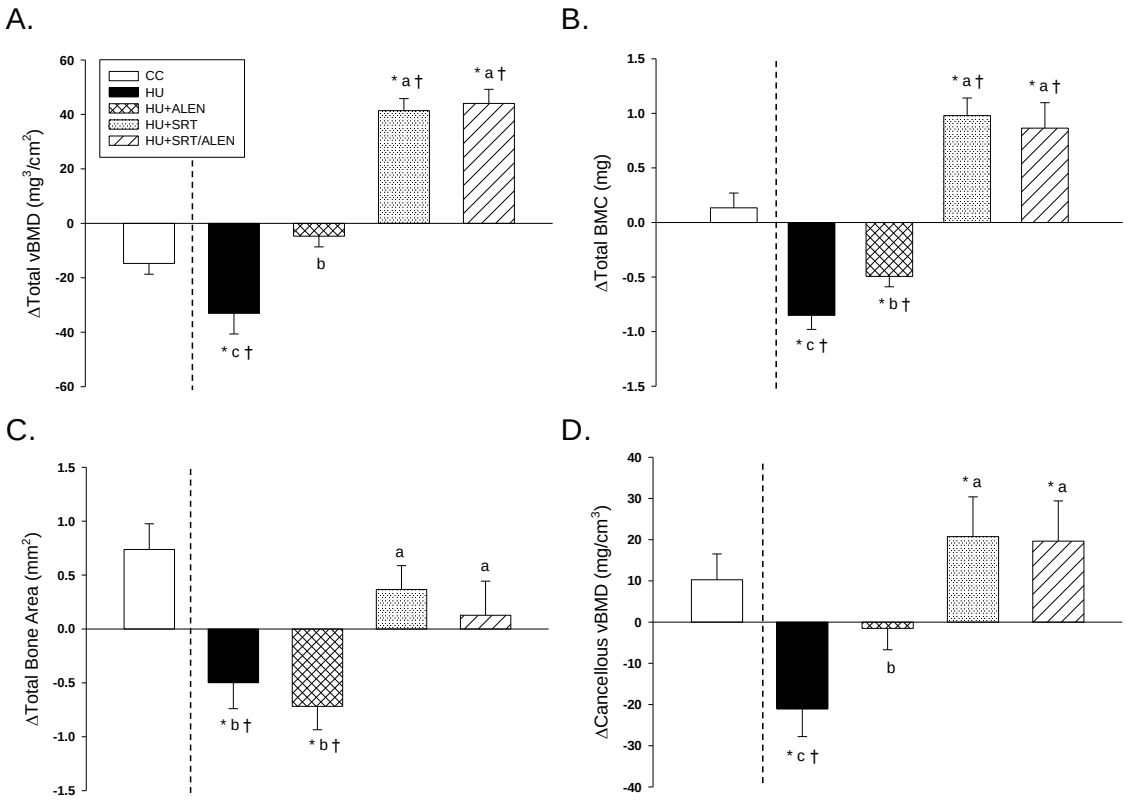

Fig. 8. Effects of hindlimb unloading (HU) with or without alendronate (ALEN) treatment and/or simulated resistance training (SRT) on changes in structural and geometric properties of the proximal tibia metaphysis as taken by in vivo peripheral quantitative computed tomography scans. *A*: Total volumetric bone mineral density (vBMD). *B*: Total bone mineral content (BMC). *C*: Total bone area. *D*: Cancellous volumetric bone mineral density (vBMD). Vertical dashed line indicates separation of CC from the experimental groups for preliminary ANOVA. Those HU groups not sharing the same letter for each variable are significantly different from each other ($p<0.05$); comparisons with CC: †Significantly different vs. CC ($p<0.05$); *$p<0.05$ vs. pre value.

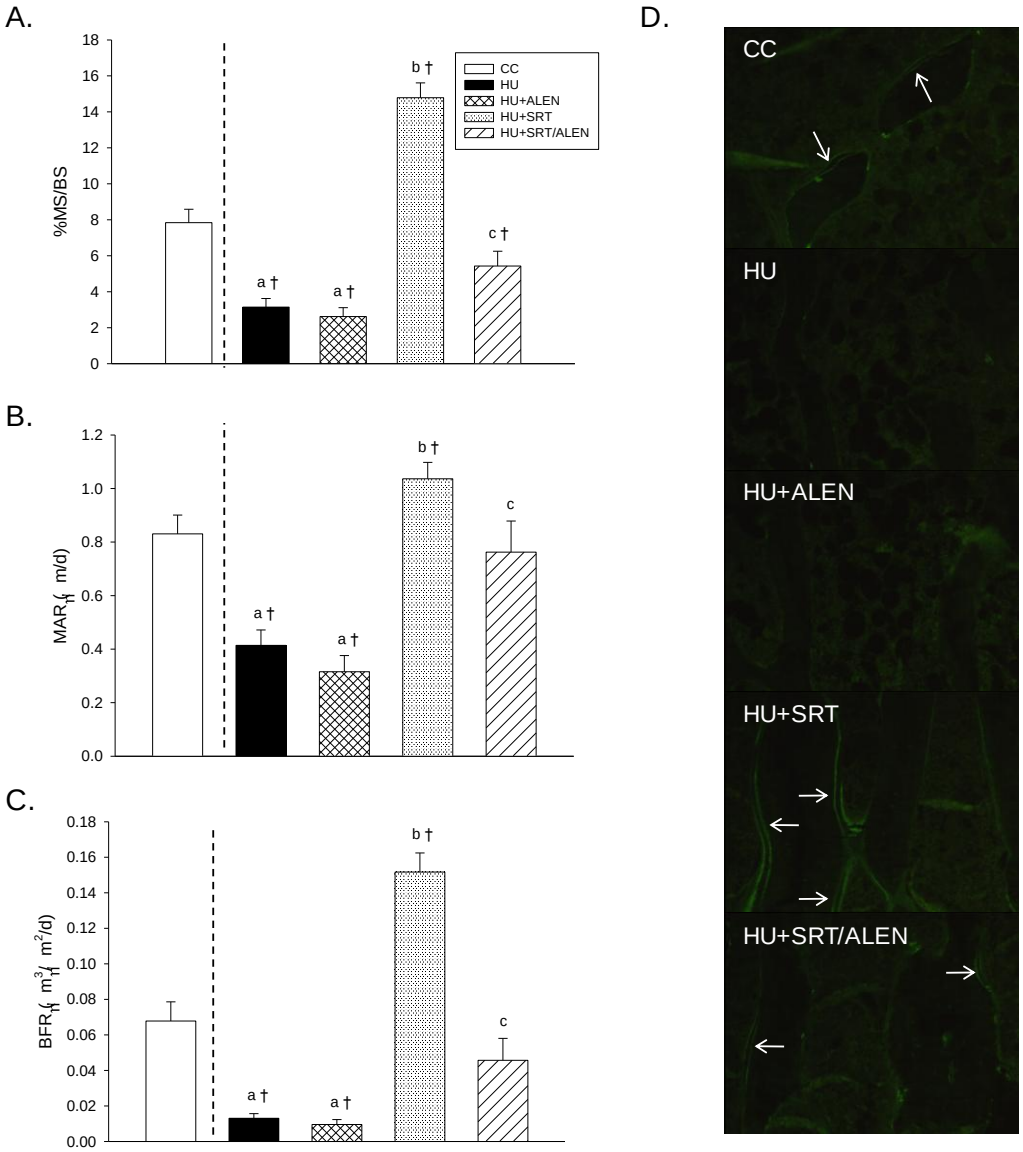

Fig. 9. Effects of hindlimb unloading (HU) with or without alendronate (ALEN) treatment and/or simulated resistance training (SRT) on cancellous bone dynamic histomorphometry analyses measured at the proximal tibia metaphysis. *A*: Mineralizing Surface (%MS/BS). *B*: Mineral Apposition Rate (MAR). *C*: Bone Formation Rate (BFR). *D*: Visual depiction (100x magnification) of calcein labeling of cancellous bone. Note the extensive fluorochrome labeling (arrows) in CC, HU+SRT, and HU+SRT/ALEN and large interlabel width (HU+SRT). Vertical dashed line indicates separation of CC from the experimental groups for preliminary ANOVA. Those HU groups not sharing the same letter for each variable are significantly different from each other ($p<0.05$); comparisons with CC: †Significantly different vs. CC ($p<0.05$).

Alendronate reduces the cancellous bone formation response to simulated resistance training during disuse. Hindlimb unloading produced significantly lower PTM cancellous bone mineralizing surface (-60%) and mineral apposition rate (-50%), resulting in 81% lower bone formation as compared to ambulatory controls (Figure 9 A-C). ALEN administration had no effect on HU-induced reductions in cancellous bone formation. SRT, undertaken during unloading, not only inhibited deficits in cancellous bone formation, but led to significantly greater %MS/BS (90%), MAR (25%), and BFR (2-fold increase) vs. CC. When SRT was completed in combination with ALEN, %MS/BS and BFR were 63-70% lower than HU+SRT. Few fluorochrome labels were present on cancellous bone surface of HU and HU+ALEN rodents (Fig 9D).

Simulated resistance training improves metaphyseal bone microarchitecture and reduces adipocyte density. HU did not significantly affect cancellous bone microarchitecture at the proximal tibia as compared to controls (Fig 10). However, ALEN treatment during unloading resulted in reduced BV/TV and Tb.Th (9-12%) vs. CC (Fig 10 A-B). Greater cancellous bone formation resulted in enhanced proximal tibia microarchitecture in HU+SRT and HU+SRT/ALEN groups. BV/TV (+15%) and Tb.Th (+32%) were significantly greater in both SRT groups as compared to HU group. Furthermore, ALEN+SRT during HU produced smaller Tb.Sp (-17%) and greater Tb.N (+14%) as compared to HU (Fig 10 C-D).

Hindlimb unloading resulted in significantly lower OS/BS (-40%) and Oc.S/BS (-45%), in addition to a 2-fold greater adipocyte density as compared to ambulatory

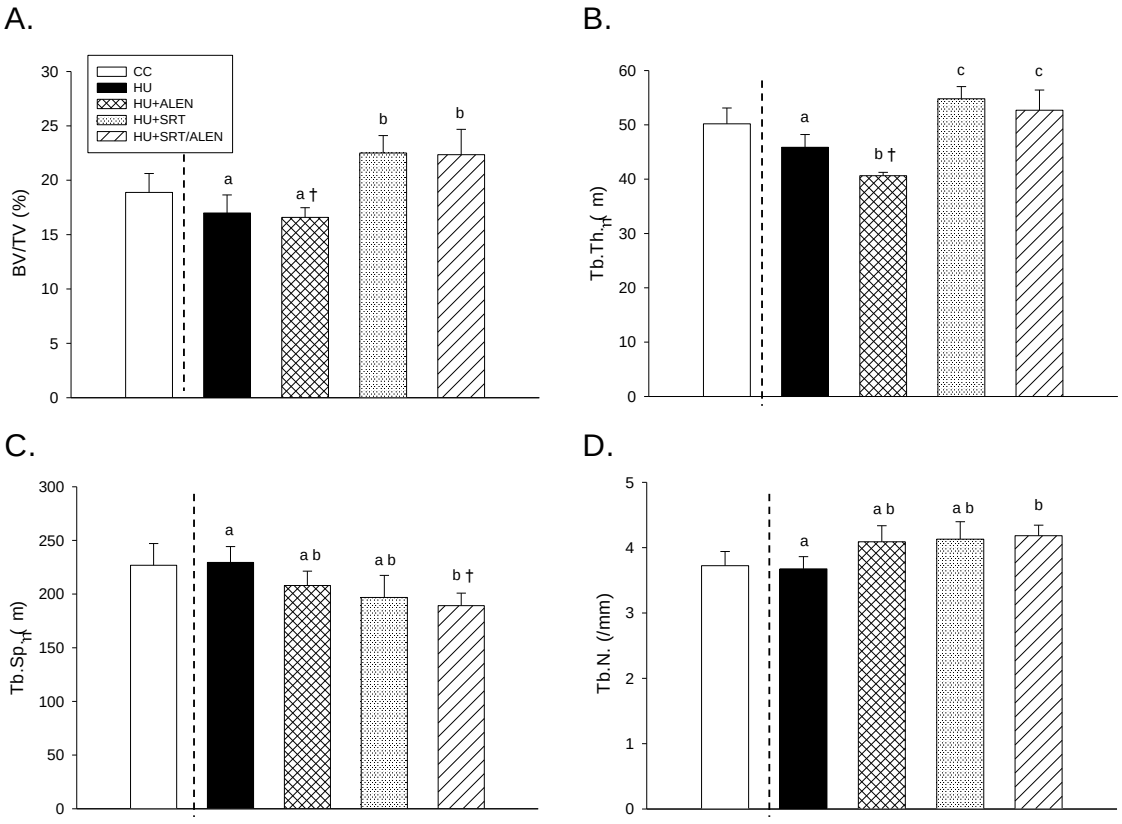

Fig. 10. Effects of hindlimb unloading (HU) with or without alendronate (ALEN) treatment and/or simulated resistance training (SRT) on cancellous bone microarchitecture. *A*: Bone Volume (%BV/TV). *B*: Trabecular Thickness (Tb.Th.). *C*: Trabecular Spacing (Tb.Sp.). *D*: Trabecular Number (Tb.N.). Vertical dashed line indicates separation of CC from the experimental groups for preliminary ANOVA. Those HU groups not sharing the same letter for each variable are significantly different from each other ($p<0.05$); comparisons with CC: †Significantly different vs. CC ($p<0.05$).

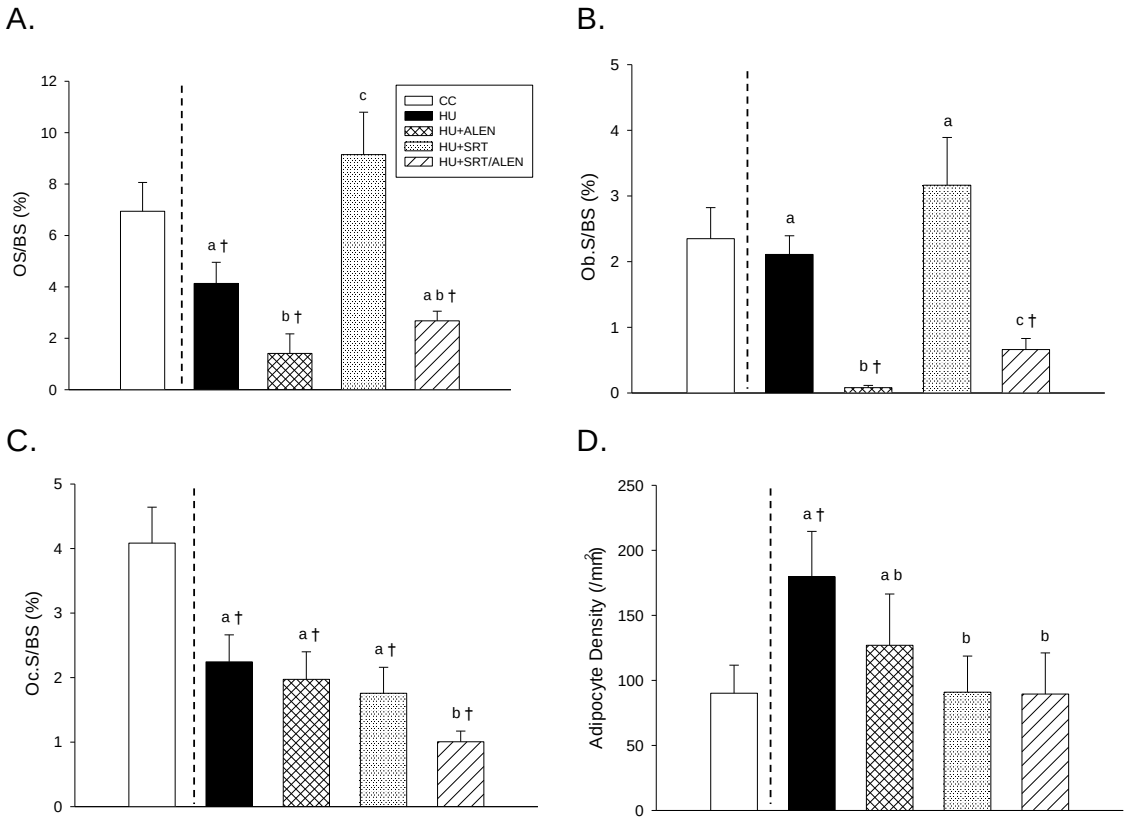

Fig. 11. Effects of hindlimb unloading (HU) with or without alendronate (ALEN) treatment and/or simulated resistance training (SRT) on cancellous bone cell activity. *A*: Osteoid Surface (OS/BS). *B*: Osteoclast Surface (OcS/BS). *C*: Osteoblast Surface (ObS/BS). *D*: Adipocyte Density (N.Ad/Ma.Ar). Vertical dashed line indicates separation of CC from the experimental groups for preliminary ANOVA. Those HU groups not sharing the same letter for each variable are significantly different from each other ($p<0.05$); comparisons with CC: †Significantly different vs. CC ($p<0.05$).

controls (Fig 11 A,B,D). ALEN treatment exacerbated HU-induced decreases in osteoid surface (-80%) and produced a nearly complete suppression of osteoblast surface (-97%) vs. CC group. SRT inhibited disuse-induced reductions in OS/BS and increased adipocyte density; the addition of ALEN treatment during SRT significantly lessened the beneficial effects of high intensity muscle contractions. HU+SRT/ALEN rats' OS/BS

and Ob.S/BS were 61-72% lower vs. those of controls. On the other hand, Oc.S/BS was reduced to a greater extent in HU+SRT/ALEN rats than in all other HU groups.

Osteocyte apoptosis is independently maintained by both muscle contractions and alendronate during disuse. Unloading resulted in a significantly greater percentage of apoptotic cancellous osteocytes (+74%) as compared to ambulatory controls (Fig 12). SRT and ALEN, independently and in combination, retarded HU-associated increases in prevalence of apoptotic osteocytes within cancellous bone.

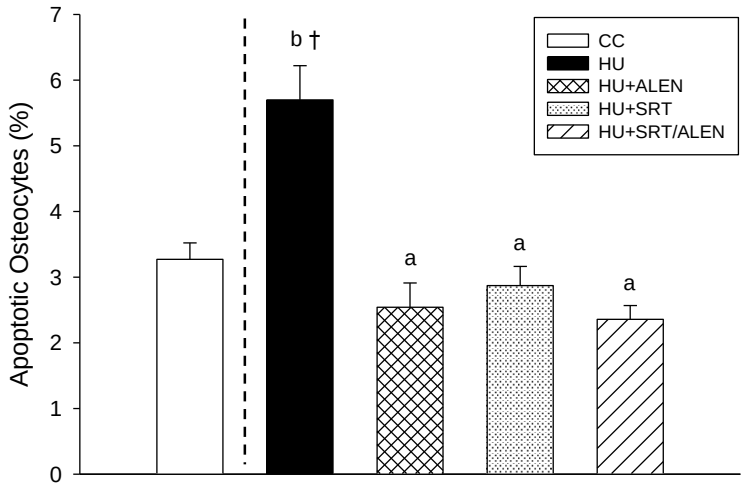

Fig. 12. Effects of hindlimb unloading (HU) with or without alendronate (ALEN) treatment and/or simulated resistance training (SRT) on cancellous bone TUNEL+ osteocytes (%) measured at the distal femur. Vertical dashed line indicates separation of CC from the experimental groups for preliminary ANOVA. Those HU groups not sharing the same letter for each variable are significantly different from each other ($p<0.05$); comparisons with CC: †Significantly different vs. CC ($p<0.05$).

Discussion

The main purpose of our study was to determine if a reduced volume of high intensity muscle contractions simulating resistance training (RT), coupled with the anti-resorptive effects of alendronate (ALEN), would benefit unloaded cancellous bone. We hypothesized that, by combining simulated RT (SRT) and alendronate, the metaphyseal bone response would be greater than either of them alone and would result in decreased prevalence of apoptotic osteocytes.

Contrary to our hypothesis, adding alendronate to simulated resistance training during disuse did not have a greater positive impact on metaphyseal bone as compared to either of these interventions alone. SRT with ALEN during HU resulted in similar changes in proximal tibia bone mass and microarchitecture. Both the HU+SRT and HU+SRT/ALEN groups experienced significant increases in proximal tibia cancellous vBMD (Fig 8D), associated with greater bone volume, trabecular thickness and trabecular number as compared to untreated HU rats (Fig 9). Additionally, both exercise trained groups exhibited a reduced prevalence of cancellous osteocyte apoptosis (Fig 12). However, when simulated RT was added to alendronate treatment during disuse, we observed a 70% suppression in cancellous bone formation as measured during the final week of disuse (Fig 9C). Furthermore, ALEN treatment inhibited the dramatic response of osteoid and osteoblast cells to SRT (Fig 11 A-B), with values similar to the HU-only group. Since the combined treatment did not provide any advantage in terms of cancellous bone mass gains beyond that observed in the HU+SRT animals, our data suggest that absolute gains in metaphyseal bone mass in the HU+SRT/ALEN group

occurred because of the anabolic effect on bone with the loading provided by these high-force muscle contractions and not because of anti-resorptive effects of alendronate.

Although this is the first study, to our knowledge, to investigate the effects of alendronate treatment in conjunction with exercise (engaged without weightbearing) during hindlimb unloading, there are a limited number of investigations on this topic testing their efficacy during estrogen deficiency using ovariectomized (OVX) rodents. Fuchs et al. (112) administered 15 μg/kg ALEN (given 2x/week) to OVX rats in combination with moderate treadmill running and found that the effects of the combined therapy are superior in maintaining bone mass and strength as compared to either individual treatment. Similar to this study, Tamaki et al. (115) documented significant interactions between exercise and bisphosphonate treatment on BMD of the proximal femur and trabecular bone of the proximal tibia. These studies, in contrast to our investigation, employed moderate intensity treadmill running which has been shown to be less effective than resistance exercise at increasing bone mass in rodents (49). The individual and combined effects of 12 months of jump exercise training and daily alendronate administration (5 mg/d) on bone mass in post-menopausal women demonstrates no additive effects of alendronate and exercise on bone mass or mechanical properties, although each treatment was found to independently impact bone (116).

Combined exercise and alendronate treatment has been investigated in few human studies assessing bone loss typically evidenced during long-duration spaceflight. The inability of combined anabolic and anti-resorptive therapy to inhibit reductions in

disuse-sensitive metaphyseal bone mass has also been documented during bed rest. Administration of an early generation bisphosphonate (ethane-1-hydroxy-1-disphosphonate) combined with treadmill exercise and cycling (modeling exercise regimens used by cosmonauts) during 360 days of bed rest reduced negative calcium balance, but did not significantly mitigate losses in femoral neck BMD (117). Neither flywheel resistance exercise or pamidronate (another nitrogen-containing bisphosphonate was able to rescue metaphyseal bone loss in the tibia during 90 days of bed rest (118). However, combined exercise and bisphosphonate treatment significantly mitigates reductions in tibia diaphyseal bone mass.

The simulated resistance training protocol utilized in the current study produced similar positive effects on the unweighted tibia consistent with our previous results (105). However, lacking detailed histomorphometry data, we were unable to confirm that our SRT protocol had an anabolic effect on cancellous bone. In the current investigation, we used a reduced intensity of combined isometric and eccentric muscle contractions (75% vs. 100% peak isometric torque), administered fewer training sessions (9 vs. 14), and still demonstrated absolute increases in proximal tibia cancellous bone vBMD (Fig 8D). This increase in cancellous bone mass was associated with significantly greater bone formation (Fig 9C), osteoid and osteoblast surface (Fig 11A-B), along with a suppression of the increase in adipocyte density observed in unloaded bones (Fig 11D). Furthermore, simulated RT resulted in greater trabecular thickness as compared to both unloaded and ambulatory control animals (Fig 10 B). However, the reduced volume of our training protocol used in this study was not able to mitigate the

loss of left ankle plantarflexor muscle mass (Table 1) as did our previous study. We were unable to detect any effect of alendronate treatment on unweighted skeletal muscle. Taken together, these data emphasize the dramatic anabolic response of cancellous bone to a low volume of high intensity muscle contractions engaged during periods of disuse. However, reducing the training intensity and volume (versus our previous protocol) resulted in a loss of the mitigating effect on disuse-induced muscle atrophy.

The effectiveness of alendronate to inhibit disuse-induced bone loss has been demonstrated in numerous rodent hindlimb unloading investigations. Alendronate (0.1 mg/kg), administered prior to HU, prevented reductions in unweighted bone mass by decreasing relative osteoclast surface and mitigating reductions in bone formation (26). Furthermore, alendronate treatment during 14-day HU abolished losses in tibia and femur BMD, but was unable to rescue disuse-induced reductions in bone strength (65). Apseloff et al. (66) administered 0.3 mg/kg alendronate during 28 days of unloading and revealed significant reductions in osteoid perimeter, cancellous bone formation, and bone resorption during hindlimb unloading. The resulting increase in bone mass with alendronate treatment resulted from greater inhibition of resorption. Bed rest investigations on human subjects testing the effects of alendronate have elucidated similar mechanisms of this bisphosphonate's action on bone during periods of disuse. Ruml and colleagues (63) administered 20 mg/day of alendronate during 3 weeks of bed rest and observed a reduction in urinary calcium excretion as compared to untreated controls. During a longer duration bed rest investigation (17 weeks), 10 mg/day of

alendronate successfully prevented reductions in lumbar spine and femoral neck BMD and attenuated increases in urinary markers of bone resorption (64).

Data from these previous investigations parallel findings in our current study. We found that 10 μg/kg alendronate (3x/week), given during disuse, maintained both total and cancellous vBMD at the proximal tibia, despite lower bone formation and osteoid and osteoblast surface. We were unable to detect significant reductions in osteoclast surface in alendronate-treated rodents subjected to unloading. We did measure serum TRACP 5b, a systemic marker of osteoclast activity. In postmenopausal females, serum TRACP 5b correlates significantly with changes in BMD and has been accepted as a useful marker for monitoring alendronate treatment (119). Serum TRACP 5b was significantly reduced in both HU+ALEN and HU+SRT/ALEN groups as compared to unloaded animals (data not shown). These data suggest that, although osteoclast surface measured in our proximal tibia region of interest was not suppressed with alendronate treatment during disuse, osteoclast activity across the entire skeleton may have been reduced.

Similar to previously published results, we found that 28 days of hindlimb unloading significantly increased cancellous osteocyte apoptosis (106,120). However, to our knowledge, no prior investigation has defined the role of mechanical loading, engaged during a period of imposed disuse, on osteocyte apoptosis within cancellous bone. Basso et al. (107) previously demonstrated that 2 weeks of resumption of normal weightbearing after an equal duration of hindlimb unloading returns cancellous osteocyte apoptosis to control levels. Additionally, ulnar loading has been shown to

significantly reduce cortical osteocyte apoptosis (121). Surprisingly, our data demonstrate that high intensity muscle contractions completely prevent disuse-induced increases in osteocyte apoptosis (Fig 12A). Furthermore, simulated RT prevented the reductions in cancellous bone osteocyte density observed in untreated hindlimb unloaded rats (Fig 12B). Alendronate treatment resulted in a similar protective effect. Although previously published studies have confirmed that alendronate inhibits osteocyte apoptosis (61,122), our data are the first to demonstrate the anti-apoptotic effects of alendronate during disuse.

There were a few limitations to this current investigation. We were unable to detect significant changes in cancellous bone microarchitecture by 2-D histomorphometry. Employing a more sensitive technique of measuring these variables may result in more definitive answers to the combined and individual effects of simulated RT and alendronate during unloading. Additionally, our study design did not include weightbearing control animals (CC) receiving either simulated RT or alendronate; therefore we are unable to determine the important clinical question as to whether or not our regimen of alendronate treatment combined with RT has similar negative effects on cancellous bone formation in weightbearing rodents.

In conclusion, data from this study suggests that bisphosphonate treatment, when combined with high-intensity muscle contractions during disuse, significantly reduces the anabolic response of cancellous bone to simulated resistance training. This beneficial effect of mechanical loading and alendronate treatment (acting independently and in combination) may be affected in part by inhibiting disuse-associated increases in

cancellous osteocyte apoptosis. The suggested inhibitory effects of bisphosphonate treatment on the cancellous bone formation response to high intensity resistance exercise has important implications for the efficacy of exercise countermeasures utilized during periods of disuse in any population using these pharmaceutical agents.

CHAPTER V

ADMINISTRATION OF A BETA-1 ADRENERGIC AGONIST ATTENUATES METAPHYSEAL BONE LOSS DURING UNLOADING BY MAINTAINING FORMATION

Introduction

Mechanical loading is essential to maintain bone mass during periods of disuse (i.e. bedrest or casting) or reduced weightbearing activity. Long duration exposure to microgravity leads to an accelerated loss of bone mass (~1-2%/month) and results in osteopenia (13,14). For those astronauts experiencing the greatest bone loss, reductions in modeled proximal femur strength after 6 months of microgravity exposure approach the estimated lifetime loss in stance strength for Caucasian women (16,17). Ground-based models demonstrate similar deleterious effects when mechanical loading of weightbearing bones ceases. Prolonged bed rest reduces femoral neck, lumbar spine, and lower body bone mineral density (BMD), resulting in decreased bone volume fraction (BV/TV) and trabecular thickness (Tb.Th) (54,123). In addition, spinal cord injury (SCI) patients experience severe reductions in bone, predominantly in cancellous bone compartments (124-126).

The rodent hindlimb unloading (HU) model is a well-established ground-based model for investigating disuse effects on bone and muscle (20). Hindlimb unloading results in significant reductions in disuse-sensitive cancellous bone mass, architecture

and material properties due to early increases in bone resorption followed by prolonged depression of bone formation rate (BFR) (21-24,104,105).

Beta-adrenergic receptor agonists, activated by the sympathetic nervous system (SNS), may affect bone metabolism through separate avenues and elicit opposing effects on bone mass. Three subunits of β-adrenergic receptors (Adrb1, 2, 3) are present in tissues within the body. Adrb2 receptors present in the lungs mediate bronchiolar dilation; those on osteoblasts and osteoclasts stimulate apoptosis and result in diminished bone mass (67,68). Adrb1 receptors on the heart, increase cardiac contractility when activated, and are also present on osteoblasts and osteoclasts (69,70). Activation of β-3 adrenergic receptors, the primary adrenoreceptor on adipocytes, upregulates lipolysis (71,72).

Adrb1 and Adrb2 receptors are both present on osteoblasts, but β-2 adrenergic receptors are the predominant subtype (67,68,73-75). Adrb2 receptor agonist administration leads to increased bone resorption, resulting in reduced cancellous bone mass and negative changes to microarchitecture (78,79). Stimulation of Adrb2 receptors on osteoblasts increases osteoclast differentiation and activity (81). Salbutamol, an Adrb2 receptor agonist, is unable to inhibit the deleterious effects of ovariectomy-induced cancellous bone loss (80). In addition, Adrb2 receptor knock-out (KO) and Adrb1 receptor KO mice demonstrate a high and low bone mass phenotype, respectively, whereas Adrb1/2 receptor double-KO mice exhibit a marked reduction in cancellous BFR vs. wild types (67,82,127). Adrb1 receptor deficient mice do not respond to mechanical loading, whereas Adrb2 receptor deficient and wild-type

littermates were found to respond normally (82). Taken together, these data suggest that the high bone mass phenotype in Adrb2 receptor KO mice may be caused by enhanced β-1 adrenergic receptor activity stimulating bone formation in the absence of the inhibitory effects of β-2 adrenergic receptors on osteoblasts. Therefore, the role that Adrb1 receptor stimulation during reduced mechanical loading has on disuse-sensitive cancellous bone is important to further understanding the underlying mechanisms responsible for bone loss.

Dobutamine (DOB) is a non-specific, Adrb receptor agonist with dominant β-1 adrenergic receptor activity and a small amount of Adrb2 activity (76). Its ability to primarily activate Adrb1 and makes it an attractive synthetic catecholamine to study in coordination with HU. Our previous data demonstrated that DOB administered during HU significantly blunts disuse-induced reductions in femoral midshaft bone area and cross-sectional moment of inertia (CSMI) by mitigating the decline in periosteal bone mineral apposition rate (MAR) (77).

Our aim with these experiments was to elucidate the mechanisms by which an Adrb1 agonist (DOB) mitigates losses bone (tibia) mass and strength during HU in skeletally mature rats. Secondary to this, we sought to characterize Adrb1 agonist effects on unloaded skeletal muscle strength and lean tissue mass. We hypothesized that DOB treatment during HU would diminish HU-associated reductions in bone mass and strength, and that the effects of DOB treatment would be greater during normal gravitational loading.

Materials and Methods

Animals and Experimental Design

Forty-eight male Sprague-Dawley rats were obtained from Harlan (Houston, TX) at 6 months of age and allowed to acclimate to their surroundings for 14 days prior to initiation of the study. All animals were acclimated to their surroundings for 14 days, and were then singly housed in a temperature-controlled (23 ± 2ºC) room with a 12-hour light-dark cycle in an American Association for Accreditation of Laboratory Animal Care-accredited animal care facility, where standard rodent chow (Harlan Teklad 8604) and water were provided ad-libitum. Animal care and all experimental procedures described in this investigation were approved by the Texas A&M University Institutional Animal Care and Use Committee.

One day prior to initiation of experimental treatments, all animals underwent peripheral quantitative computed tomography (pQCT) scans and were rank ordered by total volumetric bone mineral density (vBMD) of the proximal tibia metaphysis (PTM) and randomly assigned to one of two activity groups: normal ambulatory cage activity (CC; n=24) or hindlimb unloading (HU; n=24). Within each activity group, rats were randomly assigned to receive daily intraperitoneal injections of dobutamine (DOB; 4 mg/kg body mass/d; n=12) or an equal volume of saline (VEH; n=12), administered within the first 2 hours of the animals' dark cycle. The one bolus dose of DOB was found to be effective at mitigating reductions in cancellous vBMD at the PTM during 28-day HU in a small pilot study (unpublished data). Dobutamine hydrochloride

solution (Sigma-Aldrich Corp., St. Louis, MO) was made daily with sterile saline and stored at 4ºC until use.

Calcein injections (25 mg/kg body mass) were given subcutaneously on 9 and 2 days prior to sacrifice to label mineralizing bone for histomorphometric analyses. HU animals were anesthetized before removal from tail suspension at the end of the study to prevent any weight bearing by the hindlimbs. At necropsy, both right and left soleus, plantaris, and gastrocnemius muscles were excised and wet weights were recorded. Right tibia and femur were removed, cleaned of soft tissue, and stored at -80°C in PBS soaked gauze for ex vivo pQCT scans and/or mechanical testing, whereas left tibia were stored in 70% ethanol at 4°C for histology. Additionally, adrenal glands were dissected free and wet weights obtained as a marker of stress; heart wet weight was also recorded.

Hindlimb Unloading

Hindlimb unloading was achieved by tail suspension as previously described (21,103,105). Briefly, while the rat was under anesthesia, the tail was cleaned and dried thoroughly. A thin layer of adhesive (Amazing Goop, Eclectic Products, LA) was applied to the proximal half of the tail along the medial and lateral sides. A standard porous tape (Kendall, Mansfield, MA) harness was pressed firmly to the glue and allowed to dry (~30 min). A paper clip was used to attach the animal's tail harness to a swivel apparatus on the wire spanning the top of an 18" x 18" x 18" cage. The height of the animal's hindquarters was adjusted to prevent any contact of the hindlimbs with the

cage floor, resulting in approximately a 30° head-down tilt. The forelimbs of the animal maintained contact with the cage bottom, allowing the rat full access to the entire cage.

Muscle Function Testing

Peak isometric torque of the left leg plantarflexor muscles was determined on day 28 on all animals using an isokinetic dynamometer as previously described (128). Briefly, animals were anesethetized with isoflurane gas (~2.5%) mixed with oxygen while remaining suspended to prevent any weight bearing of the hindlimbs. Each rat was then placed in right lateral recumbency on a platform, the left foot was secured onto the foot pedal, and the left knee was clamped so that the lower leg was perpendicular to the foot and the femur and tibia were at right angles to each other. Plantarflexor muscle stimulation was performed with percutaneous electrodes inserted straddling the sciatic nerve in the proximal thigh region. The stimulation wires were then attached to the output poles of a Grass Instruments stimulus isolation unit (Model SIU5; Astro-Med, Inc; W. Warwick, RI) interfaced with a stimulator (S88; Astro-Med, Inc; W. Warwick, RI), which delivered current to the sciatic nerve and induced muscle contraction.

Peripheral Quantitative Computed Tomography (pQCT)

On days -1 and 28 of the study, tomographic scans were performed in vivo at the proximal and mid-diaphysis of the left tibia with a Stratec XCT Research-M device (Norland Corp., Fort Atkinson, WI), using a voxel size of 100 μm and a scanning beam thickness of 500 μm. Daily calibration of this machine was performed with a

hydroxyapatite standard cone phantom. Transverse images of the left tibia were taken at 5.0, 5.5, and 6.0 mm from the proximal tibia plateau, as well as one slice at the midshaft (50% of the total tibia length). A standardized analysis for either metaphyseal bone (contour mode 3, peel mode 2, outer threshold of 0.214 g/cm^3, inner threshold of 0.605 g/cm^3) or diaphyseal bone (separation 1, threshold of 0.605 g/cm^3) was applied to each slice.

For ex vivo scans, thawed femur and humeri were placed in a 1 mol/L PBS-filled vial to maintain hydration during the scan, after which time they were returned to the -80°C freezer. Femoral neck scanning was performed with the bone shaft, wrapped in PBS-soaked gauze, positioned on a platform with only the neck exposed in order to scan slices (2 images, 0.5 mm apart) perpendicular to the femoral neck's long axis. Additionally, one scan slice was taken at the femur mid-diaphysis. Femoral neck slices were analyzed using contour mode 3, peel mode 5, and attenuation threshold 0.214 g/cm^3. Scan speed was set at 2.5 mm/sec with a voxel resolution of 0.07 x 0.07 x 0.50 mm.

Values of total volumetric bone mineral density (vBMD), total bone mineral content (BMC) and total bone area were averaged across slices at each metaphyseal bone site to yield a mean value. Additionally, mid-diaphyseal cross-sectional moment of inertia (CSMI) was obtained with respect to the neutral bending axis during three-point bending for later calculation of material properties. Machine precision (based on manufacturer's data) is and ± 9 mg/cm^3 for cortical BMD. Coefficients of variation were ± 0.6, 1.6, and 1.9% for in vivo proximal tibia total vBMD, total BMC, and total

area, respectively, as determined from repeat scans on each of (n=6) adult male rats. In vivo coefficients of variation for cortical vBMD (0.7%), cortical BMC (1.2%), cortical bone area (1.5%), and CSMI (3.0%) were determined in a similar manner as described above.

Dual –Energy X-Ray Absorptiometry (DEXA)

One day before both initiation and cessation of the investigation, all animals were anesthetized with ketamine/medetomidine cocktail (ketamine 50 mg/kg, medetomidine 0.5 mg/kg) and dual-energy x-ray absorptiometry (DEXA; GE Lunar Prodigy using small animal software) scans were completed to assess changes in whole body composition (lean mass, fat mass). In vivo total body coefficients of variation for lean mass and fat mass are 1.07 and 2.99%, respectively, as determined from repeat scans on each of adult male rats (n=6).

Histomorphometry Analyses

Undemineralized proximal left tibia were subjected to serial dehydration and embedded in methylmethacrylate (Aldrich M5, 590-9). Serial frontal sections were cut 8 μm thick and left unstained for fluorochrome label measurements. Additionally, 4 μm thick sections for von Kossa staining for measurement of cancellous bone volume normalized to tissue volume and quantification of osteoid, osteoblast, and osteoclast surfaces as a percent of total cancellous surface. The histomorphometric analyses were performed by using the OsteoMeasure Analysis System, Version 1.3 (OsteoMetrics,

Atlanta, GA). A defined region of interest was established ~1 mm from the growth plate and within the endocortical edges encompassing 8-9 mm^2 at x40 magnification. Total bone surface (BS), single labeled surface (SLS), double-labeled surface (DLS), interlabel distances, bone volume, and osteoid/osteoclast/osteoblast surfaces were measured at x200 magnification. Mineral apposition rate (MAR, μm/day) was calculated by dividing the average inter-label width by the time between labels (7 days); mineralizing surface (MS) for cancellous bone surfaces (BS) was calculated using the formula %MS/BS = {[(SLS/2) + DLS]/surface perimeter} X 100. Bone formation rate (BFR) was calculated as (MAR x MS/BS).

Biomechanical Testing

Femur and tibia mid-diaphyseal cortical bone mechanical properties were determined using three-point bending to failure and femoral neck maximal force measured on an Instron 1125 machine as previously described (129). Sites of mechanical testing were matched to pQCT sampling sites (e.g., the femoral mid-diaphyses were analyzed at 50% of total bone length). Prior to testing, the length of each specimen was measured and the half-length was marked with Absolute Digamatic calipers (Mitutoyo Corp., Japan). In addition, the anterioposterior (AP) and mediolateral (ML) surface diameters at each testing site were similarly measured at the previously marked mid-point. On the day of testing, bones were thawed at room temperature and placed either anterior (femur) or lateral (tibia) side down on metal pin supports located ±9 mm (tibia) and ±7.5 mm (femur) from the predetermined mid-diaphysis testing site. All specimens

were sprayed with PBS immediately preceding testing to maintain hydration. Femoral necks were tested by placing the distal portion of the proximal half of the femur perpendicularly into a metal fixture and loading the femoral head in vertical direction, parallel to the long axis of the femur (129). Loading of the femoral head in this fashion creates a combination of bending, shear, and compression. Using a 1,000 lb load cell calibrated to 100 lb maximum load, all tests used quasi-static loading at a rate of 2.54 mm/min applied to the posterior surface of the femora, the medial surface of the tibia or the femoral head until fracture. Displacements of the servo-controlled Instron were monitored by a linear variable differential transformer (LVDT) interfaced with a personal computer (Gardener Systems software).

Raw data, collected at 10 Hz as load vs. displacement curves, were analyzed with Table-Curve 2.0 (Jandel Scientific; San Rafael, CA). Structural variables were obtained directly from load/displacement curves. The maximum load attained was defined as maximum force (MF) and the slope of the elastic portion of the curve defined as stiffness (S). Yield force (90%) was ascribed as a 10% deviation from the slope of the elastic portion of the load/displacement curve. Material properties of tibia and femur were calculated as previously described (swift jbmr 2010). Briefly, structural properties were normalized to bone geometry at the site of testing using cross-sectional moment of inertia (CSMI; from pQCT), bone diameter (D) measured by calipers, and a support span distance of either 18mm (tibia) or 15mm (femur). Formulas for elastic modulus (EM) and ultimate stress (US) were as follows: $EM = (S \times \text{support span}^3) / (48 \times CSMI \times 1{,}000)$; $US = [MF \times \text{support span} \times (D / 2)] / (4 \times CSMI)$.

Statistical Analyses

All data were expressed as means ± SEM and statistical relationships were evaluated using the statistical package SPSS (v.15). In vivo pQCT, DEXA, and body mass data were analyzed using a three-factor ANOVA (drug, gravity condition, time) with repeated measures on time. Paired t-tests were used on absolute values of in vivo pQCT and DEXA pre- and post-values to determine if the change score represented a significant change from Day 0. Mechanical testing, ex vivo pQCT, plantarflexor muscle strength, tissue masses, and histomorphometry data were analyzed using a two-factor ANOVA (drug, gravity condition). When a significant main effect was found, Tukey's post-hoc analyses were performed for pair-wise comparisons. For all data, statistical significance was accepted at $p<0.05$.

Results

Adrb1 receptor agonist treatment rescues unloading-associated reductions in muscle strength but not body mass. Significant reductions in body mass during HU (-3%) were accompanied by decrements in whole-body fat (-18%) by 28 days (Figure 13). HU rats did not exhibit the small non-significant lean mass gains observed in weightbearing cage controls. Dobutamine administration during unloading had no impact on HU-associated reductions in body mass; however, HU rats treated with DOB lost significantly more fat mass (- 37%). DOB treatment led to significantly higher cardiac mass in ambulatory controls (+7% vs. CC-VEH) but no differences in adrenal mass were evident among groups (Table 4).

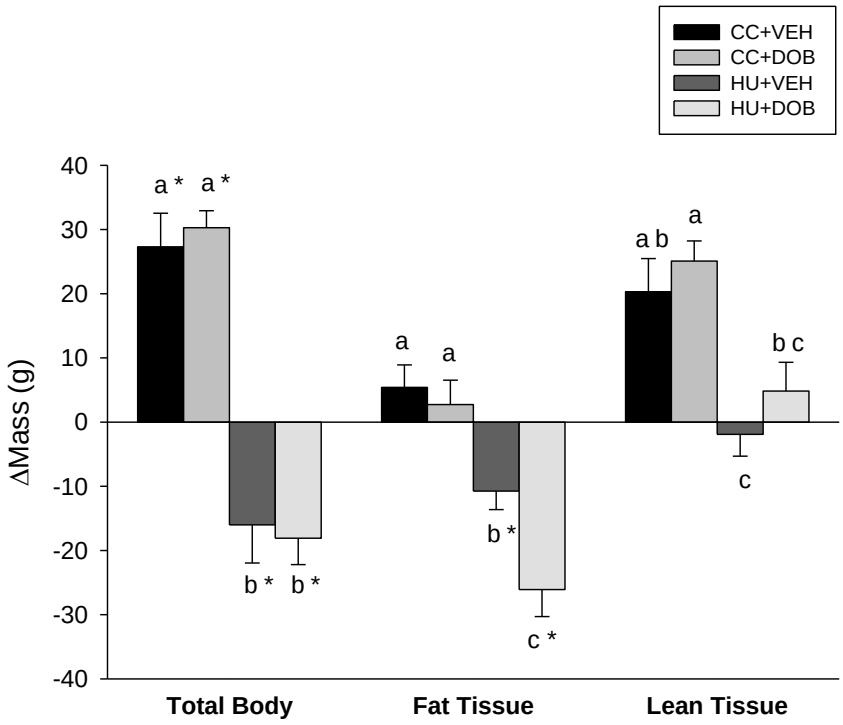

Fig. 13. Effects of dobutamine (DOB) or vehicle (VEH) administration during hindlimb unloading (HU) or ambulatory cage activity (CC) on changes in body and tissue masses as measured by in vivo DEXA scans on days -1 and 27. Values are group mean ± standard error of the mean. Those groups not sharing the same letter for each variable are significantly different from each other ($p<0.05$); $^{*}p<0.05$ vs. day 0 value.

Mechanical unloading resulted in a significant 9.7% reduction in peak isometric torque in HU-VEH rats vs. ambulatory controls ($p<0.05$). DOB treatment attenuated HU-associated losses in this measure of muscle strength compared to both CC groups (Fig 14).

Table 4. Effects of dobutamine (DOB) or vehicle (VEH) administration during hindlimb unloading (HU) or ambulatory cage activity (CC) on cardiac and adrenal mass.

		CC		HU	
		VEH	DOB	VEH	DOB
Tissue Mass (g)					
	Cardiac	1.350 ± 0.038[a]	1.442 ± 0.031[b]	1.294 ± 0.038[a]	1.375 ± 0.039[ab]
	Adrenal	0.030 ± 0.003	0.030 ± 0.001	0.041 ± 0.010	0.061 ± 0.027

CC: normal ambulatory aging controls; HU: hindlimb unloaded; VEH: vehicle (saline) administration; DOB: dobutamine administration (4 mg/kg BW/d, one bolus injection). Values presented are group mean ± standard error of the mean. Those groups not sharing the same letter for each variable are significantly different from each other ($p<0.05$). Group means with no labels are not statistically different.

Loss in bone mass and changes in bone geometry with disuse is attenuated with Adrb1 treatment. In vivo pQCT scans on days -1 and 28 revealed significant reductions in total BMC (-17%), total bone area (-8%), and total vBMD (-9%) at the PTM attributable to unloading (HU-VEH group) (Fig 15A-C). Dobutamine administration during HU (HU-DOB) was unable to mitigate associated reductions in both total BMC (-16%) or total bone area (-10%), but did significantly attenuate the loss in total vBMD (vs. HU-VEH). Additionally, beta-adrenergic agonist treatment significantly increased total bone area (+5%) at the PTM (Fig 15B) in weightbearing controls.

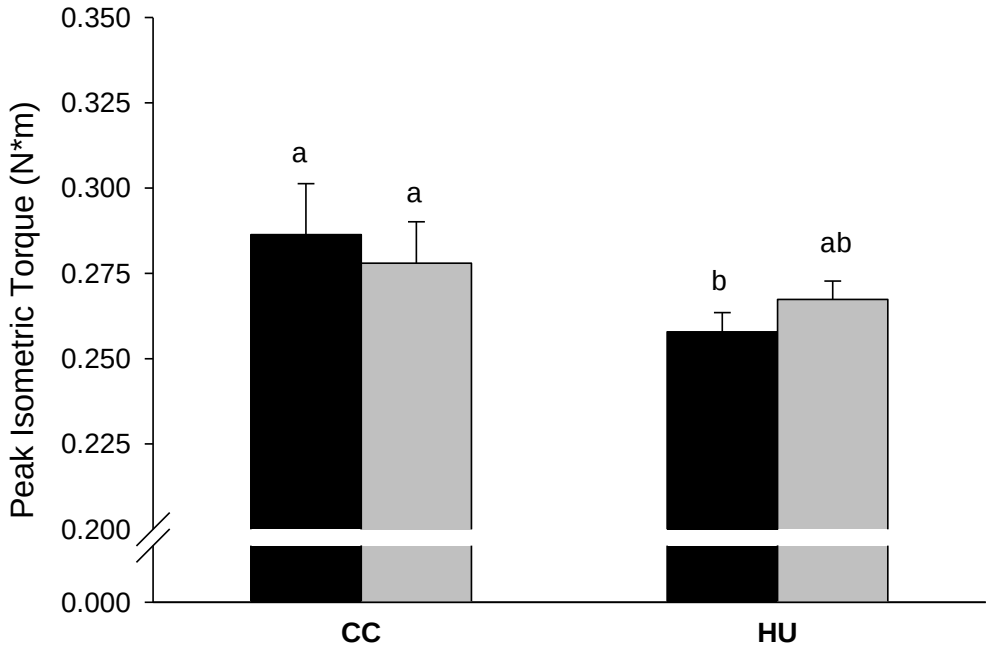

Fig. 14. Effects of dobutamine (DOB) or vehicle (VEH) administration during hindlimb unloading (HU) or ambulatory cage activity (CC) on in vivo measurement of peak isometric torque of the ankle plantarflexor muscles. VEH groups are represented by black bars; DOB groups are represented by gray bars. Values are group mean ± standard error of the mean. Those groups not sharing the same letter for each variable are significantly different from each other ($p<0.05$).

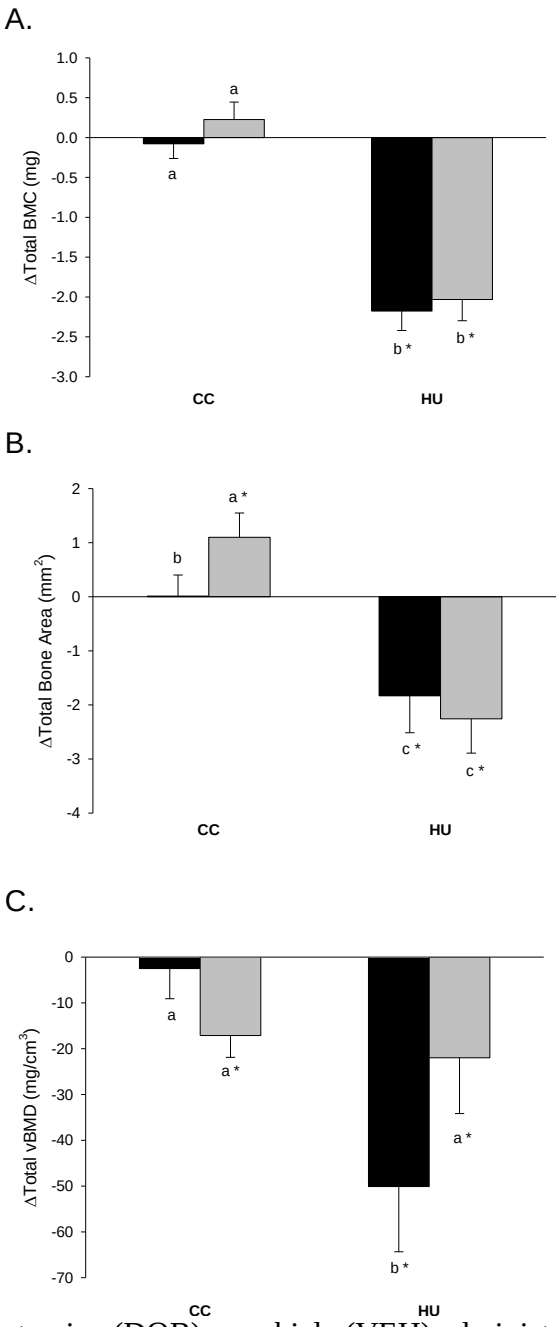

Fig. 15. Effects of dobutamine (DOB) or vehicle (VEH) administration during hindlimb unloading (HU) or ambulatory cage activity (CC) on changes in structural and geometric properties of the proximal tibia metaphysis as taken by in vivo peripheral quantitative computed tomography scans. *A*: Total bone mineral content (BMC). *B*: Total bone area. *C*: Total volumetric bone mineral density (vBMD). VEH groups are represented by black bars; DOB groups are represented by gray bars. Those groups not sharing the same letter for each variable are significantly different from each other ($p<0.05$); *$p<0.05$ vs. day 0 value.

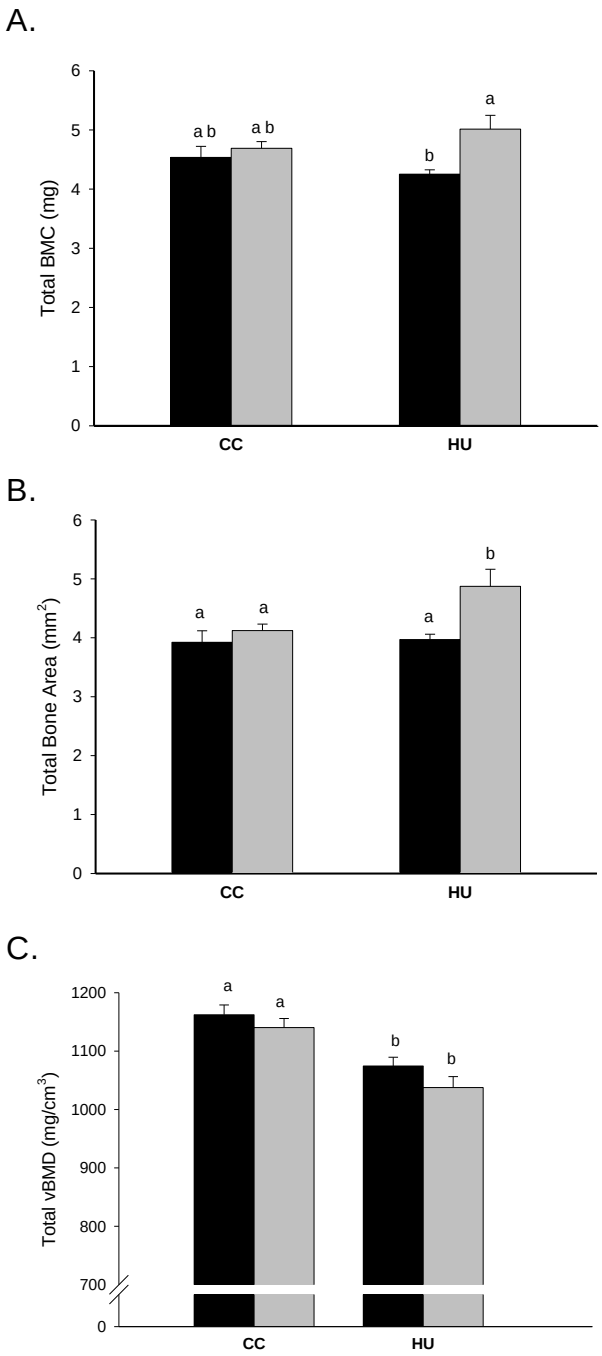

Fig. 16. Effects of dobutamine (DOB) or vehicle (VEH) administration during hindlimb unloading (HU) or ambulatory cage activity (CC) on structural and geometric properties of the femoral neck as taken by ex vivo peripheral quantitative computed tomography scans. *A*: Total bone mineral content (BMC). *B*: Total volumetric bone mineral density (vBMD). *C*: Total bone area. VEH groups are represented by black bars; DOB groups are represented by gray bars. Those groups not sharing the same letter for each variable are significantly different from each other ($p<0.05$).

Ex vivo scans of the femoral neck revealed that DOB administration during HU resulted in significantly greater total BMC and total bone area (18 and 23%, respectively) compared to the HU-VEH group (Fig 16A-B). However, significant HU-induced reductions in total vBMD; this loss was not affected by DOB treatment (Fig 16C). There were no effects of Adrb1 treatment on femoral neck bone in ambulatory cage activity animals.

In vivo pQCT scans of the mid-diaphysis tibia yielded no significant effects on changes in cortical bone structure and geometry with unloading or normal cage activity. However, daily administration of DOB during HU (HU-DOB) significantly increased cortical vBMD (+2%) (data not shown). No changes in tibia cortical bone parameters were evidenced in either ambulatory group.

The effects of disuse and/or Adrb1 treatment on mid-diaphyseal femur cortical bone structure and geometry yielded no significant differences among any of the treatment groups for cortical BMC, cortical area, cortical vBMD, or CSMI (data not shown).

Cancellous bone formation is maintained with Adrb1 receptor agonist administration during unloading. Hindlimb unloading significantly reduced %MS/BS, MAR, and BFR in proximal tibia cancellous bone (Fig 17A-C) by 43%, 26%, and 56%, respectively, vs. that observed in the CC-VEH group. In hindlimb unloaded animals given daily dobutamine treatments, %MS/BS (+105%) and MAR (+35%) were significantly greater than that measured in VEH-treated HU rats (Fig 17A-B). Most

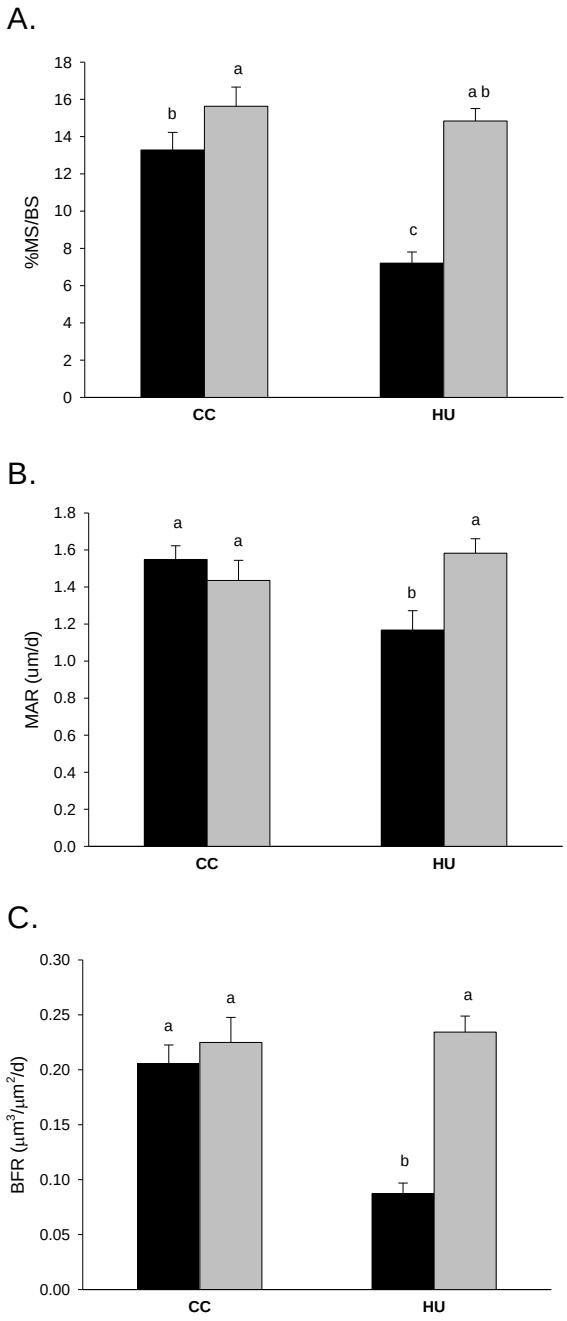

Fig. 17. Effects of dobutamine (DOB) or vehicle (VEH) administration during hindlimb unloading (HU) or ambulatory cage activity (CC) on cancellous bone dynamic histomorphometry analyses measured at the proximal tibia metaphysis. *A*: Mineralizing Surface (%MS/BS). *B*: Mineral Apposition Rate (MAR). *C*: Bone Formation Rate (BFR). VEH groups are represented by black bars; DOB groups are represented by gray bars. Those groups not sharing the same letter for each variable are significantly different from each other ($p<0.001$).

strikingly, cancellous BFR at the PTM was 168% higher in HU-DOB vs. vehicle-treated HU rats (Fig 17C). All three cancellous bone dynamic histomorphometry properties were completely restored to ambulatory control group values by Adrb1 treatment during disuse. DOB administration during normal cage activity did not alter %MS/BS, MAR, or BFR at the PTM. Rare fluorochrome labels were present on trabecular surfaces of HU rats (Fig 18A), whereas DOB treatment during HU resulted in a large amount of labeling (Fig 18B).

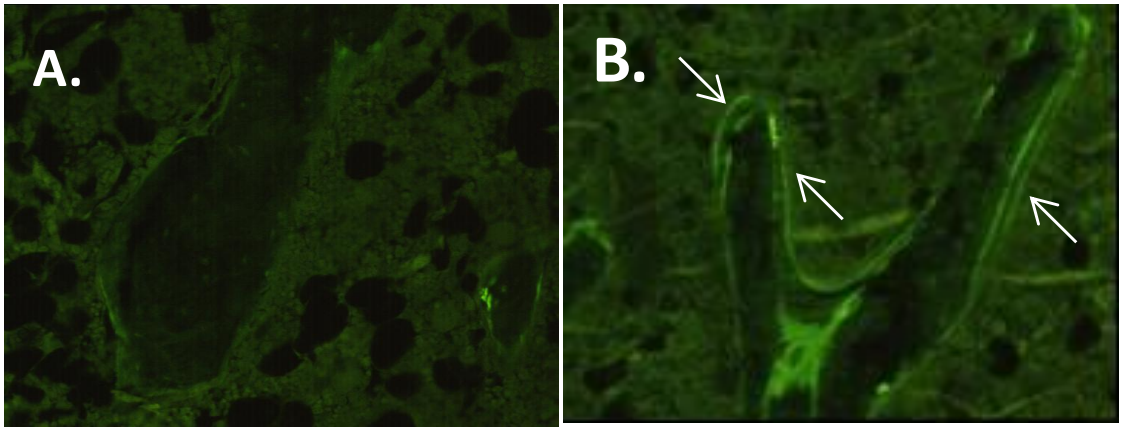

Fig. 18. Visual depiction (100x) of calcein labeling on the surface of cancellous bone located at the proximal tibia metaphysis. *A*: HU+VEH *B*: HU+DOB. Note the extensive flurochrome labeling (arrows) in HU+DOB and large interlabel width.

Adrb1 agonist treatment increases both tibia and femur bone strength during disuse. Mechanical testing of mid-diaphysis femur revealed a 14% reduction in HU-

Table 5. Effects of dobutamine (DOB) or vehicle (VEH) administration during hindlimb unloading (HU) or ambulatory cage activity (CC) on mechanical properties of mid-diaphysis tibia and femur and femoral neck.

	CC		HU	
	VEH	**DOB**	**VEH**	**DOB**
Mid-diaphysis Tibia				
Max Force (N)	120.9 ± 4.5^{bc}	125.5 ± 6.6^{ab}	119.9 ± 3.9^{bc}	137.7 ± 4.1^{a}
Yield Force (N)	100.6 ± 5.4^{ab}	101.5 ± 4.7^{ab}	94.0 ± 2.8^{b}	105.6 ± 3.6^{a}
Elastic Modulus (GPa)	1.6 ± 0.1	1.5 ± 0.1	1.6 ± 0.1	1.6 ± 0.1
Ultimate Stress (MPa)	104.1 ± 3.7	102.9 ± 4.3	102.8 ± 5.2	114.2 ± 7.0
Energy to Max Force (N/mm)	137.3 ± 13.0^{a}	139.6 ± 10.8^{a}	149.1 ± 7.6^{ab}	162.9 ± 8.2^{b}
Mid-diaphysis Femur				
Max Force (N)	246.4 ± 12.3^{ab}	253.7 ± 10.8^{a}	217.9 ± 11.5^{b}	241.2 ± 8.0^{ab}
Yield Force (N)	188.3 ± 5.8^{a}	184.8 ± 8.3^{a}	166.5 ± 6.5^{b}	159.2 ± 10.6^{b}
Elastic Modulus (GPa)	4.8 ± 0.2^{a}	4.7 ± 0.2^{ab}	4.3 ± 0.2^{b}	4.4 ± 0.3^{ab}
Ultimate Stress (MPa)	66.2 ± 6.9^{ab}	67.8 ± 6.4^{a}	63.8 ± 3.1^{a}	62.4 ± 6.4^{ab}
Energy to Max Force (N/mm)	102.3 ± 9.7^{ab}	106.1 ± 9.0^{a}	79.2 ± 9.2^{a}	93.1 ± 4.9^{ab}
Femoral Neck				
Max Force (N)	95.1 ± 5.8^{a}	87.4 ± 5.2^{ab}	81.3 ± 4.3^{b}	101.4 ± 5.2^{a}

CC: normal ambulatory aging controls; HU: hindlimb unloaded; VEH: vehicle (saline) administration; DOB: dobutamine administration (4 mg/kg BW/d, one bolus injection). Values presented are group mean ± standard error of the mean. Those groups not sharing the same letter for each variable are significantly different from each other ($p<0.05$). Group means with no labels are not statistically different.

VEH maximum force vs. CC-DOB (Table 5). Additionally, hindlimb unloading significantly reduced femur elastic modulus by 10% vs. ambulatory cage controls (CC-VEH). DOB treatment during disuse inhibited reductions in mid-diaphysis femur maximum force and elastic modulus. Dobutamine treatment during hindlimb unloading significantly enhanced tibial mid-diaphysis maximum and yield forces vs. HU-VEH (+10 and 12%, respectively).

Hindlimb unloading significantly reduced femoral neck maximum force (15%) vs. CC-VEH. This reduction in strength was abolished by DOB treatment during HU, resulting in a 25% higher max force vs. the mean value in HU-VEH animals (Table 5).

Discussion

The main objective of this study was to determine the effects of a beta-1 adrenergic agonist (Adrb1) on disuse-induced bone loss. We hypothesized that daily treatment of dobutamine (DOB), an Adrb1 agonist, during hindlimb unloading (HU) would diminish disuse-associated reductions in unweighted bone mass, and strength, and that these effects would be enhanced during normal gravitational loading.

This experiment is the first to demonstrate that DOB administration during disuse significantly blunts the catabolic effect of HU on bone mass at a mixed bone site (proximal tibia). Most significantly, daily DOB treatment during HU not only attenuated but abolished reductions in cancellous bone formation at the proximal tibia metaphysis (PTM) observed in vehicle-treated HU rats; both , mineral apposition rate and % mineralizing surface were enhanced as compared to HU-VEH (Fig 17A-C).

Additionally, we observe similar effects of this beta-agonist on disuse bone loss at another mixed bone site (femoral neck) in the unloaded hindlimb (Table 5; Fig 16A). The maintenance of bone formation at the PTM in the HU-DOB group mitigated reductions in vBMD as compared to vehicle (VEH) treatment (Fig 15C). DOB treatment during HU also resulted in significant fat, but not lean mass losses, resulting in significant reductions in total body mass (Fig 13). Furthermore, dobutamine administration during unloading attenuated reductions in lower leg muscle strength (Fig 14). Thus, our data demonstrate that daily Adrb1 agonist administration during disuse can effectively mitigate reductions in metaphyseal bone mass by maintaining cancellous bone formation.

Previous studies testing the efficacy of β-2 adrenoreceptor agonists have found no benefit in preventing bone loss due to estrogen deficiency or to disuse. Salbutamol, a selective Adrb2 agonist, is unable to inhibit ovariectomy-induced reductions in femur BMD and trabecular bone microarchitecture, resulting in decreased trabecular number and thickness (80). Zeman et. al. (130) demonstrated the ineffectiveness of another Adrb2 agonist, clenbuterol, in attenuating losses in tibia or femur bone mass during hindlimb unloading or in ovariectomized rats. However, clenbuterol was able to mitigate reductions in lower leg bone mass after surgical denervation. These data suggest that activation of Adrb2 receptors during reduced mechanical loading or estrogen deficiency does not result in any beneficial effects on cancellous bone.

We speculate that the positive effects of a β-1 adrenergic receptor agonist treatment on metaphyseal bone during disuse may be a function of reduced prevalence of

osteoblast and osteocyte apoptosis. Reductions in metaphyseal bone mass during hindlimb unloading are associated with significant and immediate increases in cancellous and cortical osteocyte apoptosis in unweighted proximal tibiae by day 3 of HU, which effect persisted for 18 days (106,107,120). Isoproterenol, an Adrb agonist (equally stimulating Adrb1 and Adrb2 receptors) has anti-apoptotic effects on cultured osteoblasts (131). Adrb1 stimulation may attenuate increases in mechanosensing osteocytes and osteoblasts, providing an explanation for the lack of reduction in cancellous bone formation in unloaded animals administered dobutamine. Evaluation of changes in osteocyte and osteoblast apoptosis, as well as bone marrow stromal cell differentiation within metaphyseal region of unweighted bone would be desirable.

We hypothesized that DOB treatment would mitigate reductions in bone mass during HU and that any effects on bone geometry or mass would be further enhanced with normal weightbearing activity in control animals. Although we did demonstrate that Adrb1 receptor agonist treatment attenuated reductions in disuse-sensitive metaphyseal bone, our data do not support the latter hypothesis. Dobutamine given during normal gravitational loading did not stimulate any additional gains in cortical or cancellous bone mass or strength as compared to the CC-VEH group. Cancellous bone mineralizing surface was greater in animals treated with DOB, but without any concordant effect on mineral apposition rate, there was no increase in bone formation rate (Fig 17 A,C).

Data from this investigation demonstrates no deleterious effects of beta-1 adrenergic agonist administration on bone during normal ambulatory activity. There

was a significant decrease in CC-DOB total vBMD at the proximal tibia, but this reduction was not significantly different from the CC-VEH group (Fig 15C). Furthermore, the mild reduction in CC-DOB total vBMD was attributable to a greater increase in proximal tibia total bone area as compared to total BMC (Fig 15A-B). Numerous other investigations have revealed significant reductions in bone mass and microarchitecture with β-2 adrenergic agonist administration. Previous studies have observed diminished tibia and femur metaphyseal BMD, trabecular bone microarchitecture, and diaphyseal bone strength in animals chronically administered clenbuterol or salbutamol (78,79,132). These detrimental effects are attributable to an increase in bone resorption, and not reduced formation (133). Contrary to these results, our data demonstrate that Adrb1 agonist administration does not result in deleterious effects on cortical or cancellous bone during normal gravitational loading, consistent with our previous findings (77).

Data from this investigation indicate that, during a period of reduced mechanical loading, dobutamine's effects are more pronounced in primarily cancellous bone compartments than at cortical bone sites. Hindlimb unloaded animals given DOB exhibited mitigated reductions in proximal tibia vBMD (Fig 15C) and higher cancellous bone formation than in vehicle-treated unloaded animals (Fig 17C). Most significantly, femoral neck BMC and bone area (Fig 16), and maximal force during mechanical testing were greater in dobutamine-treated HU rats vs. vehicle-treated unloaded animals, contributing to significantly higher femoral neck strength in the former group (Table 5). The only benefits observed to purely cortical bone sites were a slight increase in tibia

cortical vBMD (data not shown) and mid-diaphysis bone strength (Table 5); otherwise, Adrb1 agonist treatment during disuse did not result in any further enhancement of cortical bone properties.

There were several limitations in the current study. This investigation utilized a non-specific Adrb agonist (dobutamine), which may have some effects on beta 2 receptor-mediated functions. Although dobutamine functions primarily as an Adrb1 agonist, future studies involving a specific Adrb1 agonist are necessary for definitively characterizing these effects. Beta-2 adrenergic (Adrb2) stimulation increases bone resorption and results in significantly reduced bone mass, whereas Adrb2-deficient mice display a high bone mass phenotype with increased cancellous BV/TV as compared to wild-type littermates (67,69). Dobutamine's ability to stimulate Adrb2's on osteoblasts may have contributed to the reduced metaphyseal vBMD during unloading as compared to ambulatory controls (Fig 15C). An Adrb1 agonist, with no stimulation of Adrb2s, may demonstrate greater attenuation in losses of cancellous bone during disuse. Secondly, in this study, we did not assess the effect DOB administration on trabecular bone microarchitecture. Assessment of metaphyseal bone structure and bone cell surfaces are necessary to fully elucidate the effects of Adrb1 receptor agonist stimulation on metaphyseal bone during disuse.

The ability of DOB to attenuate reductions in metaphyseal bone mass during 28-day HU may be related to some mitigation of the reduced blood flow to bone during unloading. Perfusion pressure and increased vascular resistance in unweighted tibia and femur bones are observed within 10 minutes of assuming the head-down posture of

hindlimb unloading, with maintained adverse effects with 28 days of continued suspension (134). Distal femur and proximal tibia blood flow are reduced by ~40% after a 28-day HU protocol (135). Dobutamine has previously been shown to increase hindlimb blood flow during normal ambulation (136). Maintained bone blood flow to unweighted tibiae with DOB treatment may be an alternate explanation for the attenuated reductions in metaphyseal bone mass.

In summary, β-1 adrenergic receptor agonist administration during disuse attenuates reductions in metaphyseal bone mass by effectively maintaining cancellous bone formation. Dobutamine treatment significantly increased mid-diaphyseal tibia cortical vBMD in and during 28-day HU, resulting in increased bone strength as compared to VEH-treated unloaded rats. Importantly, contrary to documented effects of β-2 agonist treatment, we found no deleterious effects of dobutamine on cortical or cancellous bone with normal ambulation. These data demonstrate a potential role for β-1 adrenergic signaling in the bone response to mechanical unloading. Further investigations are necessary to define the exact mechanisms responsible for the positive effects of dobutamine or more specific Adrb1 agonists on disuse-induced bone loss.

CHAPTER VI

BETA-ADRENGERIC AGONIST ADMINISTRATION MITIGATES NEGATIVE CHANGES IN CANCELLOUS BONE MICROARCHITECTURE AND INIHIBITS OSTEOCYTE APOPTOSIS DURING DISUSE

Introduction

Osteoporosis is a debilitating skeletal disorder reportedly affecting nearly 44 million in the United States alone (137). Fragility fractures common in those with advanced osteoporosis can result in a reduced quality of life (138-141). Recently, it has been estimated that the cost associated with treating new osteoporotic fractures in the US will total $16.9 billion (142). Furthermore, a significant number of osteoporotic patients are bedridden, resulting in greater risk for debilitating secondary physiological effects and even death (143).

Similar to the effects of prolonged bed rest in humans, rodent hindlimb unloading (HU) significantly reduces cancellous bone mass and leads to deleterious changes in microarchitecture due to early increases in bone resorption followed by prolonged depressions in bone formation rate (BFR) (21-24). Unloading-associated reductions in metaphyseal bone mass are associated with increased osteocyte and osteoblast apoptosis. Dramatic increases are observed in the number of apoptotic osteocytes in cancellous bone as early as 3 days after initiation of HU (106,107). Additionally, HU increases the Bax/Bcl-2 (pro- and anti-apoptotic proteins) ratio by 2-fold in metaphyseal bone which may be responsible for the increased prevalence of osteoblast and osteocyte apoptosis

(120). Isoproterenol, an Adrb agonist (equally stimulating Adrb1 and Adrb2 receptors), has been found to have anti-apoptotic effects on cultured osteoblasts (131). Taken together, these data suggest that reducing osteocyte apoptosis during the early stages of unloading may be an effective strategy to preserve cancellous bone mass and maintain osteoblast function.

Although stimulation of the SNS has been documented to increase bone resorption, resulting in reduced cancellous bone mass and microarchitecture, this has been primarily attributed to stimulation of beta-2 adrenergic (Adrb2) receptors (78-80,144). However, the exact role that beta-1 adrenergic (Adrb1) receptors have in this process has not been elucidated. Dobutamine (DOB), primarily an Adrb1 receptor agonist, significantly blunts HU-induced reductions in cortical bone area and cross-sectional moment of inertia (CSMI), as well as mitigating the decreases in femoral mid-diaphyseal cortical bone MAR (77). Furthermore, we have previously demonstrated the ability of DOB to inhibit reductions of cancellous bone formation and mitigate losses in bone mass at the proximal tibia and femoral neck (145,146). Demonstrating a direct relationship between alterations in osteoblast activity, osteocyte apoptosis, and cancellous microarchitecture resulting from Adrb1 agonist administration during hindlimb unloading may provide useful insights into underlying mechanisms involved in disuse-induced bone loss.

Hence, the purpose of the current project was to characterize the independent and combined effects of DOB and hindlimb unloading on cancellous bone microarchitecture, osteoblast activity, and osteocyte apoptosis. Furthermore, we sought to define the

effects of DOB on the expression of pro- and anti-apoptotic genes within metaphyseal bone during normal weightbearing activity and during disuse. We hypothesized that unloading would increase the BAX/Bcl-2 ratio and osteocyte apoptosis in animals experiencing metaphyseal bone loss and that DOB administered during HU would mitigate deleterious changes in cancellous bone microarchitecture and increase osteocyte cell survival.

Materials and Methods

Animals and Experimental Design

Thirty-six male Sprague-Dawley rats were obtained from Harlan (Houston, TX) at 6 months of age and allowed to acclimate to their surroundings for 14 days prior to initiation of the study. All animals were housed in a temperature-controlled (23 ± 2ºC) room with a 12-hour light-dark cycle in an American Association for Accreditation of Laboratory Animal Care-accredited animal care facility and were provided standard rodent chow (Harlan Teklad 8604) and water ad-libitum. Animal care and all experimental procedures described in this investigation were conducted in accordance with the Texas A&M University Laboratory Animal Care Committee rules.

All animals were randomly assigned to one of two activity groups according to body mass on day -1: normal ambulatory cage activity (CC; n=18) or hindlimb unloading (HU; n=18). Each activity group was further divided by random assignment to either one daily, bolus intraperitoneal (IP) injection of 4 mg/kg body mass/day dobutamine solution (DOB; n=9) or an equal volume of inactive saline solution (VEH;

n=9), which was administered within the first 2 hours of the animals' dark cycle. Dobutamine hydrochloride solution (Sigma-Aldrich Corp.) was made daily and stored, along with saline solution, at 4ºC until usage.

Calcein injections (25 mg/kg body mass) were given subcutaneously on 9 and 2 days prior to sacrifice to label mineralizing bone for histomorphometric analyses. HU animals were anesthetized before removal from tail suspension at the end of the study to prevent any weight bearing by the hindlimbs. At necropsy, both right and left soleus, plantaris, and gastrocnemius muscles were excised and wet weights were recorded. Right femur were removed, cleaned of soft tissue, and stored at 4°C in 70% ethanol for ex vivo μCT and pQCT scans and subsequent histomorphormetry, whereas distal right femur were stored in paraformaldehyde for paraffin embedding. Right tibia were extracted, cleaned of soft tissue, and immediately frozen in liquid nitrogen and stored at -80°C for mRNA analysis.

Hindlimb Unloading

Hindlimb unloading was achieved by tail suspension as previously described (21,105). Briefly, while the rat was under anesthesia, the tail was cleaned and dried thoroughly. A thin layer of adhesive (Amazing Goop, Eclectic Products, LA) was applied to the proximal half of the tail along the medial and lateral sides. A standard porous tape (Kendall, Mansfield, MA) harness was pressed firmly to the glue and allowed to dry (~30 min). A paper clip was used to attach the animal's tail harness to a swivel apparatus on the wire spanning the top of an 18" x 18" x 18" cage. The height of

the animal's hindquarters was adjusted to prevent any contact of the hindlimbs with the cage floor, resulting in approximately a 30° head-down tilt. The forelimbs of the animal maintained contact with the cage bottom, allowing the rat full access to the entire cage.

Ex vivo Micro Computed Tomography (μCT)

Microarchitecture of cancellous bone located in the distal left femur was determined using a Skyscan 1172 (Kontich, Belgium) high-resolution desk-top micro-computed tomography system. Bones were wrapped in parafilm to prevent drying during the scanning. Scans were obtained using an x-ray source set at 60kV and 167 μA over an angular range of 180 degrees (rotational steps of 0.40 degrees) with a 6 μm pixel size. Projection images were reconstructed using standard Skyscan software. The trabecular bone compartment was segmented from the cortical shell for 50 slices in a region ~0.5 mm below the most distal portion of the growth plate for each animal. Outcomes variables include bone volume/tissue volume (BV/TV, %), trabecular number (Tb.N, μm^{-1}), and trabecular thickness (Tb.Th, μm). Values of topological parameters were calculated to describe the 3D orientation of the trabecular bone. Trabecular pattern factor (Tb.Pf) representing the amount of concave (plate-shaped bone) and convex (rodlike bone) structures was calculated; the higher the Tb.Pf, the more trabecular bone is organized in the form of rodlike structures. The structure modeling index (SMI) was measured for the prevalence of platelike or rodlike structures, where 0 represents "plates" and 3 represents "rods."

Ex vivo Peripheral Quantitative Computed Tomography (pQCT)

Scans were performed ex vivo at the distal metaphysis of the left femur with a Stratec XCT Research-M device (Norland Corp., Fort Atkinson, WI), using a voxel size of 70 μm and a scanning beam thickness of 500 μm. Daily calibration of this machine was performed with a hydroxyapatitie standard cone phantom. Transverse images of the right femur were taken at 4.5, 5.0, 5.5, and 6.0 mm from the distal femur plateau. A standardized analysis for metaphyseal bone (contour mode 3, peel mode 2, outer threshold of 0.214 g/cm^3, inner threshold of 0.605 g/cm^3) was applied to each section. Femora were placed in a 70% ethanol filled vial during the course of the scan. Values of total and cancellous volumetric bone mineral density (vBMD), total bone mineral content (BMC) and total bone area were averaged across slices at each bone site to yield a mean value.

Histomorphometry Analysis

Undemineralized proximal left femur were subjected to serial dehydration and embedded in methylmethacrylate (Sigma Aldrich, Inc.; Milwaukee, WI, USA). Serial frontal sections were cut 8 μm thick and left unstained for fluorochrome label measurements. Additionally, 4 μm thick sections treated with von Kossa staining were used for measurement of cancellous bone volume normalized to tissue volume (%BV/TV), and osteoid (OS/BS), osteoblast (Ob.S/BS), and osteoclast (Oc.S/BS) surfaces as a percent of total cancellous surface. Adipocyte density was calculated as number of adipocytes (Ad.N) divided by the marrow area (Ma.Ar) of the region of

measurement. The histomorphometric analyses were performed by using the OsteoMeasure Analysis System, Version 1.3 (OsteoMetrics, Atlanta, GA). A defined region of interest was established ~1 mm from the growth plate and within the endocortical edges encompassing 8-9 mm^2 at x40 magnification. Total bone surface (BS), single labeled surface (SLS), double-labeled surface (DLS), interlabel distances, bone volume, and osteoid/osteoclast/osteoblast surfaces were measured at x200 magnification. Mineral apposition rate (MAR, μm/day) was calculated by dividing the average interlabel width by the time between labels (7 days), and mineralizing surface (MS) for cancellous bone surfaces (BS) was calculated by using the formula %MS/BS = {[(SLS/2) + DLS]/surface perimeter} X 100. Bone formation rate (BFR) was calculated as (MAR x MS/BS). All nomenclature for cancellous histomorphometry follows standard usage (114).

Osteocyte Apoptosis

Distal left femora were fixed in 4% phosphate-buffered formalin for 48 hours at 4°C and then decalcified in 10% EDTA and 4% phosphate-buffered formalin for 14 days. Following decalcification, the distal left femora were embedded in paraffin and serial frontal sections were cut 10 μm thick and mounted on slides. Apoptosis of osteocytes were detected by in situ terminal deoxynucleotidyl transferase dUTP nick end labeling (TUNEL) using the DNA fragmentation TdT enzyme and fluorescein-dUTP label (Roche Diagnostics Corp., Indianapolis, IN) in distal femoral sections counterstained with hematoxylin QS (Vector Laboratories; Burlingame, CA).

Quantification of osteocytes within individual trabeculae was performed by using the OsteoMeasure Analysis System, Version 1.3 (OsteoMetrics, Atlanta, GA). A defined region of interest was established ~1 mm from the growth plate and within the endocortical edges encompassing 8-9 mm^2 at x40 magnification. Positive staining consisted in sections treated with DNase I (Roche Diagnostics Corp., Indianapolis, IN). Negative controls consisted of sections which were not incubated with the substrate. Apoptotic osteocytes were characterized by TUNEL-stained nucleus with condensed chromatin. The total number of osteocytes (N.Ot) within the region was first counted (under normal light), followed by identification of TUNEL+ osteocytes using ultraviolet light at 200x magnification. The number of apoptotic osteocytes was quantified in the metaphysis in the same area as for other histomorphometry variables, and was evaluated as percentage of total osteocytes.

RNA Extraction and Quantitative Real-Time PCR (RT-PCR)

Right tibiae metaphyses (proximal 25% of bone) were pulverized using a SPEX freezer mill (Model 6750; Metchum, NJ, USA) cooled with liquid nitrogen. The bone powder was suspended and isolated using RNA STAT-60 reagent (Tel-Test, Inc; Friendswood, TX, USA) and samples were then centrifuged at 12,000 g for 10 min at 4°C to precipitate RNA. Total RNA was isolated, dried, and samples were centrifuged at 7,500 g for 5 min. Samples were dried again, and then dissolved in diethylpyrocarbonate (DEPC)-treated water before their concentration was measured using a Nano-Drop spectrophotometer (ND-1000; Wilmington, DE, USA) to insure that

the A260/A280 (sample purity) ratio was > 1.6. One μg of total RNA from each sample was reverse transcribed using the Taqman RT Reagents gene expression assay kit (Applied Biosystems, Inc.; Branchburg, NJ, USA) with oligo (dT) primers. The resulting cDNA portions of the Bax, Bcl-2, and 18S sequences were amplified using Taqman RT Reagents kit. RT-PCR analysis was performed using the program SDS 2.2.2 on using a 7900 HT Fast Real-time PCR System (Applied Biosystems, Inc.; Foster City, CA, USA). For each reaction, 1-4 μl of the total RT product was amplified using the SYBR green master mix (Applied Biosystems, Inc.; Branchburg, NJ, USA) in a total of 20 μl reaction volume according to the manufacturer's standard cycling conditions. The –fold change in expression is calculated using a ΔΔCt comparative threshold cycle method. The BAX/Bcl-2 mRNA content ratio was subsequently calculated for each sample.

A negative control, consisting of sterile water, was used in place of RNA and ensured no contamination of reaction materials. 18S was used as a housekeeping gene control. Relative expression levels of Bax and Bcl-2, relative to 18S, were calculated. Primers specific for Bax and Bcl-2 were designed and purchased from Elim Biopharmaceuticals, Inc. (Hayward, CA, USA), and all were previously used in published investigations (147,148). The sequences are as follows: 5'-ATC ATG AAG ACA GGG GCC TT-3' (*Bax*, forward), 5'-TCT GGA AGA AGA TGG GCT GA-3' (*Bax*, reverse), 5'-CAG CAT GCG ACC TCT GTT TG-3' (*Bcl-2*, forward), 5'-TCT GCT GAC CTC ACT TGT GG-3' (*Bcl-2*, reverse), 5'-CCT GTA ATT GGA ATG AGT

CCA CTT T-3' (*18S*, forward), and 5'-ATA CGC TAT TGG AGC TGG AAT TAC C-3' (*18S*, reverse).

Statistical Analyses

All data were expressed as means ± SEM, and their statistical relationships were evaluated using the statistical package SPSS (v.15). Ex vivo μCT and pQCT, histomorphometry, mRNA content, and osteocyte apoptosis data were analyzed using a two-factor ANOVA (drug and gravity). When a significant main effect was found, Tukey's post-hoc analyses were performed for pairwise comparisons. For all data, statistical significance was accepted at $p<0.05$.

Results

Reductions in metaphyseal bone microarchitecture and mass during unloading are mitigated with Adrb1 treatment. To assess changes in cancellous bone microarchitecture, ex vivo μCT scans were performed on the distal femur. Unloading resulted in significantly lower BV/TV (-33%), Tb.Th (-11%), and Tb.N (-25%) compared to ambulatory controls (CC-VEH) (Table 6, Fig 19). Additionally, both Tb.Pf (+54%) and SMI (+21%) were significantly greater than in the CC-VEH group, signifying more rod-like trabeculae. Adrb1 treatment during disuse attenuated these changes in cancellous bone microarchitecture. BV/TV (+29%), Tb.Th (+7%), and Tb.N (+21%) were significantly greater in DOB-treated vs. VEH-treated animals subjected to disuse. In addition, SMI was 8% lower in animals administered DOB during HU (vs.

Table 6. Effects of dobutamine (DOB) or vehicle (VEH) administration during hindlimb unloading (HU) or ambulatory cage activity (CC) on cancellous bone microarchitecture and structure as measured by ex vivo microCT scans.

	CC		HU	
	VEH	DOB	VEH	DOB
BV/TV (%)	20.23 ± 1.36^{ab}	21.05 ± 1.24^{a}	13.46 ± 0.74^{c}	17.42 ± 0.96^{b}
Tb.Th (mm)	93.10 ± 2.09^{ab}	96.04 ± 1.39^{a}	83.36 ± 1.95^{c}	89.08 ± 1.91^{b}
Tb.N (mm^{-1})	2.16 ± 0.12^{a}	2.19 ± 0.11^{a}	1.61 ± 0.08^{b}	1.95 ± 0.09^{a}
Tb.Pf (mm^{-1})	8.99 ± 0.77^{a}	8.48 ± 0.61^{a}	13.88 ± 0.56^{b}	11.21 ± 0.71^{b}
SMI	1.64 ± 0.07^{a}	1.62 ± 0.06^{a}	1.98 ± 0.05^{c}	1.81 ± 0.05^{b}

Those groups not sharing the same letter for each variable are significantly different from each other ($p<0.05$)**.**

Table 7. Effects of dobutamine (DOB) or vehicle (VEH) administration during hindlimb unloading (HU) or ambulatory cage activity (CC) on metaphyseal bone mass and geometry at the proximal tibia as measured by ex vivo pQCT scans.

	CC		HU	
	VEH	DOB	VEH	DOB
Total BMC (mg)	12.19 ± 0.42^{a}	12.03 ± 0.29^{a}	10.10 ± 0.25^{c}	10.87 ± 0.27^{b}
Total Bone Area (mm^{2})	20.61 ± 0.76	20.25 ± 0.40	19.18 ± 0.61	20.49 ± 0.54
Total vBMD (mg/cm^{3})	593.33 ± 11.33^{a}	595.20 ± 11.58^{a}	531.02 ± 16.39^{b}	533.32 ± 11.26^{b}
Cancellous vBMD (mg/cm^{3})	329.29 ± 15.27^{a}	320.25 ± 12.12^{a}	245.96 ± 7.77^{b}	271.85 ± 6.50^{c}

Those groups not sharing the same letter for each variable are significantly different from each other ($p<0.05$)**.** Group means with no labels are not significantly different.

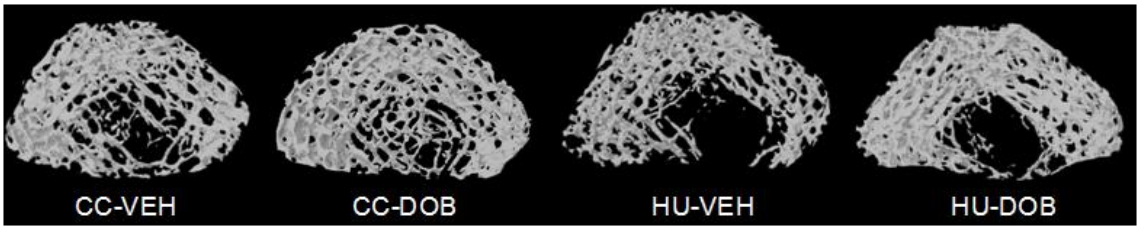

Fig. 19. Representative three-dimensional μCT images of the distal femoral metaphysis in dobutamine- (DOB) or vehicle- (VEH) treated rodents during hindlimb unloading (HU) or ambulatory cage activity (CC).

HU-VEH), indicating less of a shift towards rod-like trabeculae than in HU-VEH rats. There was no effect of Adrb1 agonist treatment on trabecular bone microarchitecture in weightbearing control rats.

Hindlimb unloading resulted in significantly reduced total BMC (-17%) and vBMD (-11%) and cancellous vBMD (-25%) as compared to ambulatory controls (CC-VEH; Table 7). DOB administration during disuse mitigated reductions in two of these parameters, resulting in greater total BMC (+8%) cancellous vBMD (+11%) compared to VEH-treated animals subjected to disuse (HU-VEH). There was no effect of either unloading or DOB on bone area. Adrb1 agonist administration did not affect metaphyseal bone mass or geometry in weightbearing cage control animals.

Adrb1 administration during disuse inhibits reductions in bone formation by maintaining osteoblast surface. Hindlimb unloading produced significantly less OS/BS (-66%) and Ob.S/BS (-49%) and greater adipocyte density (+81%) within bone marrow as compared to ambulatory controls (Fig 20 A, B, D). Adrb1 treatment during

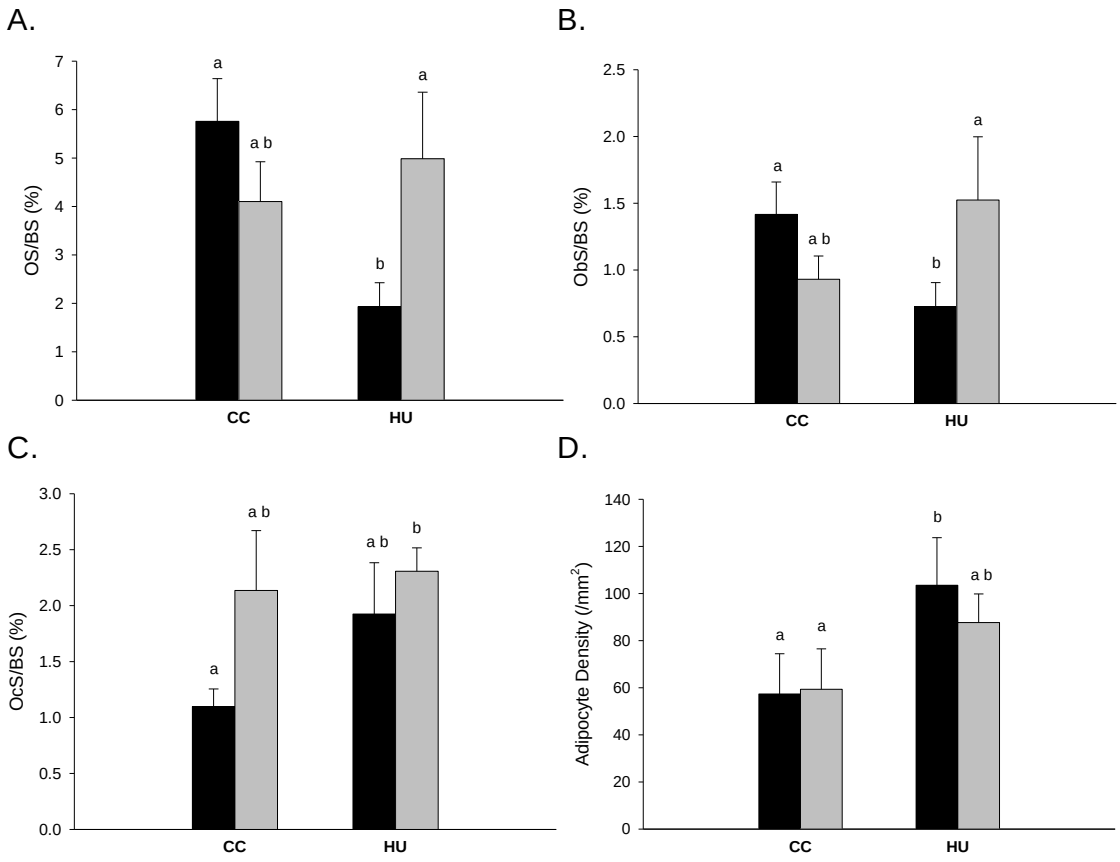

Fig. 20. Effects of dobutamine (DOB) or vehicle (VEH) administration during hindlimb unloading (HU) or ambulatory cage activity (CC) on cancellous bone measures of histomorphometry. *A*: Osteoid Surface (OS/BS). *B*: Osteoblast Surface (ObS/BS). *C*: Osteoclast Surface (OcS/BS). *D*: Adipocyte Density (N.Ad/Ma.Ar). VEH groups are represented by black bars; DOB groups are represented by gray bars. Those groups not sharing the same letter for each variable are significantly different from each other ($p<0.05$).

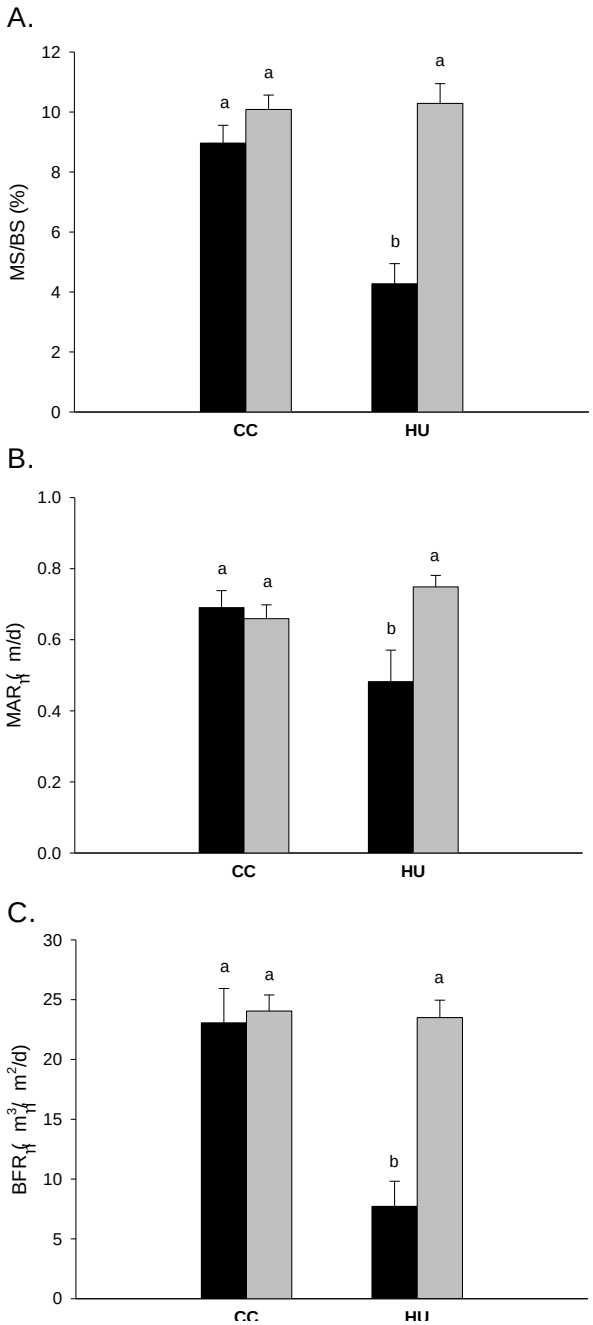

Fig. 21. Effects of dobutamine (DOB) or vehicle (VEH) administration during hindlimb unloading (HU) or ambulatory cage activity (CC) on cancellous bone measures of histomorphometry. *A*: Mineralizing Surface (%MS/BS). *B*: Mineral Apposition Rate (MAR). *C*: Bone Formation Rate (BFR). VEH groups are represented by black bars; DOB groups are represented by gray bars. Those groups not sharing the same letter for each variable are significantly different from each other ($p<0.05$).

HU resulted in significantly greater OS/BS (+158%) and Ob.S/BS (+110%) vs. VEH-treated animals subjected to HU. Furthermore, Oc.S/BS was significantly greater in HU-DOB (+110%) vs. CC-VEH group (Fig 20C). DOB administration did not affect any of these parameters in weightbearing cage controls.

Adrb1 treatment during disuse inhibited unloading-induced reductions in MS/BS, MAR, and cancellous BFR, which were 52%, 30%, and 67% lower, respectively, in HU-VEH group as compared to ambulatory controls (Fig 21 A-C). DOB treatment during unloading resulted in significantly greater MS/BS (+2.4-fold), MAR (+55%), and BFR (+3-fold) than in vehicle-treated unloaded rats. Adrb1 agonist administration did not affect dynamic histomorphometry measures of bone formation activity in weightbearing cage controls.

Increased osteocyte apoptosis during rodent hindlimb unloading is abolished with Adrb1 treatment. In situ nick-end labeling was used to determine the prevalence of osteocyte apoptosis within distal femur cancellous bone in rodents subjected to HU and/or Adrb1 agonist treatment. Unloading resulted in a significantly greater percentage of apoptotic cancellous osteocytes (+85%) as compared to both ambulatory control groups (Fig 22). DOB-treatment during disuse prevented this increase in osteocyte apoptosis, which was 36% lower than in vehicle-treated rats. There was no difference in osteocyte apoptosis between the ambulatory control groups.

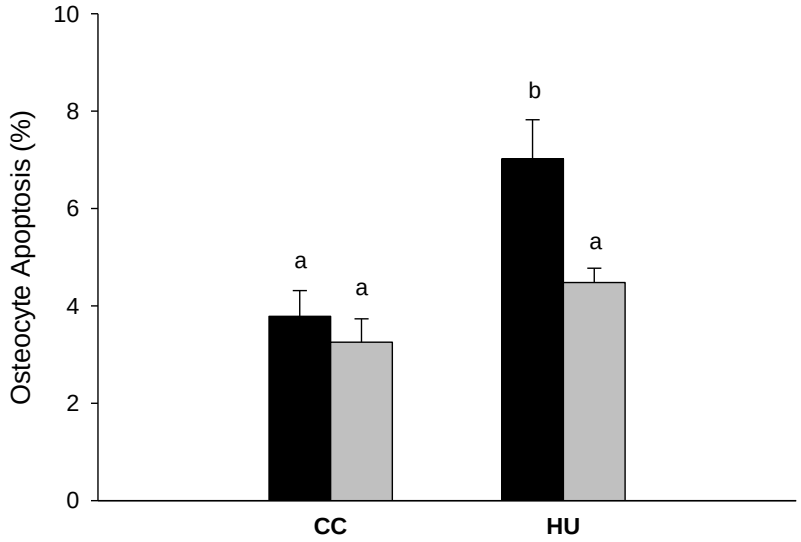

Fig. 22. Effects of dobutamine (DOB) or vehicle (VEH) administration during hindlimb unloading (HU) or ambulatory cage activity (CC) on cancellous bone TUNEL+ osteocytes (%) measured at the distal femur. VEH groups are represented by black bars; DOB groups are represented by gray bars. Those groups not sharing the same letter for each variable are significantly different from each other ($p<0.05$).

Adrb1 treatment during disuse prevents pro-apoptotic state of metaphyseal bone.

To elucidate the molecular bases underlying the effects of DOB treatment on unloading-induced gains in osteocyte apoptosis, mRNA content in the proximal tibia was analyzed. Unloading significantly enhanced the Bax/Bcl-2 mRNA content ratio in bone as compared to the CC-DOB group (Fig 23C). However, DOB-treated animals subjected to unloading did not significantly increase the Bax/Bcl-2 mRNA content ratio in metaphyseal bone. Adrb1 treatment in weightbearing cage control animals did not affect Bax/Bcl-2 levels.

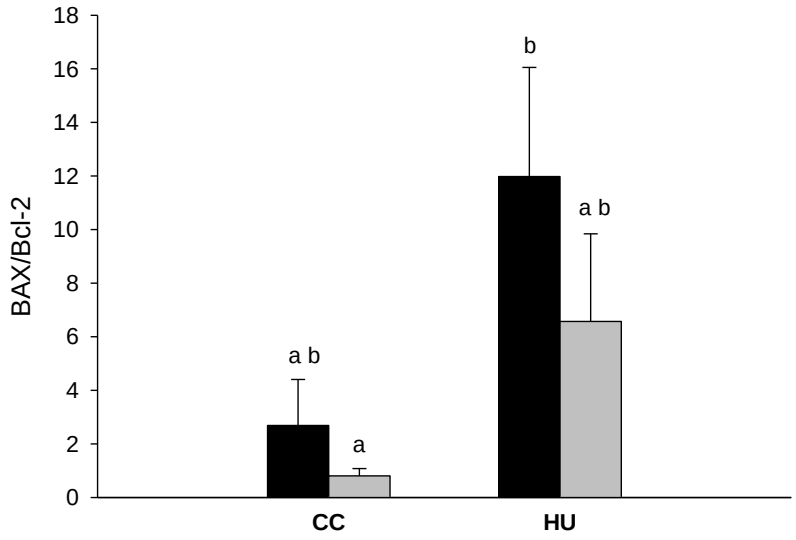

Fig. 23. Effects of dobutamine (DOB) or vehicle (VEH) administration during hindlimb unloading (HU) or ambulatory cage activity (CC) on proximal tibia mRNA content of Bcl-2 associated X protein/Bcl-2 ratio (BAX/Bcl-2). VEH groups are represented by black bars; DOB groups are represented by gray bars. Those groups not sharing the same letter for each variable are significantly different from each other ($p<0.05$). Group means with no labels are not significantly different.

Discussion

The main objective of this study was to determine the effects of a beta-1 adrenergic agonist (Adrb1), dobutamine (DOB), on metaphyseal bone microarchitecture, histomorphometric indices of osteoblast activity, and cell apoptosis. We hypothesized that unloading would result in increased osteocyte apoptosis and metaphyseal bone loss, with an associated increase in the BAX/Bcl 2 ratio, and that DOB administered during

HU would mitigate deleterious changes in cancellous bone microarchitecture and increase osteocyte cell survival.

Most strikingly, our data confirm that dobutamine treatment during unloading inhibited reductions in cancellous bone formation, resulting in attenuated losses in cancellous bone mineral density (vBMD) and bone volume (BV/TV). Dobutamine treatment prevented increased cancellous osteocyte apoptosis and may have mitigated the increase in Bax/Bcl-2 levels evidenced during disuse. We found no effect of DOB treatment on any of these outcomes when it was administered to rats experiencing normal ambulatory cage activity. Taken together, these data demonstrate the dynamic role that beta-1 adrenergic agonist signaling has on maintaining cancellous bone during periods of reduced weightbearing or unloading.

Data from this experiment demonstrate an overall increase in forming and resorbing surfaces with dobutamine treatment during unloading. DOB administration resulted in significantly greater osteoblast (+110%) and osteoid (2.6-fold) surface within cancellous bone of the distal femur as compared to vehicle-treated hindlimb unloaded rodents (Fig 20 A-B). Most strikingly, these increases in osteoblast surface were accompanied by 2.4 to 3-fold greater mineralizing surface and bone formation rate (Fig 3 A, C) and 55% greater mineral apposition rate (Fig 21B) vs. HU-VEH group. Additionally, dobutamine treatment during unloading resulted in significantly greater osteoclast surface (+110%) compared to vehicle treated ambulatory controls (Fig 20C).

Only one investigation each has assessed the effects of Adrb2 receptor agonist treatment on cancellous bone cell activity using ovariectomized (OVX) rodents or mice

subjected to unloading. Salbutamol, a β-2 adrenoreceptor agonist, administered to OVX rodents did not significantly alter osteoblast or osteoclast activity as compared to untreated estrogen deficient rats (80). However, salbutamol-treated OVX animals significantly increased both active bone resorbing and forming surfaces as compared to sham-controls. Mice administered isoproterenol (equally stimulating β-1 and β-2 adrenergic receptors) during unloading exhibit significant reductions in cancellous BV/TV, attributable to significantly lowered bone formation (149). Numerous investigations have demonstrated that Adrb2 receptor agonist administration in weightbearing rats reduces net bone formation by inhibiting osteoblast and increasing osteoclast differentiation. Takeda et al. (75) showed that isoproterenol, a non-specific β-adrenergic agonist, decreased cancellous BV/TV by significantly reducing osteoblast number and bone formation rate (-24-42% vs. controls). Furthermore, salbutamol treatment induced significant reductions in both tibia and femur cancellous bone volume as a consequence of significantly increased osteoclast surface (144). Deletion of all adrenergic receptors in skeletally mature mice results in even greater reductions in distal femur bone formation (-63% vs wild-type littermates) (83). Taken together, these data suggest opposing roles of Adrb1 and Adrb2 receptors on osteoblasts, and that, when activated, Adrb2 receptors inhibit osteoblast activity, whereas signaling via Adrb1 receptors promotes bone formation.

Administration of β-2 adrenergic agonists results in significant and deleterious modifications to cancellous bone microarchitecture. Both salbutamol and clenbuterol treatment significantly reduces metaphyseal bone volume by reducing Tb.Th and

increasing Tb.Sp, resulting in increased rodlike trabecular structures (78,79,144). Trabecular microarchitecture was similarly affected by concurrent Adrb2 administration in OVX rats (80). Data from our current investigation provide evidence for an opposing effect of Adrb1 treatment in the context of disuse. Dobutamine administration significantly mitigated unloading associated reductions in BV/TV by attenuating reduced Tb.Th and Tb.N (Table 6). Furthermore, hindlimb unloading resulted in a prevalence of more rod-like trabecular structures within the distal femur, which change was attenuated with dobutamine treatment. In contrast to the aforementioned deleterious effects of β-2 adrenergic agonists, Adrb1 administration to rats allowed normal cage activity did not produce any significant alterations in cancellous bone microarchitecture.

Reductions in metaphyseal bone mass and structure during hindlimb unloading have been characterized by immediate increases in osteocyte and osteoblast apoptosis. Recent data have demonstrated a significant increase in cancellous osteocyte apoptosis in unweighted proximal tibiae by day 3 of HU, persisting for up to 18 days after disuse (106,107,120). An in vitro study using isoproterenol, an Adrb agonist (equally stimulating Adrb1 and Adrb2 receptors), demonstrated beta-adrenergic stimulation to have anti-apoptotic effects on cultured osteoblasts (131). Data from our investigation provides further evidence that Adrb1-signaling protects osteocytes from apoptosis, as dobutamine treatment during unloading inhibited disuse-induced increases in osteocyte apoptosis in cancellous bone of the distal femur (Fig 22A). Furthermore, our current investigation implies the ability of Adrb1 agonist treatment to potentially mitigate associated increases in Bax/Bcl-2 mRNA content of metaphyseal bone (Fig 23C),

although these data are not definitive. In unloaded animals treated with vehicle, the trend towards increased Bax/Bcl-2 mRNA content of disuse-sensitive cancellous bone was attributable to a significant increase in Bax and no effect on Bcl-2 mRNA. While this finding is in agreement with data of Dufour et al. (120), the earlier study found that the HU-induced increased Bax/Bcl-2 ratio was due to decreased Bcl-2 mRNA content. Data from our current study provide preliminary evidence for the role of adrenergic signaling in inhibiting apoptosis of mechano-sensing cancellous osteocytes, possibly by mitigating increases in Bax mRNA levels during disuse.

Previously we demonstrated that dobutamine treatment during unloading significantly mitigated longitudinal reductions in proximal tibia total vBMD by maintaining bone formation (145,146). Furthermore, data from these studies showed that effects of Adrb1 treatment occurred mainly in cancellous (and mixed bone sites) and not cortical bone compartments of unweighted tibia and femur. However, lacking details about alterations in bone cell activity and cancellous bone microarchitecture, we were unable to adequately describe the effects of Adrb1 administration during normal and reduced gravitational loading. Data from this current study are in agreement with our previous studies, demonstrating that dobutamine treatment maintains cancellous bone formation during disuse. Furthermore, similar to our previous study, we demonstrate that Adrb1 receptor agonist administration mitigates losses in cancellous vBMD at the distal femur.

Hindlimb unloading increases adipocyte number, while simultaneously inhibiting osteoblast differentiation, resulting in increased adipocyte number and volume and

reducing bone mass and strength at the proximal tibia (150-152). Furthermore, beta-adrenergic stimulation has been shown to increase bone marrow adipocyte lipolysis (153). Interestingly, we demonstrated that dobutamine treatment mitigated unloading associated increases in marrow area adipocyte density (Fig 20D). While we did not measure adipocyte differentiation, data from our current study provide preliminary evidence that Adrb1 agonist administration during disuse may reduce adipocyte proliferation and result in increased osteoblast formation and activity (Fig 20, 21).

Knock-out mouse models have demonstrated the potentially unique effects of β-1 and β-2 adrenergic receptors on osteoclasts and osteoblasts, ultimately affecting cancellous bone mass and microarchitecture. Adrb2 and Adrb1 receptor knock-out (KO) mice have demonstrated a high and low bone mass phenotype, respectively, whereas Adrb1/2 receptor double-KO mice exhibit a marked reduction in cancellous BFR vs. wild types (67,82,127). Furthermore, complete deletion of all 3 Adrb receptors results in a significant reduction in bone formation, although trabecular microarchitecture and bone volume remain unchanged (83). Bonnet and colleagues (82) demonstrated that Adrb1 receptor-deficient mice do not respond to mechanical loading, whereas Adrb2 receptor KO mice and wild-type littermates were found to respond normally. Taken together, these data suggest that the higher bone mass phenotype in Adrb2 receptor KO mice may be caused by enhanced β-1 adrenergic receptor activity, stimulating bone formation in the absence of the inhibitory effects of β-2 adrenergic receptors on osteoblasts. Therefore, delineating the effects of Adrb1 receptor stimulation on disuse-

sensitive cancellous bone during reduced mechanical loading is important to defining the underlying mechanisms responsible for bone loss.

There were a few limitations of the current study. To fully elucidate the individual and, potentially, combined effects of disuse and Adrb1 receptor treatment on adrenergic receptors, immunohistochemistry analysis of osteoblast and osteoclast expression of Adrb1 and Adrb2 within weightbearing cancellous bone would be useful in elucidating mechanisms responsible for the effects demonstrated in this study. Additionally, although we did quantify osteocyte apoptosis within cancellous bone of the distal femur, we were unable to describe the effects of Adrb1 treatment during unloading on osteoblast or osteoclast apoptosis.

In conclusion, β-1 adrenergic receptor agonist treatment during unloading significantly impacted metaphyseal bone and inhibited associated increases in apoptosis. DOB administration during disuse abolished reductions in cancellous bone formation and resulted in significantly greater bone volume, trabecular thickness, and trabecular number as compared to vehicle-treated animals. Furthermore, Adrb1 treatment inhibited increased prevalence of apoptotic osteocytes and may have maintained Bax/Bcl-2 levels within cancellous bone during disuse. Similar to our previous findings, we demonstrate no deleterious effects of Adrb1 agonist treatment on cancellous bone during normal ambulation. These data further define the role that β-adrenergic receptors have in mediating bone's response to periods of disuse or unloading. However, further studies are necessary to determine the precise mechanisms involved with adrenergic signaling in bone during disuse.

CHAPTER VII

CONCLUSIONS

The ultimate goals of the first two studies were to determine the role that high intensity muscle contractions and bisphosphonate treatment, initiated during an extended period of mechanical unloading, have on maintaining disuse-sensitive cancellous bone. Eccentric- and combined isometric+eccentric-based simulated resistance training (SRT) protocols were used alone or in combination with alendronate (ALEN) treatment and compared to unloaded controls. The second two studies were completed to determine the role that beta-1 adrenergic (Adrb1) agonist administration has on metaphyseal bone during disuse. Dobutamine (DOB), an Adrb1 receptor agonist, was administered during 28-day hindlimb unloading (HU) or during normal ambulation. Measurements of bone mass and geometry (via pQCT), metaphyseal bone microarchitecture and structure (μCT), dynamic and static histomorphometry, bone biomechanical properties (reduced platen compression and 3-point bending tests), osteocyte apoptosis, and mRNA content of specific genes (real-time quantitative polymerase chain reaction) were used to assess the efficacy of these different treatments.

Data from these investigations document that (1) high-intensity, eccentric-based resistive exercise, begun early during the period of unloading, can prevent the loss of bone mass and muscle strength routinely observed during a period of disuse or exposure to microgravity; (2) ALEN treatment, when combined with high-intensity muscle contractions during disuse, significantly reduces the anabolic response of cancellous

bone to SRT; (3) mechanical loading (due to muscle contractions) and ALEN treatment (acting independently and in combination) inhibit disuse-associated increases in cancellous osteocyte apoptosis; (4) Adrb1 receptor agonist administration during HU attenuates reductions in metaphyseal bone mass by effectively maintaining cancellous bone formation; (5) DOB administration during rodent HU inhibits disuse-associated increases in osteocyte apoptosis by preventing increases in the ratio of Bax/Bcl-2 mRNA content within metaphyseal bone; (6) the mitigation of reductions in metaphyseal bone microarchitecture and cancellous bone mineral density in DOB-treated animals, as compared to unloaded controls, is primarily due to greater increases in bone formation than increased resorption; (7) beta-1 adrenergic receptor agonist administration during normal ambulation is not deleterious to bone.

The first two studies provide preliminary data on the impact that resistance exercise has on maintaining bone mass and strength during periods of disuse or reduced weightbearing activity. Recent data has demonstrated the effectiveness of mechanical loading to significantly diminish sclerostin (SOST) expression within osteocytes using immunohistochemistry (IHC) techniques (154). SOST, a key inhibitory regulating protein in bone, as well as canonical Wnt/β-catenin signaling within osteoblasts may be crucial mediators of unloading-related reductions in bone mass and formation associated with disuse. Future, mechanistically-driven investigations are necessary to outline the effects of resistive exercise during unloading on potential signaling pathways so that effective interventions targeting these proteins can be established and applied to other models attempting to address the mechanisms responsible for osteoporosis.

The second two studies provide preliminary data on the effects of Adrb1 receptor agonist administration during HU and demonstrate the basic cellular mechanisms responsible for the positive effects of DOB treatment. Further research defining the exact role of disuse on Adrb2 and Adrb1 receptors within osteoblasts and osteoclasts is necessary to help explain data from these current investigations and can be accomplished with in situ immunohistochemistry. Additionally, Adrb1receptor knock-out mice studies would help explain the differentiating results on cancellous bone demonstrated in DOB treatment during disuse and normal ambulation. Data from these investigations can help further elucidate those mechanisms responsible for bone loss and potentially assist in determining the exact role of beta-adrenergic signaling within bone cells.

REFERENCES

1. Duque G, Troen BR 2008 Understanding the mechanisms of senile osteoporosis: new facts for a major geriatric syndrome. J Am Geriatr Soc **56**(5)**:**935-41.

2. Sipos W, Pietschmann P, Rauner M, Kerschan-Schindl K, Patsch J 2009 Pathophysiology of osteoporosis. Wien Med Wochenschr **159**(9-10)**:**230-4.

3. Duplomb L, Dagouassat M, Jourdon P, Heymann D 2007 Concise review: embryonic stem cells: a new tool to study osteoblast and osteoclast differentiation. Stem Cells **25**(3)**:**544-52.

4. Silver IA, Murrills RJ, Etherington DJ 1988 Microelectrode studies on the acid microenvironment beneath adherent macrophages and osteoclasts. Exp Cell Res **175**(2)**:**266-76.

5. Leach CS, Rambaut PC, Di Ferrante N 1979 Amino aciduria in weightlessness. Acta Astronaut **6**(10)**:**1323-33.

6. Smith SM, Nillen JL, Leblanc A, Lipton A, Demers LM, Lane HW, Leach CS 1998 Collagen cross-link excretion during space flight and bed rest. J Clin Endocrinol Metab **83**(10)**:**3584-91.

7. Caillot-Augusseau A, Lafage-Proust MH, Soler C, Pernod J, Dubois F, Alexandre C 1998 Bone formation and resorption biological markers in cosmonauts during and after a 180-day space flight (Euromir 95). Clin Chem **44**(3)**:**578-85.

8. Caillot-Augusseau A, Vico L, Heer M, Voroviev D, Souberbielle JC, Zitterman A, Alexandre C, Lafage-Proust MH 2000 Space flight is associated with rapid decreases of undercarboxylated osteocalcin and increases of markers of bone resorption without changes in their circadian variation: observations in two cosmonauts. Clin Chem **46**(8 Pt 1)**:**1136-43.

9. Collet P, Uebelhart D, Vico L, Moro L, Hartmann D, Roth M, Alexandre C 1997 Effects of 1- and 6-month spaceflight on bone mass and biochemistry in two humans. Bone **20**(6)**:**547-51.

10. Smith SM, Wastney ME, O'Brien KO, Morukov BV, Larina IM, Abrams SA, Davis-Street JE, Oganov V, Shackelford LC 2005 Bone markers, calcium metabolism, and calcium kinetics during extended-duration space flight on the mir space station. J Bone Miner Res **20**(2)**:**208-18.

11. Smith SM, Wastney ME, Morukov BV, Larina IM, Nyquist LE, Abrams SA, Taran EN, Shih CY, Nillen JL, Davis-Street JE, Rice BL, Lane HW 1999 Calcium metabolism before, during, and after a 3-mo spaceflight: kinetic and biochemical changes. Am J Physiol **277**(1 Pt 2)**:**R1-10.

12. Smith SM, Heer M 2002 Calcium and bone metabolism during space flight. Nutrition **18**(10)**:**849-52.

13. Holick MF 1998 Perspective on the impact of weightlessness on calcium and bone metabolism. Bone **22**(5 Suppl)**:**105S-111S.

14. Vico L, Collet P, Guignandon A, Lafage-Proust MH, Thomas T, Rehaillia M, Alexandre C 2000 Effects of long-term microgravity exposure on cancellous and cortical weight-bearing bones of cosmonauts. Lancet **355**(9215)**:**1607-11.

15. Lang T, LeBlanc A, Evans H, Lu Y, Genant H, Yu A 2004 Cortical and trabecular bone mineral loss from the spine and hip in long-duration spaceflight. J Bone Miner Res **19**(6)**:**1006-12.

16. Lang TF, Leblanc AD, Evans HJ, Lu Y 2006 Adaptation of the proximal femur to skeletal reloading after long-duration spaceflight. J Bone Miner Res **21**(8)**:**1224-30.

17. Keyak JH, Koyama AK, LeBlanc A, Lu Y, Lang TF 2009 Reduction in proximal femoral strength due to long-duration spaceflight. Bone **44**(3)**:**449-53.

18. Sibonga JD, Evans HJ, Sung HG, Spector ER, Lang TF, Oganov VS, Bakulin AV, Shackelford LC, LeBlanc AD 2007 Recovery of spaceflight-induced bone loss: bone mineral density after long-duration missions as fitted with an exponential function. Bone **41**(6)**:**973-8.

19. Morey ER, Sabelman EE, Turner RT, Baylink DJ 1979 A new rat model simulating some aspects of space flight. Physiologist **22**(6)**:**S23-4.

20. Morey-Holton E, Globus RK, Kaplansky A, Durnova G 2005 The hindlimb unloading rat model: literature overview, technique update and comparison with space flight data. Adv Space Biol Med **10:**7-40.

21. Bloomfield SA, Allen MR, Hogan HA, Delp MD 2002 Site- and compartment-specific changes in bone with hindlimb unloading in mature adult rats. Bone **31**(1)**:**149-57.

22. Allen MR, Bloomfield SA 2003 Hindlimb unloading has a greater effect on cortical compared with cancellous bone in mature female rats. J Appl Physiol **94**(2)**:**642-50.

23. Baek K, Barlow AA, Allen MR, Bloomfield SA 2008 Food restriction and simulated microgravity: effects on bone and serum leptin. J Appl Physiol **104**(4)**:**1086-93.

24. Turner RT, Lotinun S, Hefferan TE, Morey-Holton E 2006 Disuse in adult male rats attenuates the bone anabolic response to a therapeutic dose of parathyroid hormone. J Appl Physiol **101**(3)**:**881-6.

25. Barou O, Palle S, Vico L, Alexandre C, Lafage-Proust MH 1998 Hindlimb unloading in rat decreases preosteoblast proliferation assessed in vivo with BrdU incorporation. Am J Physiol **274**(1 Pt 1)**:**E108-14.

26. Bikle DD, Morey-Holton ER, Doty SB, Currier PA, Tanner SJ, Halloran BP 1994 Alendronate increases skeletal mass of growing rats during unloading by inhibiting resorption of calcified cartilage. J Bone Miner Res **9**(11)**:**1777-87.

27. Machwate M, Zerath E, Holy X, Hott M, Godet D, Lomri A, Marie PJ 1995 Systemic administration of transforming growth factor-beta 2 prevents the impaired bone formation and osteopenia induced by unloading in rats. J Clin Invest **96**(3)**:**1245-53.

28. Casey DP, Joyner MJ 2009 Skeletal muscle blood flow responses to hypoperfusion at rest and during rhythmic exercise in humans. J Appl Physiol **107**(2)**:**429-37.

29. Parkhouse WS, Coupland DC, Li C, Vanderhoek KJ 2000 IGF-1 bioavailability is increased by resistance training in older women with low bone mineral density. Mech Ageing Dev **113**(2)**:**75-83.

30. Ryan AS, Treuth MS, Rubin MA, Miller JP, Nicklas BJ, Landis DM, Pratley RE, Libanati CR, Gundberg CM, Hurley BF 1994 Effects of strength training on bone mineral density: hormonal and bone turnover relationships. J Appl Physiol **77**(4)**:**1678-84.

31. Shepherd JT 1987 Circulatory response to exercise in health. Circulation **76**(6 Pt 2)**:**VI3-10.

32. Farrell PA, Fedele MJ, Hernandez J, Fluckey JD, Miller JL, 3rd, Lang CH, Vary TC, Kimball SR, Jefferson LS 1999 Hypertrophy of skeletal muscle in diabetic rats in response to chronic resistance exercise. J Appl Physiol **87**(3)**:**1075-82.

33. Fluckey JD, Kraemer WJ, Farrell PA 1995 Pancreatic islet insulin secretion is increased after resistance exercise in rats. J Appl Physiol **79**(4)**:**1100-5.

34. Gasier HG, Wiggs MP, Buentello JA, Previs SF, Riechman SE, Fluckey JD 2008 The assessment of in vivo protein synthesis following chronic resistance exercise using $^{2}H_2O$. FASEB J **22:**LB91.

35. Fluckey JD, Knox M, Smith L, Dupont-Versteegden EE, Gaddy D, Tesch PA, Peterson CA 2006 Insulin-facilitated increase of muscle protein synthesis after resistance exercise involves a MAP kinase pathway. Am J Physiol Endocrinol Metab **290**(6)**:**E1205-11.

36. Hawkins SA, Schroeder ET, Wiswell RA, Jaque SV, Marcell TJ, Costa K 1999 Eccentric muscle action increases site-specific osteogenic response. Med Sci Sports Exerc **31**(9)**:**1287-92.

37. Nickols-Richardson SM, Miller LE, Wootten DF, Ramp WK, Herbert WG 2007 Concentric and eccentric isokinetic resistance training similarly increases muscular strength, fat-free soft tissue mass, and specific bone mineral measurements in young women. Osteoporos Int **18**(6)**:**789-96.

38. Westerlind KC, Fluckey JD, Gordon SE, Kraemer WJ, Farrell PA, Turner RT 1998 Effect of resistance exercise training on cortical and cancellous bone in mature male rats. J Appl Physiol **84**(2)**:**459-64.

39. Fuchs RK, Bauer JJ, Snow CM 2001 Jumping improves hip and lumbar spine bone mass in prepubescent children: a randomized controlled trial. J Bone Miner Res **16**(1)**:**148-56.

40. Kelley GA, Kelley KS, Tran ZV 2001 Resistance training and bone mineral density in women: a meta-analysis of controlled trials. Am J Phys Med Rehabil **80**(1)**:**65-77.

41. Martyn-St James M, Carroll S 2006 High-intensity resistance training and postmenopausal bone loss: a meta-analysis. Osteoporos Int **17**(8)**:**1225-40.

42. Kerr D, Ackland T, Maslen B, Morton A, Prince R 2001 Resistance training over 2 years increases bone mass in calcium-replete postmenopausal women. J Bone Miner Res **16**(1)**:**175-81.

43. Nichols DL, Sanborn CF, Love AM 2001 Resistance training and bone mineral density in adolescent females. J Pediatr **139**(4)**:**494-500.

44. Singh JA, Schmitz KH, Petit MA 2009 Effect of resistance exercise on bone mineral density in premenopausal women. Joint Bone Spine **76**(3)**:**273-80.

45. Woitge HW, Friedmann B, Suttner S, Farahmand I, Muller M, Schmidt-Gayk H, Baertsch P, Ziegler R, Seibel MJ 1998 Changes in bone turnover induced by aerobic and anaerobic exercise in young males. J Bone Miner Res **13**(12)**:**1797-804.

46. Taaffe DR, Robinson TL, Snow CM, Marcus R 1997 High-impact exercise promotes bone gain in well-trained female athletes. J Bone Miner Res **12**(2)**:**255-60.

47. Kohrt WM, Bloomfield SA, Little KD, Nelson ME, Yingling VR 2004 American College of Sports Medicine Position Stand: physical activity and bone health. Med Sci Sports Exerc **36**(11)**:**1985-96.

48. Notomi T, Lee SJ, Okimoto N, Okazaki Y, Takamoto T, Nakamura T, Suzuki M 2000 Effects of resistance exercise training on mass, strength, and turnover of bone in growing rats. Eur J Appl Physiol **82**(4)**:**268-74.

49. Notomi T, Okazaki Y, Okimoto N, Saitoh S, Nakamura T, Suzuki M 2000 A comparison of resistance and aerobic training for mass, strength and turnover of bone in growing rats. Eur J Appl Physiol **83**(6)**:**469-74.

50. Umemura Y, Baylink DJ, Wergedal JE, Mohan S, Srivastava AK 2002 A time course of bone response to jump exercise in C57BL/6J mice. J Bone Miner Metab **20**(4)**:**209-15.

51. Welch JM, Turner CH, Devareddy L, Arjmandi BH, Weaver CM 2008 High impact exercise is more beneficial than dietary calcium for building bone strength in the growing rat skeleton. Bone **42**(4)**:**660-8.

52. Umemura Y, Ishiko T, Yamauchi T, Kurono M, Mashiko S 1997 Five jumps per day increase bone mass and breaking force in rats. J Bone Miner Res **12**(9)**:**1480-5.

53. Smith SM, Zwart SR, Heer M, Lee SM, Baecker N, Meuche S, Macias BR, Shackelford LC, Schneider S, Hargens AR 2008 WISE-2005: supine treadmill exercise within lower body negative pressure and flywheel resistive exercise as a countermeasure to bed rest-induced bone loss in women during 60-day simulated microgravity. Bone **42**(3)**:**572-81.

54. Shackelford LC, LeBlanc AD, Driscoll TB, Evans HJ, Rianon NJ, Smith SM, Spector E, Feeback DL, Lai D 2004 Resistance exercise as a countermeasure to disuse-induced bone loss. J Appl Physiol **97**(1)**:**119-29.

55. Rubin C, Xu G, Judex S 2001 The anabolic activity of bone tissue, suppressed by disuse, is normalized by brief exposure to extremely low-magnitude mechanical stimuli. Faseb J **15**(12)**:**2225-9.

56. Midura RJ, Dillman CJ, Grabiner MD 2005 Low amplitude, high frequency strains imposed by electrically stimulated skeletal muscle retards the development of osteopenia in the tibiae of hindlimb suspended rats. Med Eng Phys **27**(4)**:**285-93.

57. Fluckey JD, Dupont-Versteegden EE, Montague DC, Knox M, Tesch P, Peterson CA, Gaddy-Kurten D 2002 A rat resistance exercise regimen attenuates losses of musculoskeletal mass during hindlimb suspension. Acta Physiol Scand **176**(4)**:**293-300.

58. Lam H, Qin YX 2008 The effects of frequency-dependent dynamic muscle stimulation on inhibition of trabecular bone loss in a disuse model. Bone **43**(6):1093-1100.

59. Rodan GA, Fleisch HA 1996 Bisphosphonates: mechanisms of action. J Clin Invest **97**(12)**:**2692-6.

60. van Beek ER, Cohen LH, Leroy IM, Ebetino FH, Lowik CW, Papapoulos SE 2003 Differentiating the mechanisms of antiresorptive action of nitrogen containing bisphosphonates. Bone **33**(5)**:**805-11.

61. Plotkin LI, Weinstein RS, Parfitt AM, Roberson PK, Manolagas SC, Bellido T 1999 Prevention of osteocyte and osteoblast apoptosis by bisphosphonates and calcitonin. J Clin Invest **104**(10)**:**1363-74.

62. Plotkin LI, Manolagas SC, Bellido T 2006 Dissociation of the pro-apoptotic effects of bisphosphonates on osteoclasts from their anti-apoptotic effects on osteoblasts/osteocytes with novel analogs. Bone **39**(3)**:**443-52.

63. Ruml LA, Dubois SK, Roberts ML, Pak CY 1995 Prevention of hypercalciuria and stone-forming propensity during prolonged bedrest by alendronate. J Bone Miner Res **10**(4)**:**655-62.

64. LeBlanc AD, Driscol TB, Shackelford LC, Evans HJ, Rianon NJ, Smith SM, Feeback DL, Lai D 2002 Alendronate as an effective countermeasure to disuse induced bone loss. J Musculoskelet Neuronal Interact **2**(4)**:**335-43.

65. Apseloff G, Girten B, Walker M, Shepard DR, Krecic ME, Stern LS, Gerber N 1993 Aminohydroxybutane bisphosphonate and clenbuterol prevent bone changes and retard muscle atrophy respectively in tail-suspended rats. J Pharmacol Exp Ther **264**(3)**:**1071-8.

66. Apseloff G, Girten B, Weisbrode SE, Walker M, Stern LS, Krecic ME, Gerber N 1993 Effects of aminohydroxybutane bisphosphonate on bone growth when administered after hind-limb bone loss in tail-suspended rats. J Pharmacol Exp Ther **267**(1)**:**515-21.

67. Elefteriou F, Ahn JD, Takeda S, Starbuck M, Yang X, Liu X, Kondo H, Richards WG, Bannon TW, Noda M, Clement K, Vaisse C, Karsenty G 2005 Leptin regulation of bone resorption by the sympathetic nervous system and CART. Nature **434**(7032)**:**514-20.

68. Moore RE, Smith CK, 2nd, Bailey CS, Voelkel EF, Tashjian AH, Jr. 1993 Characterization of beta-adrenergic receptors on rat and human osteoblast-like cells and demonstration that beta-receptor agonists can stimulate bone resorption in organ culture. Bone Miner **23**(3)**:**301-15.

69. Bonnet N, Pierroz DD, Ferrari SL 2008 Adrenergic control of bone remodeling and its implications for the treatment of osteoporosis. J Musculoskelet Neuronal Interact **8**(2)**:**94-104.

70. Zheng M, Han QD, Xiao RP 2004 Distinct beta-adrenergic receptor subtype signaling in the heart and their pathophysiological relevance. Sheng Li Xue Bao **56**(1)**:**1-15.

71. Bojanic D, Nahorski SR 1983 Identification and subclassification of rat adipocyte beta-adrenoceptors using (+/-)-[125I]cyanopindolol. Eur J Pharmacol **93**(3-4)**:**235-43.

72. Kurabayashi T, Tomita M, Matsushita H, Honda A, Takakuwa K, Tanaka K 2001 Effects of a beta 3 adrenergic receptor agonist on bone and bone marrow adipocytes in the tibia and lumbar spine of the ovariectomized rat. Calcif Tissue Int **68**(4)**:**248-54.

73. Bonnet N, Benhamou CL, Malaval L, Goncalves C, Vico L, Eder V, Pichon C, Courteix D 2008 Low dose beta-blocker prevents ovariectomy-induced bone loss in rats without affecting heart functions. J Cell Physiol **217**(3)**:**819-27.

74. Elefteriou F 2005 Neuronal signaling and the regulation of bone remodeling. Cell Mol Life Sci **62**(19-20)**:**2339-49.

75. Takeda S, Elefteriou F, Levasseur R, Liu X, Zhao L, Parker KL, Armstrong D, Ducy P, Karsenty G 2002 Leptin regulates bone formation via the sympathetic nervous system. Cell **111**(3)**:**305-17.

76. Williams RS, Bishop T 1981 Selectivity of dobutamine for adrenergic receptor subtypes: in vitro analysis by radioligand binding. J Clin Invest **67**(6)**:**1703-11.

77. Bloomfield SA, Girten BE, Weisbrode SE 1997 Effects of vigorous exercise training and beta-agonist administration on bone response to hindlimb suspension. J Appl Physiol **83**(1)**:**172-8.

78. Bonnet N, Benhamou CL, Brunet-Imbault B, Arlettaz A, Horcajada MN, Richard O, Vico L, Collomp K, Courteix D 2005 Severe bone alterations under beta2 agonist treatments: bone mass, microarchitecture and strength analyses in female rats. Bone **37**(5)**:**622-33.

79. Bonnet N, Brunet-Imbault B, Arlettaz A, Horcajada MN, Collomp K, Benhamou CL, Courteix D 2005 Alteration of trabecular bone under chronic beta2 agonists treatment. Med Sci Sports Exerc **37**(9)**:**1493-501.

80. Bonnet N, Laroche N, Beaupied H, Vico L, Dolleans E, Benhamou CL, Courteix D 2007 Doping dose of salbutamol and exercise training: impact on the skeleton of ovariectomized rats. J Appl Physiol **103**(2)**:**524-33.

81. Togari A, Arai M 2008 Pharmacological topics of bone metabolism: the physiological function of the sympathetic nervous system in modulating bone resorption. J Pharmacol Sci **106**(4)**:**542-6.

82. Bonnet N, Pierroz DD, Ferrari SL 2008 Low bone mass and decreased biomechanical response in beta 1 adrenergic receptor ko but not in beta 2 adrenergic receptor ko mice. J Bone Miner Res **23**(Supplement 1)**:**S41.

83. Bouxsein ML, Devlin MJ, Glatt V, Dhillon H, Pierroz DD, Ferrari SL 2009 Mice lacking beta-adrenergic receptors have increased bone mass but are not protected from deleterious skeletal effects of ovariectomy. Endocrinology **150**(1)**:**144-52.

84. Mendell WW 2005 Meditations on the new space vision: the Moon as a stepping stone to Mars. Acta Astronaut **57**(2-8)**:**676-83.

85. Trappe S, Costill D, Gallagher P, Creer A, Peters JR, Evans H, Riley DA, Fitts RH 2009 Exercise in space: human skeletal muscle after 6 months aboard the International Space Station. J Appl Physiol **106**(4)**:**1159-68.

86. Macias BR, Cao P, Watenpaugh DE, Hargens AR 2007 LBNP treadmill exercise maintains spine function and muscle strength in identical twins during 28-day simulated microgravity. J Appl Physiol **102**(6)**:**2274-8.

87. Zwart SR, Hargens AR, Lee SM, Macias BR, Watenpaugh DE, Tse K, Smith SM 2007 Lower body negative pressure treadmill exercise as a countermeasure for bed rest-induced bone loss in female identical twins. Bone **40**(2)**:**529-37.

88. Belanger M, Stein RB, Wheeler GD, Gordon T, Leduc B 2000 Electrical stimulation: can it increase muscle strength and reverse osteopenia in spinal cord injured individuals? Arch Phys Med Rehabil **81**(8)**:**1090-8.

89. Bloomfield SA, Mysiw WJ, Jackson RD 1996 Bone mass and endocrine adaptations to training in spinal cord injured individuals. Bone **19**(1)**:**61-8.

90. Mohr T, Podenphant J, Biering-Sorensen F, Galbo H, Thamsborg G, Kjaer M 1997 Increased bone mineral density after prolonged electrically induced cycle training of paralyzed limbs in spinal cord injured man. Calcif Tissue Int **61**(1)**:**22-5.

91. Shields RK, Dudley-Javoroski S 2006 Musculoskeletal plasticity after acute spinal cord injury: effects of long-term neuromuscular electrical stimulation training. J Neurophysiol **95**(4)**:**2380-90.

92. Fitts RH, Riley DR, Widrick JJ 2000 Physiology of a microgravity environment invited review: microgravity and skeletal muscle. J Appl Physiol **89**(2)**:**823-39.

93. Warren GL, Stallone JL, Allen MR, Bloomfield SA 2004 Functional recovery of the plantarflexor muscle group after hindlimb unloading in the rat. Eur J Appl Physiol **93**(1-2)**:**130-8.

94. Schneider SM, Amonette WE, Blazine K, Bentley J, Lee SM, Loehr JA, Moore AD, Jr., Rapley M, Mulder ER, Smith SM 2003 Training with the International Space Station interim resistive exercise device. Med Sci Sports Exerc **35**(11)**:**1935-45.

95. Adams GR, Haddad F, Bodell PW, Tran PD, Baldwin KM 2007 Combined isometric, concentric, and eccentric resistance exercise prevents unloading-induced muscle atrophy in rats. J Appl Physiol **103**(5)**:**1644-54.

96. Hogan HA, Ruhmann SP, Sampson HW 2000 The mechanical properties of cancellous bone in the proximal tibia of ovariectomized rats. J Bone Miner Res **15**(2)**:**284-92.

97. Fluckey JD, Dupont-Versteegden EE, Knox M, Gaddy D, Tesch PA, Peterson CA 2004 Insulin facilitation of muscle protein synthesis following resistance exercise in hindlimb-suspended rats is independent of a rapamycin-sensitive pathway. Am J Physiol Endocrinol Metab **287**(6)**:**E1070-5.

98. Thomason DB, Herrick RE, Surdyka D, Baldwin KM 1987 Time course of soleus muscle myosin expression during hindlimb suspension and recovery. J Appl Physiol **63**(1)**:**130-7.

99. Hurst JE, Fitts RH 2003 Hindlimb unloading-induced muscle atrophy and loss of function: protective effect of isometric exercise. J Appl Physiol **95**(4)**:**1405-17.

100. Haddad F, Adams GR, Bodell PW, Baldwin KM 2006 Isometric resistance exercise fails to counteract skeletal muscle atrophy processes during the initial stages of unloading. J Appl Physiol **100**(2)**:**433-41.

101. Allen MR, Hogan HA, Hobbs WA, Koivuniemi AS, Koivuniemi MC, Burr DB 2007 Raloxifene enhances material-level mechanical properties of femoral cortical and trabecular bone. Endocrinology **148**(8)**:**3908-13.

102. Lawler A 2004 Space exploration. Scientists add up gains, losses in Bush's new vision for NASA. Science **303**(5657)**:**444-5.

103. Baek K, Bloomfield SA 2009 Beta-adrenergic blockade and leptin replacement effectively mitigate disuse bone loss. J Bone Miner Res **24**(5)**:**792-9.

104. Dehority W, Halloran BP, Bikle DD, Curren T, Kostenuik PJ, Wronski TJ, Shen Y, Rabkin B, Bouraoui A, Morey-Holton E 1999 Bone and hormonal changes induced by skeletal unloading in the mature male rat. Am J Physiol **276**(1 Pt 1)**:**E62-9.

105. Swift JM, Nilsson MI, Hogan HA, Sumner LR, Bloomfield SA 2010 Simulated resistance training during hindlimb unloading abolishes disuse bone loss and maintains muscle strength. J Bone Miner Res **25**(3):564-574.

106. Aguirre JI, Plotkin LI, Stewart SA, Weinstein RS, Parfitt AM, Manolagas SC, Bellido T 2006 Osteocyte apoptosis is induced by weightlessness in mice and precedes osteoclast recruitment and bone loss. J Bone Miner Res **21**(4)**:**605-15.

107. Basso N, Heersche JN 2006 Effects of hind limb unloading and reloading on nitric oxide synthase expression and apoptosis of osteocytes and chondrocytes. Bone **39**(4)**:**807-14.

108. LeBlanc A, Schneider V, Shackelford L, West S, Oganov V, Bakulin A, Voronin L 2000 Bone mineral and lean tissue loss after long duration space flight. J Musculoskelet Neuronal Interact **1**(2)**:**157-60.

109. Russell RG, Rogers MJ 1999 Bisphosphonates: from the laboratory to the clinic and back again. Bone **25**(1)**:**97-106.

110. Sato M, Grasser W, Endo N, Akins R, Simmons H, Thompson DD, Golub E, Rodan GA 1991 Bisphosphonate action. Alendronate localization in rat bone and effects on osteoclast ultrastructure. J Clin Invest **88**(6)**:**2095-105.

111. Schenk R, Eggli P, Fleisch H, Rosini S 1986 Quantitative morphometric evaluation of the inhibitory activity of new aminobisphosphonates on bone resorption in the rat. Calcif Tissue Int **38**(6)**:**342-9.

112. Fuchs RK, Shea M, Durski SL, Winters-Stone KM, Widrick J, Snow CM 2007 Individual and combined effects of exercise and alendronate on bone mass and strength in ovariectomized rats. Bone **41**(2)**:**290-6.

113. Rodan GA, Seedor JG, Balena R 1993 Preclinical pharmacology of alendronate. Osteoporos Int **3 Suppl 3:**S7-12.

114. Parfitt AM, Drezner MK, Glorieux FH, Kanis JA, Malluche H, Meunier PJ, Ott SM, Recker RR 1987 Bone histomorphometry: standardization of nomenclature, symbols, and units. Report of the ASBMR Histomorphometry Nomenclature Committee. J Bone Miner Res **2**(6)**:**595-610.

115. Tamaki H, Akamine T, Goshi N, Kurata H, Sakou T 1998 Effects of exercise training and etidronate treatment on bone mineral density and trabecular bone in ovariectomized rats. Bone **23**(2)**:**147-53.

116. Uusi-Rasi K, Kannus P, Cheng S, Sievanen H, Pasanen M, Heinonen A, Nenonen A, Halleen J, Fuerst T, Genant H, Vuori I 2003 Effect of alendronate and exercise on bone and physical performance of postmenopausal women: a randomized controlled trial. Bone **33**(1)**:**132-43.

117. Grigoriev AI, Morukov BV, Oganov VS, Rakhmanov AS, Buravkova LB 1992 Effect of exercise and bisphosphonate on mineral balance and bone density during 360 day antiorthostatic hypokinesia. J Bone Miner Res **7 Suppl 2:**S449-55.

118. Rittweger J, Frost HM, Schiessl H, Ohshima H, Alkner B, Tesch P, Felsenberg D 2005 Muscle atrophy and bone loss after 90 days' bed rest and the effects of

flywheel resistive exercise and pamidronate: results from the LTBR study. Bone **36**(6)**:**1019-29.

119. Nenonen A, Cheng S, Ivaska KK, Alatalo SL, Lehtimaki T, Schmidt-Gayk H, Uusi-Rasi K, Heinonen A, Kannus P, Sievanen H, Vuori I, Vaananen HK, Halleen JM 2005 Serum TRACP 5b is a useful marker for monitoring alendronate treatment: comparison with other markers of bone turnover. J Bone Miner Res **20**(8)**:**1804-1812.

120. Dufour C, Holy X, Marie PJ 2007 Skeletal unloading induces osteoblast apoptosis and targets alpha5beta1-PI3K-Bcl-2 signaling in rat bone. Exp Cell Res **313**(2)**:**394-403.

121. Noble BS, Peet N, Stevens HY, Brabbs A, Mosley JR, Reilly GC, Reeve J, Skerry TM, Lanyon LE 2003 Mechanical loading: biphasic osteocyte survival and targeting of osteoclasts for bone destruction in rat cortical bone. Am J Physiol Cell Physiol **284**(4)**:**C934-43.

122. Plotkin LI, Aguirre JI, Kousteni S, Manolagas SC, Bellido T 2005 Bisphosphonates and estrogens inhibit osteocyte apoptosis via distinct molecular mechanisms downstream of extracellular signal-regulated kinase activation. J Biol Chem **280**(8)**:**7317-25.

123. Thomsen JS, Morukov BV, Vico L, Alexandre C, Saparin PI, Gowin W 2005 Cancellous bone structure of iliac crest biopsies following 370 days of head-down bed rest. Aviat Space Environ Med **76**(10)**:**915-22.

124. de Bruin ED, Dietz V, Dambacher MA, Stussi E 2000 Longitudinal changes in bone in men with spinal cord injury. Clin Rehabil **14**(2)**:**145-52.

125. Frey-Rindova P, de Bruin ED, Stussi E, Dambacher MA, Dietz V 2000 Bone mineral density in upper and lower extremities during 12 months after spinal cord injury measured by peripheral quantitative computed tomography. Spinal Cord **38**(1)**:**26-32.

126. Giangregorio L, McCartney N 2006 Bone loss and muscle atrophy in spinal cord injury: epidemiology, fracture prediction, and rehabilitation strategies. J Spinal Cord Med **29**(5)**:**489-500.

127. Pierroz DD, Baldock P, Bouxsein ML, Ferrari SL 2006 Low cortical bone mass in mice lacking beta 1 and beta 2 adrenergic receptors is associated with low bone formation and and circulating IGF-1. J Bone Miner Res **21**(Supplement 1)**:**S277.

128. Allen MR, Hogan HA, Bloomfield SA 2006 Differential bone and muscle recovery following hindlimb unloading in skeletally mature male rats. J Musculoskelet Neuronal Interact **6**(3)**:**217-25.

129. Prisby RD, Swift JM, Bloomfield SA, Hogan HA, Delp MD 2008 Altered bone mass, geometry and mechanical properties during the development and progression of type 2 diabetes in the Zucker diabetic fatty rat. J Endocrinol **199**(3)**:**379-88.

130. Zeman RJ, Hirschman A, Hirschman ML, Guo G, Etlinger JD 1991 Clenbuterol, a beta 2-receptor agonist, reduces net bone loss in denervated hindlimbs. Am J Physiol **261**(2 Pt 1)**:**E285-9.

131. Chen X, Song IH, Dennis JE, Greenfield EM 2007 Endogenous PKI gamma limits the duration of the anti-apoptotic effects of PTH and beta-adrenergic agonists in osteoblasts. J Bone Miner Res **22**(5)**:**656-64.

132. Kitaura T, Tsunekawa N, Kraemer WJ 2002 Inhibited longitudinal growth of bones in young male rats by clenbuterol. Med Sci Sports Exerc **34**(2)**:**267-73.

133. Cavalie H, Lac G, Lebecque P, Chanteranne B, Davicco MJ, Barlet JP 2002 Influence of clenbuterol on bone metabolism in exercised or sedentary rats. J Appl Physiol **93**(6)**:**2034-7.

134. Colleran PN, Wilkerson MK, Bloomfield SA, Suva LJ, Turner RT, Delp MD 2000 Alterations in skeletal perfusion with simulated microgravity: a possible mechanism for bone remodeling. J Appl Physiol **89**(3)**:**1046-54.

135. Roer RD, Dillaman RM 1994 Decreased femoral arterial flow during simulated microgravity in the rat. J Appl Physiol **76**(5)**:**2125-9.

136. Robie NW, Nutter DO, Moody C, McNay JL 1974 In vivo analysis of adrenergic receptor activity of dobutamine. Circ Res **34**(5)**:**663-71.

137. National Osteoporosis Foundation 2002 America's bone health: the state of osteoporosis and low bone mass in our nation. National Osteoporosis Foundation, Washington, DC.

138. Adachi JD, Loannidis G, Berger C, Joseph L, Papaioannou A, Pickard L, Papadimitropoulos EA, Hopman W, Poliquin S, Prior JC, Hanley DA, Olszynski WP, Anastassiades T, Brown JP, Murray T, Jackson SA, Tenenhouse A 2001 The influence of osteoporotic fractures on health-related quality of life in community-dwelling men and women across Canada. Osteoporos Int **12**(11)**:**903-8.

139. Cooper C 1997 The crippling consequences of fractures and their impact on quality of life. Am J Med **103**(2A)**:**12S-17S; discussion 17S-19S.

140. Ensrud KE, Thompson DE, Cauley JA, Nevitt MC, Kado DM, Hochberg MC, Santora AC, 2nd, Black DM 2000 Prevalent vertebral deformities predict mortality and hospitalization in older women with low bone mass. Fracture Intervention Trial Research Group. J Am Geriatr Soc **48**(3)**:**241-9.

141. Oleksik A, Lips P, Dawson A, Minshall ME, Shen W, Cooper C, Kanis J 2000 Health-related quality of life in postmenopausal women with low BMD with or without prevalent vertebral fractures. J Bone Miner Res **15**(7)**:**1384-92.

142. Burge R, Dawson-Hughes B, Solomon DH, Wong JB, King A, Tosteson A 2007 Incidence and economic burden of osteoporosis-related fractures in the United States, 2005-2025. J Bone Miner Res **22**(3)**:**465-75.

143. Ehrlich PJ, Lanyon LE 2002 Mechanical strain and bone cell function: a review. Osteoporos Int **13**(9)**:**688-700.

144. Bonnet N, Benhamou CL, Beaupied H, Laroche N, Vico L, Dolleans E, Courteix D 2007 Doping dose of salbutamol and exercise: deleterious effect on cancellous and cortical bones in adult rats. J Appl Physiol **102**(4)**:**1502-9.

145. Swift JM, Ali JT, Stallone JL, Hogan HA, Bloomfield SA 2007 Beta-adrenergic receptor agonist administration during hindlimb unloading attenuates losses in bone geometry, structure, and mechanical properties. J Bone Miner Res **22**(Supplement 1)**:**S134.

146. Swift JM, Swift SN, Bloomfield SA 2008 Beta-adrenergic receptor agonist administration during hindlimb unloading effectively mitigates reductions in cancellous bone formation. J Bone Miner Res **23**(Supplement 1)**:**S231.

147. Ishijima M, Ezura Y, Tsuji K, Rittling SR, Kurosawa H, Denhardt DT, Emi M, Nifuji A, Noda M 2006 Osteopontin is associated with nuclear factor kappaB gene expression during tail-suspension-induced bone loss. Exp Cell Res **312**(16)**:**3075-83.

148. Xian CJ, Cool JC, Pyragius T, Foster BK 2006 Damage and recovery of the bone growth mechanism in young rats following 5-fluorouracil acute chemotherapy. J Cell Biochem **99**(6)**:**1688-704.

149. Kondo H, Nifuji A, Takeda S, Ezura Y, Rittling SR, Denhardt DT, Nakashima K, Karsenty G, Noda M 2005 Unloading induces osteoblastic cell suppression and

osteoclastic cell activation to lead to bone loss via sympathetic nervous system. J Biol Chem **280**(34)**:**30192-200.

150. Ahdjoudj S, Lasmoles F, Holy X, Zerath E, Marie PJ 2002 Transforming growth factor beta2 inhibits adipocyte differentiation induced by skeletal unloading in rat bone marrow stroma. J Bone Miner Res **17**(4)**:**668-77.

151. Hamrick MW, Shi X, Zhang W, Pennington C, Thakore H, Haque M, Kang B, Isales CM, Fulzele S, Wenger KH 2007 Loss of myostatin (GDF8) function increases osteogenic differentiation of bone marrow-derived mesenchymal stem cells but the osteogenic effect is ablated with unloading. Bone **40**(6)**:**1544-53.

152. Hino K, Nifuji A, Morinobu M, Tsuji K, Ezura Y, Nakashima K, Yamamoto H, Noda M 2006 Unloading-induced bone loss was suppressed in gold-thioglucose treated mice. J Cell Biochem **99**(3)**:**845-52.

153. Laharrague P, Larrouy D, Fontanilles AM, Truel N, Campfield A, Tenenbaum R, Galitzky J, Corberand JX, Penicaud L, Casteilla L 1998 High expression of leptin by human bone marrow adipocytes in primary culture. FASEB J **12**(9)**:**747-52.

154. Robling AG, Niziolek PJ, Baldridge LA, Condon KW, Allen MR, Alam I, Mantila SM, Gluhak-Heinrich J, Bellido TM, Harris SE, Turner CH 2008 Mechanical stimulation of bone in vivo reduces osteocyte expression of Sost/sclerostin. J Biol Chem **283**(9)**:**5866-75.

APPENDIX A

TERMINAL DEOXYNUCLEOTIDYL TRANSFERASE dUTP NICK END LABELING (TUNEL) ASSAY FOR PARAFFIN-EMBEDDED BONE SECTIONS

Melt paraffin on slides

You can complete up to 18 slides (with duplicate bone slices on each slide, of course) per day; each fluorescein *in-situ* cell death kit (Roche Diagnostics, Inc.; Indianapolis, IN) allows for only 50 samples (25 slides). This procedure will take you around 3-4 hours. Place slides in glass holders (empty bottom) and put in a 56-58°C oven for 10-15 minutes, or just until the paraffin melts. After paraffin melts, immediately turn oven down to 31°C.

1. Deparaffinize slides

Before the paraffin hardens dehydrate the slides in the following graded series of xylenes and alcohol (thus, the slide holders must physically fit in the ~ 300 ml jars that hold these liquids):

1. Xylene 5 min
2. Xylene 5 min
3. 100% ethanol 3 min
4. 100% ethanol 3 min
5. 95% ethanol 3 min
6. 70% ethanol 3 min

Don't reuse these solutions!

2. Rehydrate sections with 0.3% H_2O_2 (594 ml DI water, 6 ml 0.3% H_2O_2) in DI water for 30 minutes. Use the same glass slide holders as before and quench in 300 ml jars.

3. Make "wells" with Liquid Blocker pen (Accurate Chemical and Scientific Corp, Westbury, NY) around each bone slice. It is very important that these wells will keep the fluids and don't leak. Take your time when you are doing this step, but make sure that the bone samples are well-hydrated.

3. Incubate tissue section for 15-30 minutes at 21-37°C with Proteinase K recombinant (PCR Grade; Roche Diagnostics, Indianapolis, IN) in oven. Proteinase K has been aloquated out in 1 ml vials in a concentration of 20 mg/ml. To make up Proteinase K

solution for TUNEL assay, thaw out aliquot and remove 2 vials of 10 μl; dilute 10 μl in 1 ml of 10mM Tris-HCl (2 vials total).

After incubation is complete place a steel pan filled with dd H_2O and 3 drops of Clear Bath Algicide (NWR International; Polyscience, Niles, IL) in bottom of oven (humidifies oven).

4. Rinse slides 2x with freshly made PBS (*make with Distilled H_2O).*

5. Remove TUNEL reaction mixtures from ice.

a) Remove 100 μl Label Solution (vial 2) for two negative controls.
b) Add total volume (50 μl) of Enzyme Solution (vial 1) to remaining 450 μl Label Solution in vial 2 to obtain 500 μl of TUNEL reaction mixture.
c) Mix well to equilibrate components.
d) Remember to complete 1 positive control (DNase I recombinant) for each TUNEL kit. To make DNase I recombinant (Roche Diagnostics, Inc.; Indianapolis, IN): 1) combine 0.788g Tris-HCl (157.6g/M; Sigma, St. Louis, MO) with 100mL Di H_2O_2, 2) add 1 mg/ml BSA (Bovine Serum Albumin; in this case, add exactly 0.1g BSA because we are using 150 ml solution), 3) combine 6.7 μl of DNase I (concentration is 10 U/μl; need concentration of 1500 U/ml; have 10,000 units in 1 ml; therefore, use 6.7 μl DNase I) with 150 μl of Tris-HCl/BSA solution.

6. Rinse slides 2x with PBS (place slides in PBS-filled jar for 2 minutes); subsequently dry area around samples with cotton-tipped swab.

7. Add 50 μl TUNEL reaction mixture on samples (NOTE: for negative control, add 50 μl Label Solution each instead of TUNEL reaction mixture; for positive control, add 50 μl DNase I solution, then add 50 μl TUNEL reaction mixture).

8. Incubate slides in a humidified atmosphere for 60 min at 37°C.

9. Rinse slides 3x with fresh PBS.

10. Counterstain with 1 ml drop of hematoxylin (Hematoxylin QS; Vector Laboratories; Burlingame, CA) for 10-15 seconds of exposure (less time if stain is too bright).

11. Rinse slides for 3-5 seconds under faucet with tap water and return to slide holder.

12. Immediately coverslip one slide at a time under dark conditions until all slides are complete, and place slides in a box. Do not allow for extended UV light exposure by slides (i.e. sunlight)! This light will fade fluorescent labeling of cells & inhibit accurate measurement of TUNEL+ cells.

13. Measure positive & negative controls first under UV light (SWB) at x200 or x400 magnification to ensure quality of solutions.

VITA

Joshua Michael Swift
Texas A&M University
Department of Health and Kinesiology; MS4243
College Station, TX 77843-4243
jms1017@hlkn.tamu.edu

EDUCATION

2002	B.S.	The Pennsylvania State University	Kinesiology
2010	Ph.D.*	Texas A&M University	Kinesiology

* certificate in Space Life Sciences, awarded by Texas A&M University

HONORS AND AWARDS

2010	Distinguished Graduate Student Award for Excellence in Doctoral Research
2010	Research Presentation Award, Annual NASA HRP Workshop
2009	Oral Presentation Award, American Society of Bone and Mineral Research 31st Annual Meeting
2009	Texas Chapter of the American College of Sports Medicine, Manuscript Award, 1st Place
2008-2010	US Navy Health Services Collegiate Scholarship; Commissioned Navy Lieutenant upon Graduation as Research Physiologist
2007	Plenary Poster Presentation Award, American Society of Bone and Mineral Research 29th Annual Meeting
2006-2008	National Space Biomedical Research Institute Pre-Doctoral Training Fellowship
2006	Texas Chapter of the American College of Sports Medicine, Research Award in the Master's Category, 1st Place

PUBLICATIONS

1. Prisby, R.D., J.M. Swift, S.A. Bloomfield, H.A. Hogan, M.D. Delp. 2008 Altered bone mass, geometry, and mechanical properties during the development and progression of type 2 diabetes in the Zucker diabetic fatty rat. Journal of Endocrinology 199(3): 379-388.
2. Swift, J.M., H.A. Hogan, M.I. Nilsson, L.R. Sumner, S.A. Bloomfield. 2010 Simulated resistance training during hindlimb unloading abolishes disuse bone loss and maintains muscle strength. Journal of Bone and Mineral Research (In Press)
3. Swift, J.M., H.G. Gasier, M.P. Wiggs, S.N. Swift, H.A. Hogan, J.D. Fluckey, and S.A. Bloomfield. Reduced load increases the cancellous bone response to rodent voluntary jump exercise.(Submitted to Bone)
4. Swift, J.M., S.D. Bouse, H.A. Hogan, S.A. Bloomfield. Cancellous bone response to simulated resistance training is blunted by concomitant alendronate treatment during disuse. (In preparation)